

**POLYSACCHARIDE SOLUTIONS FROM A  
STATISTICAL THERMODYNAMIC  
PERSPECTIVE AND THE DEVELOPMENT  
OF CELLULOSE ANALOGUES**

**Thomas William John Nicol (MChem MRSC)**

**PhD Thesis**

**University of York**

**Chemistry (Green Chemistry & YSBL Cohort)**

**May 2020**

## ABSTRACT

The development of new cellulose solvents, motivated by environmental concerns, would greatly benefit from a full understanding of the cellulose dissolution mechanism. With a focus on aqueous solvents, this thesis made progress towards understanding the molecular interactions in solution that lead to successful dissolution of cellulose. These molecular interactions were quantified by using statistical thermodynamic theory based on the Kirkwood-Buff (KB) theory of solutions. This was applied to cellobiose and gave insights into the interactions present in its solubility, highlighting the importance of preferential salt-cellobiose interaction and lending support to the hypothesis of “cellulose charging up” seen in the literature. However, extension of this theory for application to cellulose requires improvement in both accuracy and reliability of solubility quantification. An experimental investigation identified the problem of incomplete dissolution below the saturation point, which is responsible for major inaccuracies in solubility measurements of amorphous cellulose. The requirements for an analogue of cellulose and the correct choice of measurement protocol for solubility of cellulose were identified.

In addition to molecular level interactions, macroscopic scale phenomena such as gelation and precipitation could be seen as equally important for understanding cellulose behaviour in solvents. Design of new methods of analysis is required to understand these phenomena in a manner beyond the capabilities of traditional polymer theory. Hence an extension of KB theory using starch gelatinisation as a basis was developed. When applied to starch gelatinisation, this theory clarified the mechanism behind the effect of salt concentration on temperature dependence of gelatinisation. (Salts are excluded from gelatinised starch at low salt concentrations and anions can access inside the starch granule at higher concentration.) Similar theory could be applied to cellulose gelation, or precipitation, to glean information about the interactions present in their mechanisms.

# LIST OF CONTENTS

ABSTRACT.....	2
LIST OF CONTENTS.....	3
LIST OF TABLES.....	8
LIST OF FIGURES.....	9
LIST OF NOTATION.....	13
ACKNOWLEDGEMENTS.....	14
DECLARATION.....	16
CHAPTER 1: SOLUTIONS FOR POLYSACCHARIDE DISSOLUTION.....	17
1.1 Physical characteristics and uses of cellulose.....	17
1.2 Why is it difficult to break down cellulose?.....	19
1.3 Importance of understanding solvents for environmentally friendly biomass utilisation.....	24
1.4 Cellulose solubilisation: hypotheses & the importance of theory.....	27
1.5 Theoretical approaches to understand cellulose solutions.....	29
1.5.1 Statistical thermodynamics reveals molecular interactions.....	29
1.5.2 The link between solubility and free energy.....	33
1.5.3 Transfer free energy interpretation.....	36
Relationship between concentration and chemical potential relies on statistical thermodynamics.....	36
Standard chemical potential and pseudo-chemical potential in dilute solutions.....	37
Psuedo-chemical potential's effect on interpreting thermodynamic quantities of transfer.....	38

1.6 Quantifying cellulose solubility and the use of analogues .....	39
1.6.1 Problems in cellulose solubility .....	39
1.6.2 Employing cellulose analogues.....	40
1.7 Thesis strategy and motivation .....	42
CHAPTER 2: SOLUTION MOLECULAR INTERACTIONS FROM CELLOBIOSE AS AN ANALOGUE OF CELLULOSE .....	43
2.1 Predominant hypotheses of cellulose interactions.....	45
2.2 From solubility to the solvation mechanism.....	47
2.3. Quantifying interactions in solutions.....	49
2.3.1 Expressing solubility in terms of KBIs .....	50
2.4 Quantifying affinities from experimental data .....	52
2.4.1 Calculation of Equation 2.6 .....	52
2.4.2 Calculation of Equation 2.7 .....	54
2.5 Results and Discussion.....	56
2.5.1 Driving forces of solubilisation: Preferential cellobiose-salt interaction versus preferential self-aggregation of salts .....	56
2.5.2 Salt accumulation around cellulose as a driving force.....	58
2.6 Cellobiose dehydration – water structure hypothesis .....	60
2.7 Cellobiose solubilisation and the Hofmeister effect .....	63
2.8 Summary and cellobiose as an analogue.....	64
2.8.1 molecular scale solubility explanation.....	64
2.8.2 Cellobiose as a cellulose analogue.....	65
CHAPTER 3: DEVELOPMENT OF CELLULOSE SOLUBILITY METHODS FOR STATISTICAL THERMODYNAMIC DATA ACQUISITION .....	67

3.1 Introduction.....	67
3.1.1 Quantification methods .....	69
Single aliquot addition .....	70
Incremental addition.....	71
3.1.2 Choice of samples and solvent.....	72
3.2 Experimental .....	75
3.2.1 Materials .....	75
3.2.2 Sample preparation.....	75
Preparation of amorphous cellulose through phosphoric acid hydrolysis ...	75
End group reduction .....	76
Preparation of amorphous cellulose samples through dissolution and coagulation.....	76
3.2.3 Solubility test protocols.....	76
Solubility determination using single aliquot addition with solute recovery	76
Solubility determination using incremental addition with solute recovery...	77
Solubility determination using incremental addition with visual quantification .....	77
SEC-MALLS analysis .....	78
3.3 Results and discussion .....	81
3.3.1 Comparison with cellulose: DP dependence in dissolution behaviour for Single Aliquot experiments .....	81
3.3.2 Influence of incremental addition on solute recovery measurements ....	83
3.3.4 Incremental Addition: Visual/Optical measurement of saturation point .	85
3.3.5 Origin of incomplete dissolution .....	86

3.3.6 Comparison between methods .....	89
3.4 Conclusions .....	91
3.4.1 Insights into quantification problems .....	91
3.4.2 Design of an analogue .....	92
CHAPTER 4: UNDERSTANDING MOLECULAR INTERACTIONS IN MACROSCOPIC TRANSITIONS .....	93
4.1 Introduction.....	93
4.2 Statistical thermodynamics of starch gelatinisation in the presence of salts	97
4.2.1 Thermodynamics of starch gelatinisation .....	97
4.2.2. Statistical thermodynamics of starch gelatinisation.....	99
4.2.3 Determining starch-water and starch-salt affinity changes .....	101
4.2.4 The effect of bulk solution structure.....	102
4.2.5 Source and analysis of experimental data – non-linear regressions.....	102
4.3 Data processing methods .....	104
4.3.1 Enthalpy fitting .....	104
4.3.2 Salt activity fitting.....	107
4.4 Starch gelatinisation under dilute salt concentration .....	109
4.5. Starch gelatinisation under increased salt concentration .....	114
4.5.1. The origin of the $T_g$ maxima.....	114
4.5.2. Salt accessibility to, and association with, starch .....	115
4.6. Advantages over the current polymer theory.....	117
4.6.1. Quantifying co-solute exclusion .....	117
4.6.2. Other processes involving starch .....	117
4.6.3 Extension and application to cellulose .....	118

4.7. Conclusion .....	119
CHAPTER 5: CONCLUSION AND FUTURE WORK.....	121
5.1 Insights into the mechanism of cellulose solubility in aqueous solvents .....	121
5.2. Improvements to the experimental quantification of cellulose solubility ...	122
5.3. Future work based on this thesis .....	123
5.3.1 Experimental improvements .....	123
Understanding the impact of filtration or centrifugation on quality of supernatant sampling .....	123
5.3.2 Additional research into dissolution mechanism .....	124
Applying thermodynamics to understand cellulose solubility driving forces .....	124
Simulation to complete the molecular level picture of cellulose's dissolution mechanism.....	125
Extending KB theory to cellulose particles.....	127
Final thoughts.....	128
Appendix – Fitting and methodology for salt activities in starch systems .....	129
References .....	134

## LIST OF TABLES

Table 2.1: Heat capacity of cellobiose dissolution, calculated from literature enthalpy data.

Table 3.1: Schematic depictions of relevant quantification methods in cellulose solubility measurement, separated by method of addition and of measurement.

Table 3.2: Deconvoluted SEC-MALLS peaks describing the DP distribution within Initial, Dissolved and Undissolved samples.

Table 4.1: Coefficients from the equation,  $\Delta H_g = A + Bc_2 + Cc_2^2$ , used for fitting calorimetric  $\Delta H_g$  data. These coefficients have no physical meaning and exist simply to provide a continuous set of data.

Table 4.2: Coefficients from the equation,  $T_g = A + Bc_2 + Cc_2^2 + Dc_2^Z$ , to fit experimental gelatinisation temperature data.

Table 4.3:  $\Delta G_{u1}^0$  and  $\Delta G_{u2}^0$  of a range of salts upon gelatinisation of sago and wheat (for KI only) starch.

Table A.1: Fitting coefficients for osmotic coefficient in equation B5.



## LIST OF FIGURES

Figure 1.1: Glucose, the monomer unit of cellulose, (left) and how it is arranged as the constituent unit in celluloses' molecular structures.

Figure 1.2: Changing Markets' "Dirty Fashion" report showing pollution in rivers around viscose producing factories.

Figure 1.3: Schematic depiction of the description of a system considering short range interactions only and a system including long range interactions.

Figure 1.4: KBIs quantify the differences in distribution of molecules between these two states. In this example there is negative accumulation of solvent (blue) around solute (red) and therefore  $G_{u1}$  has a negative value.

Figure 1.5: Schematic depiction of pseudo-chemical potential ( $\mu_u^*$ ) of the solute (u) in red.

Figure 1.6: Schematic depicting the origin of transfer free energy ( $\Delta\mu_{tr}$ ).

Figure 1.7: Schematic depiction of transfer free energy and its relationship to dissolution.

Figure 2.1: Solubility enhancement of cellobiose by Chloride salts, data from Liu et al.

Figure 2.2: Polynomial fitting of  $\Delta\mu_c^*$  plotted against  $-RT \ln a_w$  to provide a function which can be differentiated as per Eq. 2.9 to calculate preferential interaction. The fitting equation used was:  $\Delta\mu_c^* = a(-RT \ln a_w)^2 + b(-RT \ln a_w)$ .

Figure 2.3: Preferential cellobiose-ion interactions characterised quantitatively via the Kirkwood-Buff integrals ( $G_{cs} - G_{cw}$ ) for NaCl, KCl, LiCl and ZnCl<sub>2</sub> calculated from the solubility data. Error bars shown as blocks in corresponding colours.

Figure 2.4: Solubilisation inefficiency due to the preferential self-aggregation of salt ions in bulk aqueous solution, which has been quantified by the KBIs via Eq. 2.7, plotted for KCl, NaCl, LiCl and ZnCl<sub>2</sub>. Error bars shown as blocks in corresponding colours.

Figure 2.5: Individual Kirkwood-Buff integrals that lead to preferential association of cellobiose in solutions of ZnCl<sub>2</sub>, LiCl, NaCl and KCl. Error bars shown as blocks in corresponding colours.

Figure 3.1: DP distribution of amorphous Avicel, CC31, and filter paper pulp (FP) regenerated from LiCl/DMAc system and amorphous hydrolysed Avicel regenerated from H<sub>3</sub>PO<sub>4</sub> system.

Figure S1: Raw data of all single aliquot/solute recovery experiments on hydrolysed Avicel.

Figure S2: Schematic depiction of apparent solubility value calculation.

Figure 3.2: Solubility of cellulose samples in 2 molar LiOH (aq) solution at 10 °C plotted against the size of the aliquot of solute added, in weight percent. (Error bars calculated by procedure in Box 1.4. and not available for CC31 and FP due to the small quantity of available sample.)

Figure 3.3: Solubility of hydrolysed cellulose measured by the addition of incremental aliquots of < 1.5 wt%. Compared with the solubility profile obtained from single aliquot/solute recovery measurements.

Figure 3.4 Saturation point determined by incremental addition of hydrolysed Avicel regenerated from H<sub>3</sub>PO<sub>4</sub> and Avicel regenerated from LiCl/DMAc at 10 °C in 2 molar LiOH (aq) (Shown in purple, line thickness represents error bars) compared with the solubility profile obtained from single aliquot/solute recovery measurements.

Figure 3.5: SEC-MALLS elution profiles for hydrolysed Avicel (HA) before solubility tests ("Input") overlaid with elution profiles for the dissolved ("D") and undissolved ("U") fractions of HA. The "D" and "U" samples were taken from the SA/SR batch at  $11.85 \pm 0.19$  wt% added (Figure 2). The concentration of profiles "D" and "U" were normalised with respect to the peak area of "Input" by taking account of the mass recovered for each fraction (Where D was  $66.2 \pm 1.6$  % and undissolved was  $36.0 \pm 1.6$  % of the mass of "Input").

Figure 4.1: DSC thermogram of wheat starch within a range of water contents (25-90%) as seen in Day et al.

Figure 4.2: Fitting of enthalpy data collected from the literature <sup>1,2</sup> using parameters summarised in Table 4.1. Unfitted points highlighted with black outline.

Figure 4.3: Fitting of  $T_g$  data from the literature to obtain  $\frac{dT_g}{dc_2}$ , using parameters summarised in Table 4.2.

Figure 4.4: Preferential affinity of salt with starch or water with starch, described by  $\Delta G_{u2} - \Delta G_{u1}$  values from Eq. (4.11) for all of the salts studied, and its dependence on salt ion concentration. The individual data points in the  $\text{Na}_2\text{SO}_4$  dataset that lay outside of smoothed data fit (Figure 4.1) are denoted by yellow square markers.

Figure 4.5:  $c_2(G_{22} - G_{21})$ , the salt ion self-association in bulk solution and its dependence on salt concentration. Calculated using Eq. (4.9).

Figure A.1: Osmotic coefficient of NaCl at 348K (75 °C).

Figure A.2: Osmotic coefficient of KCl at 353K (80 °C).

Figure A.3: Osmotic coefficient of  $\text{Na}_2\text{SO}_4$  at 353K (80 °C).

Figure A.4: Osmotic coefficient of NaI at 353K (80 °C) (extrapolated from trend seen in reference).

Figure A.5: Osmotic coefficient of KI at 333K (60C).

# LIST OF NOTATION

Reference page for notation used throughout the thesis.

- $a_i$  - chemical activity of i
- $c_i$  - molar concentration of i
- $C_p$  - constant pressure heat capacity
- $G$  - Gibbs free energy
- $G_{ij}$  - Kirkwood-Buff integral between species i and j
- $g_{ij}(r)$  - radial distribution function between species i and j at distance r
- k - Boltzmann coefficient
- $m_i$  - molal concentration of i
- $N$  - number of particles
- P - pressure
- R - gas constant
- T - temperature
- $T_g$  - temperature of gelatinisation
- V - volume
- $V_i$  - partial molar volume of i
- $\gamma_i$  - activity coefficient of i
- $\Delta H_g$  - enthalpy change of gelatinisation
- $\Delta S_g$  - entropy change of gelatinisation
- $\Delta\mu_{g,u}$  - partial molar free energy of gelatinisation of u ( $\Delta\mu_u$  for simplicity)
- $\Delta\mu_{tr}^*$  - partial molar transfer free energy ( $\Delta\mu_{tr,c}^*$  is referred to as  $\Delta\mu_c^*$  for simplicity)
- $\varphi$  - osmotic coefficient
- $\Lambda^3$  - momentum partition function in 3 dimensions
- $\mu_i^*$  - pseudo-chemical potential of i
- $\mu_i$  - chemical potential of i
- $\mu_i^\theta$  - standard chemical potential

Superscript 0 is used to define a quantity in pure water or the dilute limit of a solution (e.g. of concentration ( $c_i^0$   $_{j \rightarrow 0}$ ) or chemical potential ( $\mu_i^0$   $_{j \rightarrow 0}$ ) where  $j \rightarrow 0$  is often omitted in the notation for simplicity).

Subscript g is used to denote gelatinisation processes.

$\Delta$  is used to denote that a transition is occurring, this could either be a transfer of a solute from one phase to another (in transfer free energy) or a phase transition (in gelatinisation processes).

## ACKNOWLEDGEMENTS

Seishi, without you I would not be the scientist I am today. You've been an instrumental force in my growth as a person and as a researcher. Thank you for everything science dad! To Noriyuki Isobe, your guidance and support in the development of my experimental abilities have made it possible to find a place in research where I feel satisfied. Your expert knowledge and understanding have helped me escape many pitfalls. Also, I enjoyed our trip to Kamakura, your family is lovely!

To Mum, Dad, Laura and Grace, and to all the rest of my own family. You are wonderful and kind. Thank you for your unwavering support. Soph, our time together has been sweet. I hope that we can explore more beaches and cities together once we are free again! You're a lovely bean and you mean the world to me. David, you're my friend and I like you. All my friends, top gods and discord boys, you're fab! Izzi, thank you for the years of support and sparkling conversation, and for your continued friendship. Anna, thanks for telling me like it is and supporting me throughout, thanks for friends-giving and friendship. Here's some bedtime story for J! Andy, you're a cool guy, I don't care what you say! Josh, you're an inspiration. Laura, you're a boss, give me job one day?

Thanks to James Clark and Martin Bates for insight and direction in my TAP meetings. Thanks to Simon Grist for your technical expertise and friendly chats. Thanks to Louise Haigh, Julie Borgia, Jane Harrison, Richard Gammons, Rachel Crooks and many other staff members in YSBL and Chemistry for your support and kindness. Dr Andrew Leech for friendly chats and the density meter. Matubayasi, it was a pleasure to meet you and I hope to work with you again in the future. Thanks to Shigeru Deguchi and all at JAMSTEC for making my research trips out to Japan such a pleasure.

For funding, I would like to acknowledge the EPSRC, the Gen Foundation and the RSC Chem community fund.

To everybody who has given me their time and support through this process I am truly thankful.

My heart goes out to the victims of the covid-19 pandemic, which is active as I write this.

## DECLARATION

I declare that this thesis is a presentation of original work and I am the sole author. The content of chapters 2 and 4 are adapted from the following publications, of which I am first author:

*"Statistical thermodynamics unveils the dissolution mechanism of cellobiose"* by Thomas W. J. Nicol, Noriyuki Isobe, James H. Clark, and Seishi Shimizu.<sup>3</sup>

And

*"The mechanism of salt effects on starch gelatinization from a statistical thermodynamic perspective"* by Thomas W.J. Nicol, Noriyuki Isobe, James H. Clark, Nobuyuki Matubayasad, and Seishi Shimizu.<sup>4</sup>

Chapter 3 is adapted from a publication in preparation titled "Towards quantitative cellulose solubility: causes and cures for systematic inaccuracies", by Authors: Thomas W. J. Nicol, Noriyuki Isobe, Yuko Ono, Akira Isogai, Shigeru Deguchi, James H. Clark, and Seishi Shimizu.

Box 1.3 is adapted from Appendix A of my MChem dissertation *"A statistical thermodynamic approach to quantifying non-specific interactions in cyclodextrin induced drug solubilisation."*, York, 2015.

This work has not been previously presented for an award at this, or any other, University. All sources are acknowledged as References.



# CHAPTER 1: SOLUTIONS FOR POLYSACCHARIDE DISSOLUTION

## 1.1 Physical characteristics and uses of cellulose

It is well known that cellulose is an extremely abundant biopolymer which occurs naturally in plant cell walls.<sup>5,6</sup> The fact that it is so abundant in nature makes it a prime target for use as a renewable feedstock for various industrial sectors which rely heavily on fossil fuels and unsustainably produced precursors.<sup>7-9</sup> Additionally, the chemical structure and composition of cellulose that enable its use in biology are advantageous for its industrial uses, as discussed below.

Firstly, cellulose is a polysaccharide, comprised of glucose monomer units,<sup>10</sup> which have been photosynthesised and exist in plant cells as structural components.<sup>11</sup> On a molecular level, these glucose units have glycosidic linkages between the 1 and 4 positions of the pyranose form of the ring,<sup>12</sup> this leads to an unbranched polymer which can extend up to thousands of monomer units.<sup>13</sup>

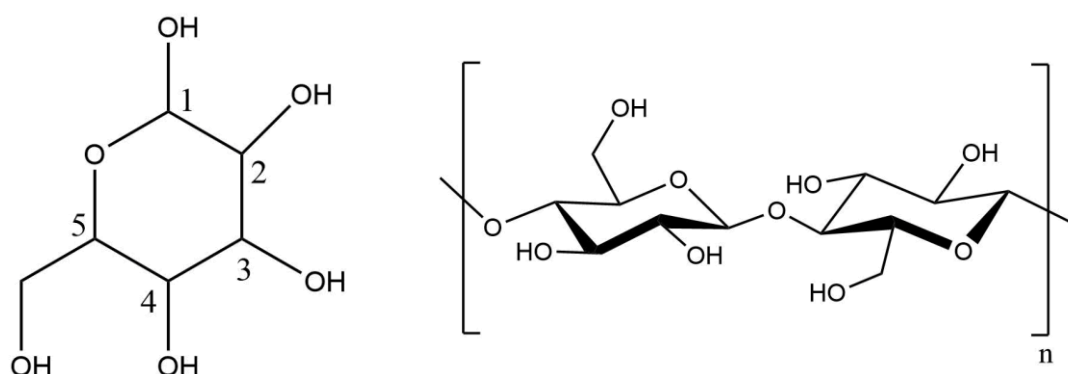


**Figure 1.1:** Glucose, the monomer unit of cellulose, (left) and how it is arranged as the constituent unit in celluloses' molecular structures.

These molecular properties enable its use as a structural component in the plant cell.<sup>14</sup> In the solid form of cellulose, the OH groups' ability to form hydrogen

bonds means that glucan chains can interact with one another, producing microfibrils which bundle to become fibres,<sup>15</sup> an important structural component of cell walls.<sup>11</sup> These structures have been utilised by humans throughout the history of civilisation because fibres from plants containing cellulose are widely available and inexpensive. Additionally, they have many useful physical properties including toughness, high tensile strength and biodegradability.<sup>16</sup> These properties makes biomass containing cellulose an excellent target as a natural fibre in fabrics and as a structural component in materials such as bio-composites.<sup>17</sup>

Secondly, the organic nature of cellulose provides the additional benefit that it can be chemically modified to produce derivatives such as cellulose acetate (which has uses as a biodegradable plastic substitute),<sup>17</sup> amino-celluloses (which can be used as bio-derived reaction scaffolds),<sup>18</sup> cellulose esters, ethers and many more examples.<sup>14,19</sup>

The combination of these structural and chemical properties lead to the possibility of other functionalised materials such as hydrogels.<sup>20-23</sup> Hydrogels are structures formed from polymer networks with large amounts of trapped water.<sup>24</sup> These materials have applications in medicine and biomaterials.<sup>25,26</sup> The key in their manufacturing is the use of aqueous solvents to facilitate the penetration of water into the polymer network.

Thirdly, the presence of carbon and hydrogen in cellulose makes it a prime target for hydrolysis and catalytic conversion. This can yield a range of commodity chemicals, ready to substitute starting materials and fuels in various established processes.<sup>27-29</sup>

In order to be utilised for this wide range of applications, cellulose is frequently required to be dissolved, derivatised or broken down.<sup>30-32</sup>

## 1.2 Why is it difficult to break down cellulose?

Cellulose is not easily extracted directly from its biomass source. Plant biomass in most cases is “lignocellulosic”, which means it contains lignin (an amorphous aromatic polymer)<sup>33</sup> and hemicellulose (a branched hetero-polysaccharide)<sup>34</sup> as structural components alongside cellulose.<sup>8</sup> The structural stability from the combination of these components, which affords useful mechanical properties to the fibres of lignocellulosic biomass, is a large part of why biomass is resistant (or recalcitrant) to processing. The pre-treatments required to overcome this recalcitrance depend on the end use for their requirements.

In pre-treatment, alongside physical pulping, cellulose dissolution is required (See Box 1.2).<sup>35,36</sup> Furthermore, after these pre-treatments, cellulose must often be stable in solution to enable further processing.<sup>14</sup> This dissolution is one of the most significant barriers to cellulose utilisation and is either achieved by derivatisation of the cellulose molecules into a form which allows them to be dissolved more easily,<sup>37</sup> or by using a solvent which is able to penetrate the chains and dissolve without derivitisation.<sup>38</sup> However, even when separated from lignin, cellulose is extremely resistant to dissolution in almost all environmentally “acceptable” solvents.<sup>39,40</sup> Box 1.1. lists the key variables that can lead to this resistance.

**Box 1.1 – Key factors affecting cellulose’s resistance to dissolution.**

**Crystallinity.** The ratio of cellulose that is crystalline vs amorphous.<sup>41,42</sup> The amorphous regions are more easily dissolved.<sup>43</sup> De-crystallisation is an important kinetic step in the cellulose dissolution mechanism.<sup>44</sup>

**Crystalline allomorph.** The arrangement of chains in the crystal state of cellulose. Cellulose’s native (Cellulose I) form exists in two versions Cellulose I $\alpha$  and I $\beta$ ,<sup>41</sup> which have differences in structure and H bonding. Upon processing via a method known as regeneration (Box 1.2), cellulose is most often converted to Cellulose II, with anti-parallel chain arrangements leading to a more easily dissolved substance.<sup>45</sup>

**Degree of polymerisation (DP).** The number of glucose units in the polymer molecule. It is well established that lower DP (or molecular weight (MW)) cellulose is easier to dissolve.<sup>46,47</sup> A reduction of DP is often carried out during pre-processing.

**Fibre structure/ macroscopic structure.** Less processed cellulose will exist in its native form which includes macroscopic assemblies such as fibrils or the matrices in cell walls.<sup>11,15</sup> This leads to multiple stages in the dissolution mechanism which must be overcome (See Box 1.2).

Separation of the contributions of each of these variables in Box 1.1. is difficult, because of their interdependence on one another. This hampers the establishment of causal links between one variable and improved dissolution. (This will be discussed later, in Chapter 3.) Cellulose samples can exhibit large variation in all of these properties which, each in turn, affect solubility. Extracting the individual contributions these properties have to solubility is difficult, because both macroscopic and microscopic factors resist solubilisation at different levels and stages of dissolution.

**Macroscopic** – (i) Fibre structure and the macroscopic crystalline arrangements that relate to crystalline allomorph and (ii) the native cell-wall structure, which includes bundles of fibrils incorporated within hemi-cellulose and lignin, in which cellulose exists within plants are both likely to affect the earlier stages in dissolution. These are usually reduced when extracting cellulose but they must be overcome before solubilisation begins. The most prominent example of an early stage in dissolution is known as “swelling”, a phenomenon in which solvent penetrates the structure of cellulose, which will be discussed later in this chapter (Box 1.2) and in Chapter 3. Eliminating some of the above during pre-processing for cellulose samples leads to increased cellulose solubility due to the reduction of intermediate steps between solid to solution.

**Microscopic** – After pre-treatments to overcome macroscopic structures have been completed, the cellulose molecules need to be dispersed into solution. Degree of polymerisation and the molecular structure of cellulose affect this final step which determines the energy and conditions required for solubility.<sup>46</sup> Cellulose is dissolved only when the intermolecular interactions between cellulose chains are overcome by the solute-solvent interactions, a well-known requirement for solubility.<sup>48</sup>

Solutions of native, or unmodified, cellulose are usually not completely dispersible on a molecular scale without derivatisation or reduction of some of the above macroscopic or microscopic properties.<sup>14,49</sup> To address the latter, pre-processing methods are used to overcome these macroscopic and microscopic factors relevant to solubility. These methods are discussed below in Box 1.2. and are used to make cellulose more easily soluble or usable.

## **Box 1.2 – Overcoming barriers to solubility via pre-treatment**

**Delignification and Fractionation.** To use cellulose from lignocellulosic sources, pre-processing steps known as delignification are applied to either solubilise lignin or extract cellulose.<sup>32</sup> Alternatively, processes known as fractionation separate out lignin, hemi-cellulose and cellulose by solubility and reactivity, again making cellulose more accessible.<sup>35</sup> In general these methods physically separate out the fibres and attempt to reduce the lignin content to provide easier access to cellulose.<sup>50,51</sup>

**Regeneration.** The reformation of solid cellulose from solution, applied once cellulose is extracted from biomass. The process leads to a change in the crystalline allomorph of cellulose, most often from I to II.<sup>52</sup> It also alters the crystallinity, depending on the conditions, to be more or less amorphous.<sup>13,52,53</sup> In addition to making cellulose more soluble, the process is utilised in the production of fibres (shown in section 1.3).

**Swelling.** Cellulose fibres and micro-crystalline cellulose both require solvent penetration into their structure as a step in their dissolution mechanism.<sup>54</sup> The process of solvent penetration is known as swelling and is sometimes taken advantage of during pre-processing to enhance dissolution. Swelling allows co-solutes to have access to the internal molecules in cellulose structures. It leads to decrystallisation and enables the next step of the cellulose dissolution mechanism.<sup>44,55</sup>

**Hydrolysis.** The reduction of cellulose DP by acid,<sup>56</sup> heat,<sup>57</sup> or enzyme.<sup>30</sup> This can be controlled to produce short chain cellulose oligomers,<sup>58-60</sup> or it can proceed to completion to provide glucose as a starting material for biosynthesis.<sup>61,62</sup>

All of these methods are crucial in utilising cellulose for industry. However, many of the chemicals used to enable this industrial use lead to environmental and human health problems as will be discussed in the next section.

## 1.3 Importance of understanding solvents for environmentally friendly biomass utilisation

Fabric processing is an example of an industrial process which is of pressing concern. Processing of natural fibres for use in fabrics has been ubiquitous in the history of human civilisation. However, only in the last 150 years modification, or derivatisation, of these fibres to give them different properties was introduced, along with the utilisation of other cellulose sources to make up for the increasing demand of globalised consumerism.<sup>63-65</sup> Even though biomass is a renewable feedstock, it is the processing methods that can cause pollution and problems for public health. Examples of these harmful processes are:

**Mercerisation.** A processing method introduced to produce better quality fibres from cellulose, mostly cotton. Improving strength and softness, it produces cotton fibres superior for textile manufacture.<sup>66</sup> This is achieved through swelling and derivatisation.

**Rayon.** Another manufactured cellulose fibre, which allows production of fibres processed from wood pulps and other biomass sources that do not naturally form fibres.<sup>67</sup> There are several variants of rayon which are comprised of partially derivatised regenerated cellulose of different degrees.<sup>66</sup>

Both mercerisation and rayon production require the use of caustic chemicals, primarily NaOH. Also, rayon production has further problems inherent in its processing steps. For example, the viscose process, developed in the late 1800s, is still a prominent manufacturing method for rayon fibres and cellulose-based films.<sup>65,68</sup> This process, however, has been internationally identified as a problematic environmental concern: The process comprises of several steps which include swelling by NaOH and eventually derivatisation into sodium cellulose xanthate using CS<sub>2</sub>. The material safety data sheets of these chemicals



show the dangers that they could pose if not properly disposed of.<sup>69,70</sup> These chemicals have been allowed to escape into waterways, leading to risks to public and environmental health.<sup>71</sup>



**Figure 1.2:** Changing Markets' "Dirty Fashion" report showing pollution in rivers around viscose producing factories.<sup>71</sup>

Less harsh chemicals are required by new solvent spinning techniques, to produce rayon fibres known as Lyocell®, which has helped to reduce the risk of this pollution.<sup>63</sup> However, global uptake is limited by licensing.

The environmental problems with the use of cellulose also extend beyond its application as a fibre in textiles. Even after the removal of cellulose's fibrous structures, it is still difficult to dissolve without the use of harsh chemicals. Through the years, significant efforts have been made to develop new solvents for cellulose, both derivatising and non-derivatising.<sup>72-76</sup> The following organic-based solvents have some success in reasonably environmentally friendly dissolution of cellulose:

- N-Methylmorpholine N-oxide (NMMO) is an industrially used solvent not only in Lyocell production,<sup>77</sup> but also for coatings, hydrolysis and films of cellulose.<sup>78-80</sup> However, it is solid at room temperature (and consequently can be expensive to use) and highly explosive.<sup>75</sup>
- N,N-Dimethylacetamide (DMAc) is combined with LiCl (which acts as a cosolvent) to form a functional solvent for synthesis and analytical purposes.<sup>14,81-83</sup> However, it has been labelled a substance of “Very High Concern” due to human toxicity.<sup>84</sup>

Even though environmental hazard has been reduced for these solvents, the risks for humans are still problematic.

Exploring aqueous solvents is important for the development of green solvents because water is sourced renewably. However, aqueous solvents able to dissolve cellulose are still very harsh. A large proportion of them use transition metals, targeted at derivatisation or coordination of cellulose.<sup>85</sup> Components of these solvents can pose severe health and environmental hazards,<sup>86-88</sup> and have been shown to lead to heavy metal build-up in materials.<sup>89</sup> Other aqueous solvents for cellulose are often alkaline solutions, as seen in mercerisation, which pose their own hazards. Disposal of even moderately hazardous waste leads to significant expenses for companies.<sup>71,90</sup> Consequently, in less highly regulated areas, waste can leak into the environment.<sup>91</sup>

Due to the environmental problems and health hazards associated with current solvents for cellulose, the field of green or eco-friendly aqueous solvents has recently been a focus of this development.<sup>92-94</sup> This development is hampered by a lack of sufficient understanding of the mechanisms at play in the dissolution of cellulose. An understanding of the mechanism and conditions required to dissolve cellulose would be indispensable for the continued development of these solvents.

## 1.4 Cellulose solubilisation: hypotheses & the importance of theory

Cellulose's dissolution mechanism remains a very active field of research to this day without reaching any consensus. There are a range of different views on the mechanism of cellulose dissolution but studies are generally limited to a specific solvent system.<sup>43,82,95-98</sup>

However, two important general driving forces that lead to the difficulties in the microscopic process of dissolving cellulose have been hypothesised:

- 1) **Hydrogen bonding**<sup>43,97,99</sup> has been highlighted both as a reason for strong crystal cohesion<sup>43,100</sup> and the general basis for the resistance to complete dissolution in cellulose.<sup>101</sup> Consequently, hydrogen bonding must be disrupted for dissolution to occur due to the large number of inter- and intra- molecular hydrogen bond interactions present in cellulose's crystal forms.<sup>102</sup>
- 2) **Hydrophobic interactions.** Due to amphiphilic nature of cellulose, it has been suggested that the tendency for cellulose to stack (i.e., to aggregate) in aqueous solutions is a source for the difficulties seen in dissolving it.<sup>39,101</sup> Co-solvents known to modulate hydrophobicity, such as urea, have been shown to improve cellulose solubility in some solvents.<sup>103</sup>

Aqueous solvents that are able to overcome the above interactions, (1) and (2), often contain co-solutes that are ionic.<sup>104,105</sup> Upon study of these solutions, cellulose charging, the formation of a poly-electrolyte form of cellulose, has been recently suggested as a cause for their ability to improve cellulose solubility. This occurs from either ion/hydrate association or pH changes.<sup>106-108</sup>

The importance of each driving force (1) and (2) can be demonstrated in a range of systems, even though there has yet to be a consensus on which contribution

is dominant. The only consensus is that hydrogen bonding has previously been over-emphasised and that neither hydrogen bonding nor the hydrophobic effect can be the sole driving force.<sup>40,101,109</sup> This thesis will attempt to contribute to this debate.

Limitations of the studies of cellulose dissolution mechanism are primarily due to the lack of solid, quantitative evidence on the extent that each of the existing driving forces, and their combination and interplay, contribute to dissolution in each system.\*<sup>99</sup> These studies require theory. Empirical measures without theory cannot identify the cause of phenomena.<sup>110</sup> It is important, however, that any theory we apply has grounding in the fundamental laws of physics and is not simply speculative correlation. To provide insights into explaining the cause of observed phenomena, when taking measurements, the quantities which have a proven connection to trustworthy theories through physical chemistry should be used.

---

\* It may be noted here that limitations in the understanding of cellulose solubility are also likely linked to the misuse of terminology. One example of this is that cellulose fibres are referred to as "hydrophilic" by materials scientists due to the fact that they absorb water.<sup>111</sup> Perhaps the term "hygroscopic" should be used here, as this does not mis-assign cellulose as hydrophilic. Unclear terminology could lead to miscommunication between researchers of different backgrounds.

## 1.5 Theoretical approaches to understand cellulose solutions

Understanding the in-solution molecular interactions is indispensable for understanding the state that cellulose needs to get to in order to be completely dissolved. This section will discuss the microscopic (molecular level) theory we can apply to understand solutions that are able to dissolve cellulose and how to link experimental measurements with molecular interactions.

### 1.5.1 Statistical thermodynamics reveals molecular interactions

To understand solubility the underlying molecular interactions, attractive or repulsive forces between molecules, in solution must be quantified. However, in the past, short range or direct binding interactions (often treated as stoichiometric) were the main focus in the solubility of small molecules and the stability of macro-molecules alike.<sup>112-114</sup> This approach only takes into account the molecules in solution which make direct contact with the solute. A true description of the system will include the weaker forces from components in the solution which are not in direct contact and also the influence of the structural changes in the solvent induced by the presence of the solute.<sup>113,114</sup> This can be visualised by the schematic in Figure 1.3.

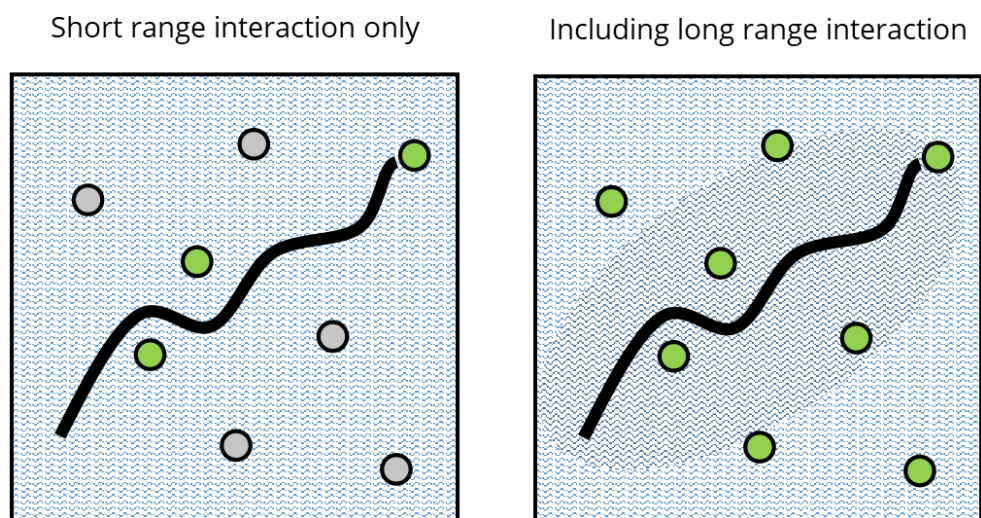


**Figure 1.3:** Schematic depiction of the description of a system considering short range interactions only and a system including long range interactions.

This is especially important for polymeric solutes as the sum of weaker interactions contribute more significantly as molecular size increases.<sup>115,116</sup>

Attempts to understand interactions in solution from measurements that only observe a small section of the system do not take these long range interactions into account, making these techniques ineffective for understanding solubility mechanisms quantitatively.

For example, many studies (including those establishing the importance of hydrogen bonding in cellulose solubility<sup>43</sup>) use nuclear magnetic resonance (NMR) spectroscopy to determine the molecular level interactions involved in mechanism.<sup>40,95,117,118</sup> NMR is useful for determining position of interaction as shielding and de-shielding changes can give us information on the localised, short-ranged, interactions in solutions and in solubility mechanisms. The direct-interaction nature of these measurements means that long range non-specific interactions, which have considerable effect on solution, are neglected.

Although one can determine the location and nature of molecular interaction due to chemical shift fluctuations of a certain assigned atom or group, this can

lead to assumptions being drawn in which a specific pair of short-range interactions is assumed to be dominant for solubilisation. However, the strength of that interaction is only qualitatively known and assignment of mechanistic behaviour from the simple presence of these interactions assumes a degree of causality from their presence alone that is not supported by a full quantitative interaction measurement. A more quantitative method is needed to show which driving force is dominant.

If we start from theory which gives a quantitative measure of all of the contributions, long range and short, the specific interaction information from methods such as NMR can give complimentary insight into mechanisms. To quantitatively study molecular level interactions specifically, a connection between the macroscopic quantities (accessible via thermodynamic and solubility measurements) and the microscopic interactions must be established.

One useful statistical thermodynamic theory which can do so, and provides clear evidence of the dominance and magnitude of interactions between components is Kirkwood Buff theory of solutions.<sup>119</sup> This theory will be discussed in more detail when it is applied later in the thesis, however, briefly: the inversion of the KB theory, initiated academically by Hall and Ben-Naim in 1970s,<sup>120,121</sup> theoretically allows conversion of thermodynamic quantities into quantitative information about molecular interactions in a solution.

These interactions are quantified in terms of the Kirkwood-Buff integral (KBI) defined, between a pair of species  $i$  and  $j$  as:

$$G_{ij} = \int dr 4\pi r^2 [g_{ij}(r) - 1] \quad (1.1)$$

where  $g_{ij}(r)$  is the radial distribution function between the species  $i$  and  $j$ .

The KBI,  $G_{ij}$ , represents the net affinity between the species  $i$  and  $j$  because it is the integral of the total distribution of molecules (or particles) of  $i$  around  $j$ .<sup>121</sup> If  $i$  is the solute (u) and  $j$  is the solvent (1),  $G_{u1}$  quantifies the extent to which solvent (1) accumulates around solute (u). This is achieved by comparing the particle distribution in solution with and without solute (Figure 1.4).

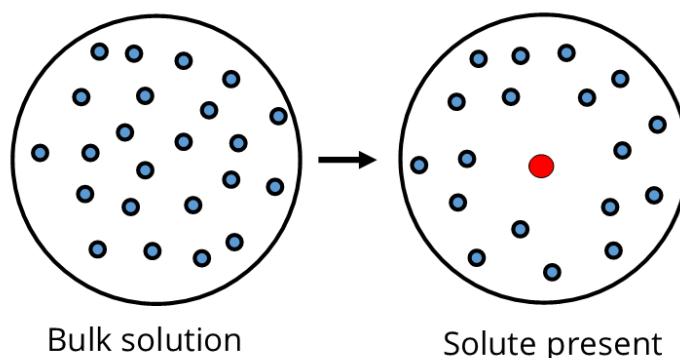


**Figure 1.4:** KBIs quantify the differences in distribution of molecules between these two states. In this example there is negative accumulation of solvent (blue) around solute (red) and therefore  $G_{u1}$  has a negative value.

Using KBIs, and comparisons between them, one can extract important information about the effects of each component in solution on a solute's solubility. A clear link to macromolecular solvation interactions was established through these KBIs.<sup>113,116,122</sup> Indeed, polysaccharides such as cellulose form aggregates in solution, even when completely dissolved. Hence, the applicability of KBIs to both particles and molecules is crucial as cellulose in solution show close to particulate behaviour.<sup>123,124</sup> Through this development experimental quantities such as concentration (solubility), molar volume, and solution activity can be used to extract molecular interactions defined in terms of KBIs.

In summary, quantitative measures of the molecular level interactions from statistical thermodynamics, combined with an understanding of the thermodynamics of a system, gives insight into the mechanism of solubilisation and can determine the driving forces behind it. To enable this, accurate



experimental data, from which quantitative measures such as KBIs can be calculated, must be used.

## 1.5.2 The link between solubility and free energy

As a first step towards linking solubility measurements to microscopic interactions, a link between solubility and the free energy of dissolution needs to be established. This can be done using chemical potential (partial molar free energy) and its definition, shown in Box 1.3.

### **Box 1.3: Connection between Chemical Potential and solubility.**<sup>125</sup>

The partial molar free energy of a solute molecule in solution can be defined in terms of the work required to introduce a particle of solute to the system. This can be done using two terms, one for inserting a particle at a fixed position ( $\mu_u^*$ ) and one for releasing the fixed particle (f). The insertion term is the pseudo-chemical potential  $\mu_u^*$ , the work required to place the particle in the system fixed at a fixed position. The second term (f) enables the fixed particle to move freely within the system, it is comprised of:

*Kinetic translational energy:  $kT \ln(\Lambda^3)$*

*Particle's freedom in the volume of solution:  $-kT \ln(V)$*

*Assimilation of one particle by N indistinguishable particles:  $kT \ln(N)$*

This leads to the liberation term:

$$f = kT \ln\left(\left(\frac{N}{V}\right) \Lambda^3\right) \quad (\#1)$$

These contributions are combined to give a statistical thermodynamic definition for chemical potential of:

$$\mu_u = \mu_u^* + kT \ln\left(\left(\frac{N}{V}\right) \Lambda^3\right) \quad (\#2)$$

Which, using the gas constant (R), gives:

$$\mu_u = \mu_u^* + RT \ln(c_u \Lambda^3) \quad (\#3)$$

Wherein  $c_u$  is first introduced. This leads to the connection between solubility and free energy, the source of which is discussed in more detail in section 1.5.3.

It should be noted that the kinetic energy consideration (which is based on the momentum partition function of the system  $\Lambda^3$ ) is dependent on temperature. Therefore, any constant temperature derivatives of Eq. #3 cancel out the contribution of  $\Lambda^3$ .

The influence of solvents on cellulose can be understood by comparing solvation between two different states. This can be done using the pseudo-chemical potentials of those states. Pseudo-chemical potential of a solute defines the energy difference between the bulk solution without a solute and the same solution with a solute inserted at a fixed position.

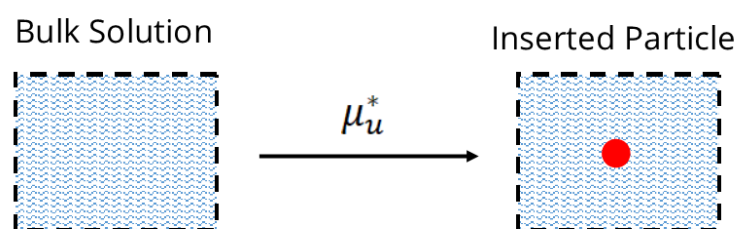


**Figure 1.5:** Schematic depiction of pseudo-chemical potential ( $\mu_u^*$ ) of the solute (u) in red.

The difference between this quantity in two different solvents is the transfer free energy ( $\Delta\mu_{tr}^*$ ).

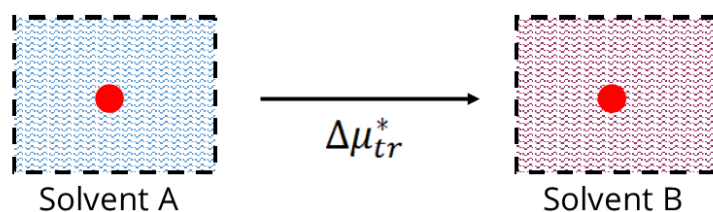


**Figure 1.6:** Schematic depicting the origin of transfer free energy ( $\Delta\mu_{tr}$ ).

$\Delta\mu_{tr}^*$  is thus the energy required to remove a solute particle from Solvent A and insert it into Solvent B. As a consequence of this,  $\Delta\mu_{tr}^*$  can be interpreted as the solvent dependence of the change in partial molar free energy of dissolution

Standard thermodynamic quantities of transfer provide a link between experimental measurements and thermodynamic theory (Box 1.3). They are widely used across many applications relating to solutions.<sup>126-128</sup> However, their interpretation and basis must be carefully examined to avoid misuse.<sup>129</sup>

Within this thesis, transfer free energy ( $\Delta\mu_{tr}$ ) is calculated as the difference between the pseudo-chemical potential (Box 1.3) of two solutions (Figure 1.6). The interpretation of TFE from one solution to another as equivalent to the difference between the partial molar free energy of dissolution in each solvent can be explained by the following schematic:

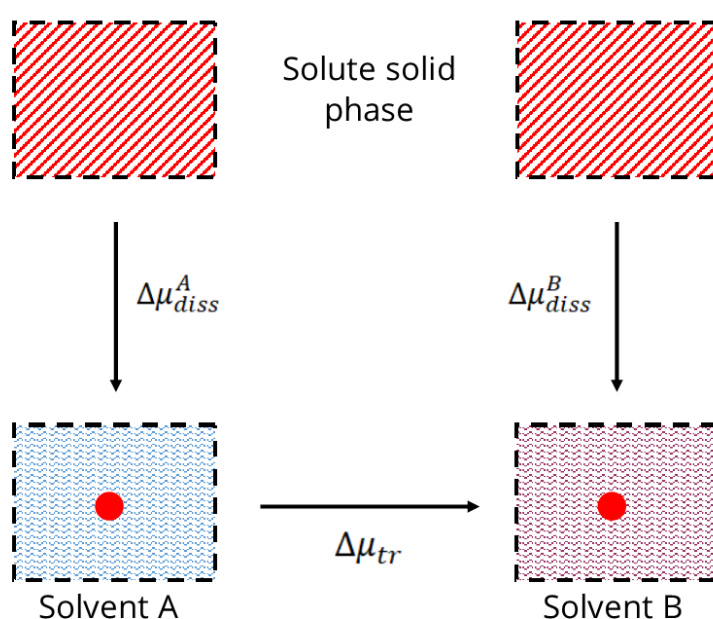


**Figure 1.7:** Schematic depiction of transfer free energy and its relationship to dissolution.

As the solute in its solid form will not change in terms of energy no matter which solvent it will be dissolved in,  $\Delta\mu_{tr}$  (the change in partial molar free energy of

transfer from A to B) only has contributions from the difference between the two solution states. Since free energy is a state function,  $\Delta\mu_{diss}^A + \Delta\mu_{tr} = \Delta\mu_{diss}^B$ . However, this is a simplification for linking transfer free energy to easily understandable quantities. Some additional considerations should be made to clarify its use and the requirements for its use (See section 1.5.3, below).

This quantity ( $\Delta\mu_{tr}$ ), most importantly, allows quantification of the interaction differences between two different solutions (through statistical thermodynamics). This enables the application of KB theory as a quantitative measure of the effect of solvents on solution molecular interactions which can help us to understand the mechanism of cellulose solvation at a molecular level. The accurate application of this theory requires robust quantitative measures of relevant experimental quantities (most importantly, solubility).

### 1.5.3 Transfer free energy interpretation

#### **Relationship between concentration and chemical potential relies on statistical thermodynamics**

The decomposition of chemical potential into insertion and liberation terms, as given in Eq. #3 (Box 1.3) relies on a statistical thermodynamic definition.

Through the extensive character of Gibbs free energy, chemical potential ( $\mu_u = \left(\frac{\partial G}{\partial N_u}\right)_{T,P}$ ) can be written in terms of:

$$\mu_u = G(T, P, N_u + 1, N_1) - G(T, P, N_u, N_1) \quad (1.2)$$

Where  $N_1$  = number of solvent molecules.

The pseudochemical potential, written in the same manner, including the fixed nature of the solute is:

$$\mu_u^* = G(T, P, N_u + 1, N_1; \mathbf{R}_0) - G(T, P, N_u, N_1) \quad (1.3)$$

Where the vector  $\mathbf{R}_0$  refers to the fixed position of the added solute.

The difference between the statistical mechanical expressions for free energy in Eq. (1.2) and (1.3) is the cause of Eq. #2 in Box 1.3.

### Standard chemical potential and pseudo-chemical potential in dilute solutions

When applying this theory, in general experimentally measured quantities from transfer free energy are not chemical potentials but *differences* in chemical potentials. Based on the free energy change between two known phases A and B:

$$\Delta G_{A \rightarrow B} = (\mu_u^B - \mu_u^A) dN_u \quad (1.4)$$

Where  $\Delta G_{A \rightarrow B}$  is the gibbs free energy of transfer of u from phase A to phase B.

A very dilute solution of u in 1, in the molar concentration scheme ( $c_u$ ) gives the standard chemical potential ( $\mu_u^\theta$ ) as:

$$\mu_u = \mu_u^\theta + RT \ln c_u \quad (1.5)$$

If the concentration of u in each phase is  $c_u^A$  and  $c_u^B$  we have, using (1.4) and (1.5):

$$\Delta G_{A \rightarrow B}(c_u^A, c_u^B) = \mu_u^B - \mu_u^A = \mu_u^{\theta B} - \mu_u^{\theta A} + RT \ln \frac{c_u^B}{c_u^A} \quad (1.6)$$

Hence, in the case of  $c_u^A = c_u^B$ , Equation 1.6 has the consequence that:

*“The differences in standard chemical potential of u is equal to the free energy of transferring u from A to B provided the concentrations  $c_u^A$  and  $c_u^B$  are the same in the two phases.”* -Ben-Naim<sup>129</sup> (Notation altered for clarity.)

However, standard chemical potential does not have an interpretable meaning as it is a constant defined by (1.5) at the dilute limit.

Pseudo-chemical potential ( $\mu_u^*$ ), on the other hand, does have an interpretable meaning (Eq. (#2, Figure 1.5). At the dilution limit where  $c_u \rightarrow 0$  in the two

phases,  $\mu_u^{*B} - \mu_u^{*A}$  becomes independent of the  $c_u$  and thus coincides with the quantity  $\mu_u^B - \mu_u^A$ . Hence, transfer free energy can be defined in terms of  $\mu_u^*$  which allows for a connection between differences in the environment around  $\mathbf{R}_0$  and the measured solubility between these two phases through:

$$\Delta G_{A \rightarrow B} = \mu_u^{*B} - \mu_u^{*A} = -RT \ln \frac{c_u^B}{c_u^A} \quad (1.7)$$

This is the source of the mathematical connection between transfer free energy and solubility.

### **Pseudo-chemical potential's effect on interpreting thermodynamic quantities of transfer**

Thermodynamic quantities of transfer calculated from Eq. (1.7), the quantities are based on the transfer of fixed solutes (AKA "local" transfer properties). This affects the interpretation of these quantities insofar as they have no contribution from the "liberation" step of introducing a particle to the solution. They simply describe the spatial arrangement of the solution around the fixed solute particle and eventually tend towards bulk solution structure. Hence,  $G_{ij}$  can be interpreted as the difference from the bulk solution of spatial arrangement of molecules of  $j$  induced by the presence of a fixed molecule of  $i$ .

## 1.6 Quantifying cellulose solubility and the use of analogues

Solubility is one of the most important parameters which can be linked to molecular interactions through transfer free energy (Section 1.5). Unfortunately, as discussed in Section 1.2, cellulose has several physical properties which can lead to problems with quantifying cellulose's solubility.

### 1.6.1 Problems in cellulose solubility

Two main factors lead to difficulties in obtaining accurate cellulose solubility data:

- 1) **Sample dependency of experiments:** Cellulose has a number of properties which lead to limitations in solubility (Box 1.1). Choice of sample leads to variation in these properties.

This can lead to solubility values between different samples that are not comparable with one another. Experimental process requires standardisation to make meaningful comparisons. Much of the time, solubility tests are measured using a brand of cellulose known as Avicel which is useful as a standard for experiments with cellulose. However, Avicel suffers from the second factor.

- 2) **Incomplete dispersion/dissolution:** Cellulose is not always dispersed at a molecular level in solution,<sup>49</sup> due to aggregation (or micelle-like supramolecular assembly)<sup>15,49</sup> and the multistage swelling process that occurs before dissolution,<sup>40,109,130,131</sup> these issues occur at higher degrees of polymerisation (DP). There is little information available on the effect of DP on interactions at a molecular level, though it is known to affect solubility.<sup>132</sup>

The incomplete dispersion observed in cellulose solutions means that aggregates are often present.<sup>49</sup> For consistent measures of solubility, this needs

to be taken into account because it can make solubility dependent on the method used to measure cellulose's solubility. Consequently, some methods may not accurately represent how much solute is dissolved. This will be investigated in greater detail in Chapter 3.

Factors (1) and (2) above are the problems with solubility that could lead to inaccuracy if such data were used in theoretical studies. These problems have led researchers to use analogues of cellulose.

## 1.6.2 Employing cellulose analogues

The analogues of cellulose focused on in this thesis are shorter chain polysaccharides produced by hydrolysis (Box 1.2). Analogue molecules should:

- Act as a reasonable representation of cellulose, with controlled differences. (eg: Similar solubility behaviour in water, similar molecular structure.)
- Allow accurate quantification of solubility.
- Be easily reproducible without specialist equipment from available materials.

Cellulose analogues may enable studies which are unfeasible with cellulose (eg: solubility in water). This information can be used to extrapolate a better understanding of cellulose.

Many studies use cellobiose as a model compound for cellulose.<sup>97,133-135</sup> The use of cellobiose is prevalent as it is experimentally simple to employ and just as cellulose is less soluble when compared to polysaccharides of a similar chain length, cellobiose is also less soluble than polysaccharides of a similar chain length (Chapter 2). Its use could also be simply due to convention. A cellobiose system is a significant simplification of cellulose solution as its behaviour differs in several ways from cellulose's on both a microscopic and macroscopic level.<sup>136</sup>



Cello-tetraose is also used at times for simulation<sup>137</sup> and as a structural analogue for crystals.<sup>138</sup> However, using cello-tetraose also neglects polymeric contributions and has a different solubility behaviour to cellulose because it is water soluble.<sup>109</sup> The details of the problems and benefits of analogues will be expanded upon in later chapters (2 and 3) when discussing the choice of model compounds for the studies herein.

Molecular interactions can be understood from studies using analogues of cellulose, or cellulose processed to eliminate macroscopic structures which complicate the solubility mechanism. However, these approaches may not be able to fully describe the cellulose dissolution mechanism as there are complicated multi-stage processes which are absent in analogues.

## 1.7 Thesis strategy and motivation

The presence of unsolved problems with cellulose solvents demonstrate that there is still a clear need for the development of new solvents (Section 1.2). This should be done in a guided manner as opposed to the trial and error (Section 1.5). To enable this, the application of statistical thermodynamics towards understanding cellulose solubility can be applied (Section 1.5.2). Hence, this thesis will attempt to adapt the theory outlined in Section 1.5.2 to understand both the microscopic molecular interactions and the macroscopic driving forces within cellulose dissolution.

The focus of this thesis will primarily be aqueous cellulose solvents. Aqueous solvents for cellulose are used in some of the larger industrial applications of cellulose such as the viscose process (Section 1.2) but also for important modern applications such as hydrogels. In addition, their multicomponent nature allows for independent variation of each component,<sup>120</sup> which is an extremely useful property for the study of mechanism and molecular interactions in a solution. Finally, water is a greener solvent, as opposed to organic solvents, because it does not require synthesis and has fewer hazards associated with it. However, water suffers from the need of hazardous chemicals to allow dissolution of cellulose (Section 1.2). Reducing the hazards of co-solutes in water would make aqueous solvents ideal targets as green solvents of cellulose. To achieve this goal, the function of currently successful aqueous solvents of cellulose must be understood. Investigation into cellulose solubility will be guided by attempts to circumvent the quantification issues present when acquiring data (Section 1.6). This will be done through experiments into cellulose and its analogues (Chapters 2 and 3). An additional study will be completed, considering the possibility of extending KB theory to be applied to the macroscopic structures present in polysaccharides aggregates, in this case starch granules (Chapter 4).

## CHAPTER 2: SOLUTION MOLECULAR INTERACTIONS FROM CELLOBIOSE AS AN ANALOGUE OF CELLULOSE

Cellulose is effectively insoluble in water, making it impossible to quantify its water solubility. In addition, cellulose solubility is poorly reproducible, due to the intricate intermediate steps such as swelling<sup>139,140</sup> and complexation<sup>141</sup>. The energetic barrier of these intermediate steps can be moderated by pre-treatment such as steam-explosion<sup>142</sup> and crystal transition<sup>143</sup>. Therefore, cellulose dissolution can exhibit strong dependency on the severity of the pre-treatment.<sup>45,142,144</sup> Consequently, literature data of cellulose solubility inherently contains inaccuracies which complicate the thermodynamic measurements (Chapter 3).<sup>145</sup> As discussed in Chapter 1 (1.5.2 and 1.6), the use of a cellulose analogue circumvents the problems arising from both water insolubility and intermediate steps.

The choice of analogue is a balancing act between loss of accuracy due to simplification and ease of study. Cellobiose, which is composed of two  $\beta$ -1,4 linked D-glucose units, has been used as an analogue for cellulose in this chapter. Cellobiose retains "cellulosic" characteristics: aqueous solubility of cellobiose is much lower (12%) than its isomeric disaccharide maltose ( $\alpha$ -1,4 linked two D-glucose units, 50%),<sup>146</sup> and dissolution of cellobiose in dimethylacetamide necessitates the addition of lithium chloride as cellulose does<sup>147</sup>. However, it should be noted that cellobiose mainly takes a cis conformation,<sup>148</sup> whereas cellulose takes a trans conformation.<sup>15</sup> Also, in contrast to cellulose, cellobiose demonstrates a non-negligible contribution from possible arrangements of its reducing end (which can exist in both  $\alpha$  and  $\beta$  anomers and open chain form<sup>15</sup>).

Nevertheless, thanks to the smaller molecular size compared with cellulose, the above-mentioned intermediate steps are rendered negligible, and thus the use of cellobiose assures the reproducibility of solubility measurement.<sup>109,149</sup> This is beneficial for the quantification of the interactions that the constituent disaccharide unit of cellulose has respectively with solvent and cosolvent molecules, neither of which have been quantified previously. From the understanding of constituent unit solvation contributions, we can build up to the understanding of cellulose solvation as a whole.

Furthermore, the true benefit that can be gained from cellobiose has not been highlighted in studies which have utilised it simply as an analogue. Cellobiose allows the comparison between solubility in pure water and a co-solute containing solution. A clear distinction between a solution containing no co-solute and a solution containing co-solute can give us a clear picture of the role of said co-solute in the molecular interactions that lead to the differences in solubility. This was made possible by the thermodynamic framework of transfer free energy from pure water to aqueous co-solute solutions (Section 1.5.2). Much of the previous work with cellobiose lacked this framework.

Thus, cellobiose may be limited as a model for cellulose itself but can be a good starting point as its solvation model. Hence, combining a rigorous statistical thermodynamic theory and cellobiose solubility data in the presence of chloride salts, whose cations progress in the Hofmeister series (KCl, NaCl, LiCl and ZnCl<sub>2</sub>), we can determine the effects of cations on the driving forces of cellobiose solubilisation.

## 2.1 Predominant hypotheses of cellulose interactions

The dissolution of cellulose requires additional components, namely co-solvents, as well as specific thermal conditions: aqueous 2 M alkali solution below 5°C,<sup>150,151</sup> aqueous 7 M lithium bromide solution above 120°C,<sup>152</sup> and 8% lithium chloride in di-methyl-acetamide solution below 4°C are the typical examples.<sup>153</sup> The origin of such a wide variety of optimal conditions, “heat or cold” and compositions “aqueous or non-aqueous”, has been an unanswered question, hindered by a lack of explicit explanation on how cellulose molecules dissolve into solvents on a molecular scale. The currently understood driving forces of cellulose’s resistance to dissolution have led to a number of hypotheses related to overcoming this resistance:

**Co-solvent binding:** It has historically been assumed that in most aqueous cellulose solvents, co-solvents play a dominant role in dissolution by interacting with hydroxyl (OH) groups of cellulose. This leads to the currently-prevailing view that co-solvent disruption of hydrogen bonding present in the cellulose crystal is crucial for dissolution of cellulose.<sup>97,154-156</sup>

**Cellulose charging up:** The OH group–cosolvent interactions are re-highlighted in recent studies as the “cellulose charging up” hypothesis. They claimed that cellulose–ion interaction can make cellulose into a “polyelectrolyte” which drives its dissolution.<sup>157,158</sup> The cellulose polyelectrolytes are in solution together with a number of small ions whose increase of the entropy of mixing is claimed to be the driving force of their cellulose solubility enhancement.<sup>159</sup>

**Amphiphilicity or “like dissolves like”:** The limitation of previous co-solvent binding hypotheses is that they do not explain the insolubility of cellulose as demonstrated in the following example: poly-vinyl alcohol (PVA), a highly water-soluble polymer, contains 3 OH groups per 6 carbons, an identical number to cellulose.<sup>101</sup> To rationalise this inconsistency, the hypothesis that insolubility is

attributed to the structure of cellulose, particularly its amphiphilic nature, was proposed.<sup>39,101,109,160,161</sup> Consequently, the “like dissolves like” principle has inspired the view that the solvent would need to be amphiphilic like cellulose. However, the discussion on such amphiphilic nature remains qualitative.<sup>162</sup>

Thus, different hypotheses co-exist for cellulose dissolution mechanisms, none of which can put numbers to each of the driving forces. Especially, to focus solely on cellulose-co-solvent interaction cannot give an accurate explanation of cellulose dissolution because it neglects another essential contributory factor, namely the cellulose–solvent interactions. It is not even clear which of the proposed hypotheses are dominant or minor, or whether some of the proposed driving forces are interrelated or equivalent to one another.

## 2.2 From solubility to the solvation mechanism

The major hindrance towards elucidating the mechanism of cellulose dissolution is the lack of a link between the proposed mechanisms and solubility on a quantitative basis. Such a hindrance towards elucidating cellulose dissolution can be overcome by employing a statistical thermodynamic theory that can explain solubility on a quantitative basis from the interactions between individual species.<sup>116,122</sup>

To this end, this chapter will begin to rationalise the dissolution mechanism of cellulose. Statistical thermodynamics can link the solubility data to the interactions between cellobiose and solvents and between the solvent species in a quantitative manner.<sup>116,121,163</sup> A quantitative evaluation will then be possible for the first time on the predominant hypotheses of cellulose dissolution mechanisms, summarised above. This information can help us to understand molecular interactions with cellulosic materials. When compared to larger solutes this quantitative information could also lead to a full understanding of cellulose solution interactions.

Experimental evidence suggests that anions and cations both contribute to cellulose dissolution in aqueous solution:

1. LiCl/water does not dissolve cellulose polymers<sup>82</sup> but LiBr/water mixture dissolves cellulose.<sup>152</sup>
2. To solubilise cellulose with LiCl, a complete removal of the solvent water is indispensable, i.e., the complete replacement of water by ethanol, acetone, or dimethylacetamide.<sup>147,164</sup>

Such a strong anion dependence suggests that both anions and cations are engaged in the interaction with cellulose molecules in a hard-to-separate manner.

Cellobiose solubility enhancement in the presence of Hofmeister cations with chloride has been reported as the function of salt concentration.<sup>165</sup> Here, this solubility data (Figure 2.1) has been complemented by the cellobiose partial molar volumes in the presence of the same salts,<sup>166,167</sup> as well as the activity coefficients of water and salts. As will be discussed in Section 2.3, the combination of solubility, volumetric and activity data are sufficient to draw a complete picture of interactions in cellobiose-water-salt solutions in a quantitative way.

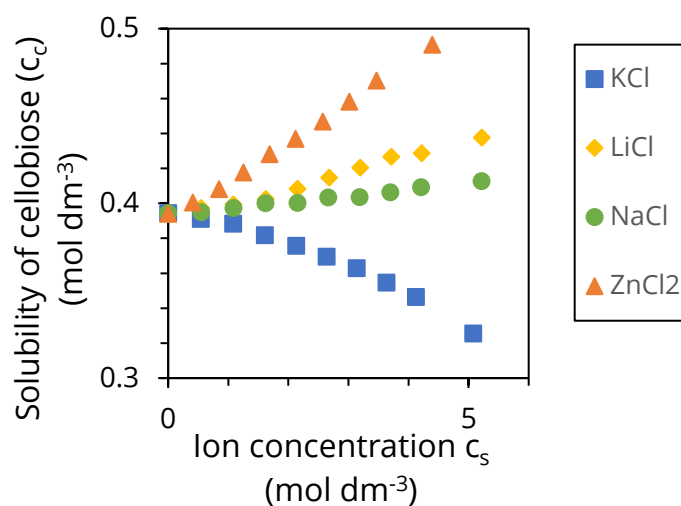


**Figure 2.1:** Solubility enhancement of cellobiose by Chloride salts, data from Liu et al.<sup>165</sup>



## 2.3. Quantifying interactions in solutions

In order to quantify how each of the interactions (cellobiose-salt, cellobiose-water, salt-salt, salt-water and water-water) contribute to the dissolution of cellobiose we will apply Kirkwood Buff (KB) theory. (Introduction, Section 1.5.2)

The interactions between a pair of species (say, between the species  $i$  and  $j$ ) can be quantified in terms of the KB integral defined as

$$G_{ij} = \int dr 4\pi r^2 [g_{ij}(r) - 1] \quad (2.1)$$

where  $g_{ij}(r)$  is the radial distribution function between the species  $i$  and  $j$ .

$G_{ij}$  is the net affinity between the species  $i$  and  $j$  (Introduction, Section 1.5.2).<sup>121</sup>

These pair affinities can be calculated from experimental data alone. Through this, the theory can quantify the dominant role in cellobiose solubility.

When applying this theory to the solutions introduced in Figure 2.1, the following convention has been used:  $c$ : cellobiose,  $w$ : water and  $s$ : salt ions. The theory itself is exact and without model assumptions, it will give a quantitative measure of cellobiose's interactions. One limitation of the theory, however, is that it is not possible to study the independent effects of each ion, due to the fact that the number of cations or anions, formed by the dissociation of salts, cannot be altered independently.<sup>168</sup> As a consequence of this, it is a standard practice to use the concentration of "indistinguishable ions" as opposed to salt concentration.<sup>120,169</sup> Therefore,  $c_s$  refers to the concentration of the salt's ions. This inability of changing anion and cation concentrations separately in solution poses difficulty from the experimental determination of separate KBIs for cations and anions, despite the seminal extension of the KB theory by Patey and coworkers.<sup>45,46</sup> Despite this difficulty, it is possible to study anion (or cation) effects by varying cation (or anion, respectively).

### 2.3.1 Expressing solubility in terms of KBIs

To quantify the relative contribution of anion and cation to the molecular interactions in these electrolyte solutions, cellobiose solubility ( $c_c$ ), when dependent on the ion concentration ( $c_s$ ), can be expressed in terms of KBIs.

According to the Kirkwood-Buff (KB) theory of solutions, the dependence of the pseudo-chemical potential (See Box 1.3, Section 1.5.2) of cellobiose,  $\mu_c^*$ , on salt concentration can be expressed as:<sup>170,171</sup>

$$-\frac{1}{RT} \left( \frac{\partial \Delta \mu_c^*}{\partial c_s} \right)_{T,P} = \frac{G_{cs} - G_{cw}}{1 + c_s(G_{ss} - G_{sw})} \quad (2.2)$$

$\left( \frac{\partial \Delta \mu_c^*}{\partial c_s} \right)_{T,P}$  can be determined from the experimental solubility data, starting from the free energy of transfer of a solute (cellobiose) molecule,  $\Delta \mu_{tr,c}^*$  which will from now on in this chapter be denoted by  $\Delta \mu_c^*$  for simplicity, from a pure water phase to an aqueous salt solution phase, defined as:

$$\Delta \mu_c^* = \mu_c^* - \mu_c^{*0} \quad (2.3)$$

where  $\mu_c^*$  and  $\mu_c^{*0}$  express the pseudo-chemical potentials of the solute c at a fixed position in aqueous salt solution and in pure water, respectively. Using the method established in Section 1.5.2, this  $\Delta \mu_c^*$  can be calculated directly from the cellobiose solubility in solution ( $c_c$ ) and pure water ( $c_c^0$ ) as:

$$\Delta \mu_c^* = -RT \ln \frac{c_c}{c_c^0} \quad (2.4)$$

Since, according to Eq. (2.3),  $\mu_c^* = \Delta \mu_c^* + \mu_c^{*0}$ , in which  $\mu_c^{*0}$  and  $c_c^0$  do not depend on the salt concentration, this independence of  $\mu_c^{*0}$  on salt concentration means that Eq. (2.2) can be rewritten to give Eq. (2.5):

$$\frac{1}{RT} \left( \frac{\partial \ln c_c}{\partial c_s} \right)_{T,P} = \frac{G_{CS} - G_{CW}}{1 + c_s(G_{SS} - G_{SW})} \quad (2.5)$$

where  $(G_{CS} - G_{CW})$ , the preferential affinity between cellobiose molecules and ions over cellobiose and water molecules, drives up the solubility.  $1 + c_s(G_{SS} - G_{SW})$ , the preferential self-association of ions, driven by ion-ion affinity ( $G_{SS}$ ) over affinity between ions and water or ion hydration ( $G_{SW}$ ) reduces the solubilisation.<sup>171</sup>  $R$  and  $T$  respectively denote the gas constant and the temperature. Eq. (2.5) thus quantifies the molecular driving forces for cellobiose dissolution in a manner that can be extracted from solubility data.

## 2.4 Quantifying affinities from experimental data

The calculation of KBIs and the above expressions from experimental data requires not only the dependence of cellulose solubility on salt ion concentration (Eq. (2.5)) but also the partial molar volume of cellobiose in aqueous salt solutions, density and activities of aqueous salt solutions, all of which can be expressed in terms of KBIs. This procedure is well-established with track record of successes in many applications.<sup>113,114,124,172-175</sup> In this section the basic relationships used in the analysis of experimental data are summarised.

In section 2.3.1 two contributions to solubilisation were identified. The first is the preferential salt-cellobiose affinity:<sup>170</sup>

$$\frac{1}{c_s} \left( \frac{\partial \Delta \mu_c^*}{\partial \mu_s} \right)_{T,P,c_c \rightarrow 0} = - (G_{cs} - G_{cw}) \quad (2.6)$$

And the second contribution is the salt self-association, given as:

$$\frac{c_s}{RT} \left( \frac{\partial \mu_s}{\partial c_s} \right)_{T,P,c_s \rightarrow 0} = \frac{1}{1 + c_s(G_{ss} - G_{sw})} \quad (2.7)$$

These parameters are isolated from equation 2.2 using the chain rule. Isolating the contributions to solubilisation in this way allows for a comparison between direct interactions with the solute (Eq. 2.6) and bulk-solution interactions (Eq. 2.7) that can describe intra-solution effects. In the following, we explain how these two contributions have been derived and evaluated from the experimental data available in the literature.

### 2.4.1 Calculation of Equation 2.6

$G_{cs} - G_{cw}$  is a measure of a solute's affinity with the "co-solvent" *relative* to that with a "solvent". This is known as preferential affinity as a positive value of  $G_{cs} - G_{cw}$  denotes that cellobiose-salt interactions are more attractive than cellobiose water interactions, meaning salt is *preferentially* interacting with cellobiose. To

obtain this from available data, such as the dependence of  $\Delta\mu_u^*$  on water activity,<sup>176</sup> Eq. (2.6) should be rewritten using the following thermodynamic relationship:

$$\frac{1}{c_s} \left( \frac{\partial \Delta\mu_c^*}{\partial \mu_s} \right)_{T,P,c_c \rightarrow 0} = - \frac{1}{c_w} \left( \frac{\partial \Delta\mu_c^*}{\partial \mu_w} \right)_{T,P,c_c \rightarrow 0} \quad (2.8)$$

Using the well-defined relationship between chemical potential and activity  $\mu_i - \mu_i^\theta = RT \ln a_i$ , given on pp 24-27 in Robinson and Stokes,<sup>177</sup> combined with the fact that  $d\mu_i = RT d \ln a_i$  (because **standard** chemical potential ( $\mu_i^\theta$ ) depends on temperature and pressure and therefore  $d\mu_i^\theta = 0$  in this context) to give the form:<sup>171</sup>

$$- \frac{1}{c_w} \left( \frac{\partial \Delta\mu_c^*}{\partial (-RT \ln a_w)} \right)_{T,P,c_c \rightarrow 0} = (G_{cs} - G_{cw}) \quad (2.9)$$

In order to evaluate the differential on the L.H.S. of Eq. (2.9), the  $RT \ln a_w$  dependence of  $\Delta\mu_c^*$  was fitted using a polynomial function. Figure 2.2 shows the polynomial fitting used to enable differentiation of  $\Delta\mu_c^*$  with respect to  $RT \ln a_w$ , where  $\Delta\mu_c^*$  was calculated using Equation 2.4 ( $\Delta\mu_c^* = -RT \ln \frac{c_c}{c_c^0}$ ),  $c_c^0$  was the cellobiose solubility in water ( $0.394 \text{ mol dm}^{-3}$ )<sup>165,178</sup> and  $c_c$  was the solubility given in Figure 2.1 for cellobiose in each salt.<sup>165</sup>  $RT \ln a_w$ , was calculated directly from osmotic coefficients ( $\phi$ ) using the following well known relationship:<sup>177</sup>

$$\ln a_w = \phi \ln x_w \quad (2.10)$$

And values of  $\phi$  were obtained from critical data tables and the literature.<sup>179-182</sup>

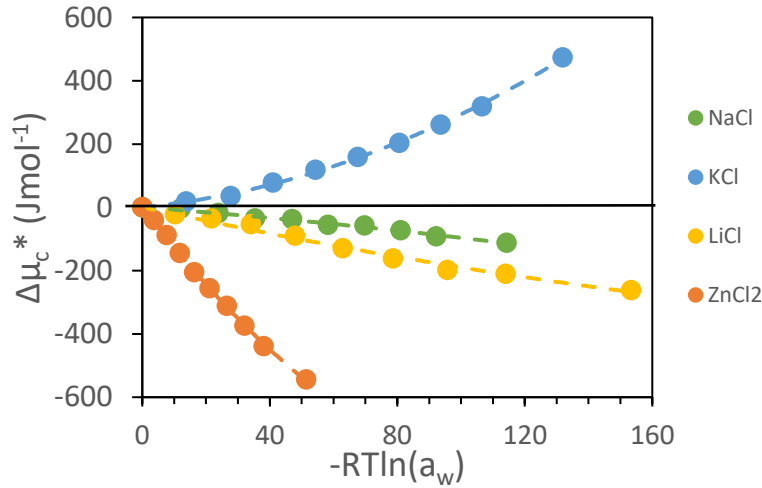


**Figure 2.2:** Polynomial fitting of  $\Delta\mu_c^*$  plotted against  $-RT \ln a_w$  to provide a function which can be differentiated as per Eq. 2.9 to calculate preferential interaction. The fitting equation used was:  $\Delta\mu_c^* = a(-RT \ln a_w)^2 + b(-RT \ln a_w)$ .

Once the differential  $\frac{\partial \Delta\mu_c^*}{\partial (-RT \ln a_w)}$  was calculated using Fig. 2.2, evaluation of Eq. 2.9 was straightforward.

## 2.4.2 Calculation of Equation 2.7

Using the relationship between activity and chemical potential denoted in section 2.4.1, combined with the relationship  $a_s = m_s \gamma_s^m$ , equation 2.7 can be rewritten as:

$$\frac{1}{1+c_s(G_{SS}-G_{SW})} = c_s \left( \frac{\partial \ln m_s}{\partial c_s} + \frac{\partial \ln \gamma_s^m}{\partial m_s} \frac{\partial m_s}{\partial c_s} \right) \quad (2.11)$$

The calculation of the  $G_{SS} - G_{SW}$  term *via* Eq. (2.11) requires the evaluation of

$\frac{\partial \ln \gamma_s^m}{\partial m_s}$ . To do so, the following fitting equation was adopted for electrolyte

osmotic coefficients based on a classical model by Stokes and Robinson:<sup>177</sup>

$$\phi - 1 = -\frac{\alpha\sqrt{m}}{3} \left( \frac{3}{(\beta\sqrt{m})^3} \left[ 1 + \beta\sqrt{m} - 2 \ln(1 + \beta\sqrt{m}) - \frac{1}{1+\beta\sqrt{m}} \right] \right) + cm + dm^2 \quad (2.12)$$

Using parameters determined by fitting Eq. (2.12) to  $\phi_s$  vs  $m_s$  data,<sup>179-182</sup>  $\frac{\partial \ln \gamma_s^m}{\partial m_s}$

was calculated as follows:

$$\frac{\partial \ln \gamma_s^m}{\partial m_s} = -\frac{\alpha}{2\sqrt{m}} \left( \frac{1}{(1+\beta\sqrt{m})^2} \right) + 2c + 3dm \quad (2.13)$$

It should be noted here that, although the functional form used in equation 2.12

was rooted in electrolyte solution theory, its purpose was simply to provide an

accurate fit to the osmotic coefficient data which would enable calculation of

$\frac{\partial \ln \gamma_s^m}{\partial m_s}$ . (Hence, the polynomial addition does not lead to any problems for the

interpretation of data at a later stage.)

## 2.5 Results and Discussion

All of the proposed classical hypotheses for the mechanism of cellulose dissolution were qualitative. To overcome such a limitation, we demonstrate in the following section that each of the driving forces for solubilisation can be quantified, through statistical thermodynamics, using the experimental data identified previously. The findings of the Kirkwood Buff theory can then be compared with those of the classical hypotheses to evaluate their veracity.

### 2.5.1 Driving forces of solubilisation: Preferential cellobiose-salt interaction versus preferential self-aggregation of salts

The preferential cellobiose salt interaction term ( $G_{cs} - G_{cw}$ ) and the preferential self-aggregation term ( $\frac{1}{1+c_s(G_{ss}-G_{sw})}$ ) were calculated as described in section 2.4 and are presented in the following figures.

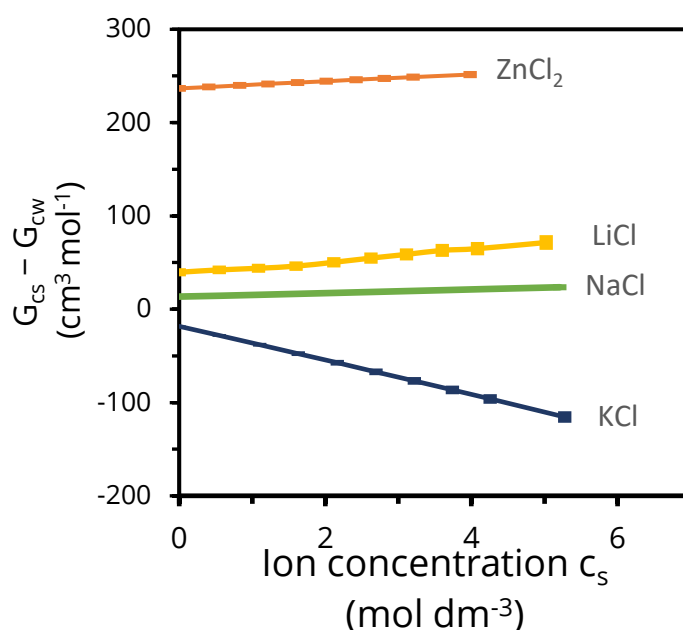


**Figure 2.3:** Preferential cellobiose-ion interactions characterised quantitatively via the Kirkwood-Buff integrals ( $G_{cs} - G_{cw}$ ) for NaCl, KCl, LiCl and ZnCl<sub>2</sub> calculated from the solubility data.<sup>165</sup> Error bars shown as blocks in corresponding colours.



The trends described in Figure 2.3 are subject to some error due to fitting, however, this error is reasonable to be taken as negligible.

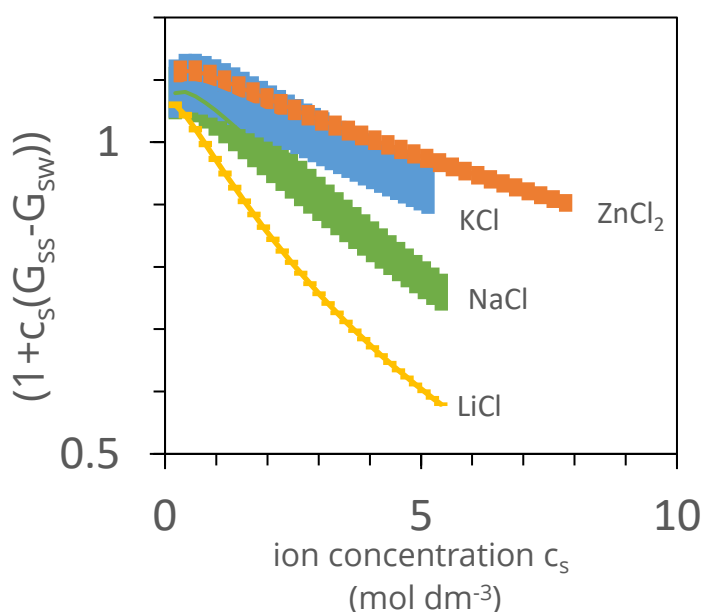


**Figure 2.4:** Solubilisation inefficiency due to the preferential self-aggregation of salt ions in bulk aqueous solution, which has been quantified by the KBIs via Equation 2.7, plotted for KCl, NaCl, LiCl and ZnCl<sub>2</sub>. Error bars shown as blocks in corresponding colours.

The trends in Figure 2.4 are subject to some error due to fitting. These errors are more significant; however, they do not alter the overall trend with respect to salt choice.

Through Figures 2.3 and 2.4, statistical thermodynamics reveals the following two major driving forces for the increase of cellobiose solubility in the presence of salts. Firstly, the preferential cellobiose-ion affinity over affinity between cellobiose and water molecules, which has historically been a dominant driving force in solubility.<sup>170</sup> The trend of  $(G_{cs} - G_{cw})$  with respect to salt choice seen in Figure 2.3 correlates with the trend in solubility enhancement (ZnCl<sub>2</sub> > LiCl > NaCl > KCl). This suggests that  $(G_{cs} - G_{cw})$  is connected to the driving force of solubility enhancement.

Secondly, preferential self-association of salts in aqueous solution, historically the minor contribution, which reduces per-ion solubilisation efficiency (Figure 2.4). From Figure 2.4 it can be seen that salt self-accumulation does not follow the same trend as cellobiose solubility enhancement (Figure 2.1) which shows that salt self-accumulation is not directly correlated with the solubilisation process to the same extent as preferential salt-cellobiose accumulation, suggesting it may be a secondary effect.

In the following section, the individual contributions to these terms are discussed in more detail to link the novel quantitative insights from the KB theory to the classical hypotheses. Quantitative comparison between the two parameters in this form is not possible as the central solute being studied differs. With modifications based on excluded volume they are comparable. However, that is outside the scope of this work and plenty of useful information can be gleaned from observing the trends in both terms.

## 2.5.2 Salt accumulation around cellulose as a driving force

The salts that enhance cellobiose aqueous solubility (NaCl, LiCl and ZnCl<sub>2</sub>) have an energetic benefit to accumulation around cellobiose as indicated by their positive preferential affinity/ interaction with cellobiose over water (Figure 2.3). Increase of cellobiose solubility is seen when the affinity of salts with cellobiose exceed that of water. Preferential salt accumulation around cellobiose should thus be considered an important contribution to cellobiose solubilisation. It may be noted, however, that the KBIs corresponding to cellobiose-salt interaction ( $G_{cs}$ ) are negative (Figure 2.5, below). This counterintuitive value arises due to the excluded volume of cellobiose contributing in a dominant manner to make the individual  $G_{cs}$  net negative.<sup>183</sup>

Salt accumulation around cellulose as a driving force provides support for the cellulose charging up hypothesis (Section 2.1) in which ion binding is an

important factor. Unlike this hypothesis, however, KB theory does not involve any need for invoking the entropy of mixing, which, despite its historical importance, is problematic as a thermodynamic concept,<sup>184</sup> because (1) it is not a reversible and hence a thermodynamic process, and (2) solubility (governed by the free energy) is the result of compensating, large entropic and enthalpic contributions of different signs. The result presented here, instead, is based on a direct relationship between salt accumulation and solvation free energy – provided by the KB theory.

## 2.6 Cellobiose dehydration – water structure hypothesis

The solution phase interaction component of the amphiphilicity hypothesis (Section 2.1) presupposes

the enhanced water structure around the hydrophobic group as a basis for insolubility.<sup>185</sup> Insolubility of cellulose has also been attributed specifically to the hydrophobic section of cellulose.<sup>39,162,186</sup> Within this framework, the effect of cosolvents on solubility, and especially Hofmeister ions, have been explained via water structure. Solubilisation according to the classical hydrophobic clathrate view in solubility theory,<sup>187,188</sup> which corresponds to the solution phase interaction portion of the aforementioned hypothesis, can be summarised as:

- The hydrophobic effect is due to the enhancement of the water structure around the solute (“clathrate” structure) which cannot hydrogen bond with water, which leads to entropic penalty;
- Species called "chaotropes" break the “water structure”, or the hydrogen bond network of water molecules;
- Chaotropes weaken the clathrate structure of water, thereby weakening the hydrophobic effect

This classical hypothesis has been the source of controversy over decades.<sup>185,189,190</sup> Indeed, the presumed hydrogen bond enhancement by ions has been challenged spectroscopically,<sup>191</sup> and the dynamic nature of the “clathrate” or “iceberg” has emerged since then.<sup>192,193</sup> The consequence of this hypothesis is that, since the clathrate structure involves more hydrogen bonds, the water molecules are kept further apart on average and consequently the density is lower. Hence “water structure breaking” increases hydration, i.e., increase of the density of water in the hydration shell. This hypothesis can be examined by breaking down the terms given in Eq. 2.6 into their individual contributions.

The individual KB integrals contributing to the preferential affinity ( $G_{cs} - G_{cw}$ ) can be determined independently, by complementing it with the partial molar volume  $V_c$  of cellobiose in the presence of the salts, which can be expressed as

$$G_{cw} = -V_c - c_s V_s (G_{cs} - G_{cw}) \quad (2.10)$$

where  $V_s$  is the partial molar volume of the salt ion.<sup>194</sup>  $G_{cs}$  was then calculated from the values of ( $G_{cs} - G_{cw}$ ) and  $G_{cw}$  combined.

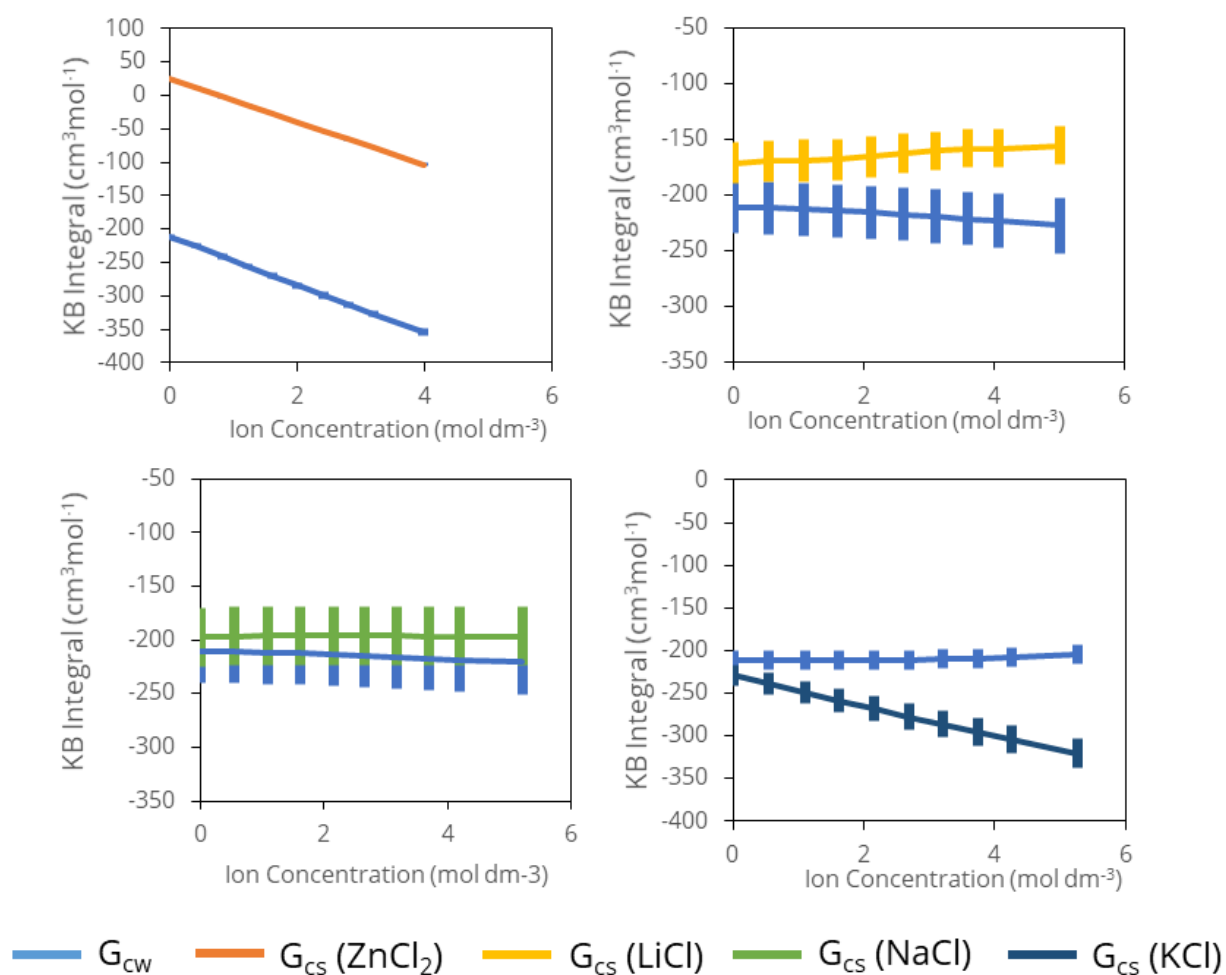


**Figure 2.5:** Individual Kirkwood-Buff integrals that lead to preferential association of cellobiose in solutions of ZnCl<sub>2</sub>, LiCl, NaCl and KCl. Error bars shown as blocks in corresponding colours.

The errors in Figure 2.5 do not affect the dominance of either  $G_{cw}$  or  $G_{cs}$ , however, for NaCl and LiCl the concentration dependence of individual KBIs becomes more difficult to clearly interpret.

In stark contrast to this classical hypothesis, Figure 2.5 shows that  $G_{cw}$  decreases as the concentration of salts that enhance cellobiose solubilisation (NaCl, ZnCl<sub>2</sub> and LiCl) increase, which means that the chaotropic salts dehydrate cellobiose instead of enhancing its hydration, which is in contradiction to the water structure hypothesis. Thus, this analysis suggests strongly that the water structure hypothesis cannot explain cellobiose solubilisation. Figure 2.5 also shows us that the relationship between the KBIs should not be neglected. As the salt ion concentration of ZnCl<sub>2</sub> increases, salt accumulation ( $G_{cs}$ ) around cellobiose decreases, which leads to a weaker contribution to solubilisation (ZnCl<sub>2</sub> - Figure 2.5). Despite this, decreasing cellobiose hydration (increasing cellobiose dehydration) indicated by decreasing  $G_{cw}$  shows that salts still interact preferentially with cellobiose, thereby increasing its solubility.

Furthermore, though KCl exhibits weak salt accumulation, this is not compensated for by the corresponding dehydration and accumulation continues to weaken as salt ion concentration increases (Figure 2.5), therefore leading to a solubility decrease, thus the salt's effect on solubility is again caused by the interplay between the two affinities.

Note here that the classical water structure hypothesis focuses exclusively on the *increase* of solute hydration with increasing salt concentration, i.e., the *increase* of  $G_{cw}$ . The rigorous statistical thermodynamic theory not only shows that *decrease* in cellobiose hydration takes place but also the crucial role of  $G_{cs} - G_{cw}$ , instead of  $G_{cw}$  on its own, that is the driving force for solubilisation.

## 2.7 Cellobiose solubilisation and the Hofmeister effect

The effect of salts on solubilisation has long been related to the Hofmeister effect, in which the ionic charge density is considered to play a crucial role on solubilisation.<sup>195</sup> According to the classical hypothesis, ions with low charge density break the “water structure” thereby weakening the hydrophobic effect, while those with high charge density enhance it and fortify the hydrophobic effect.<sup>196</sup> The water structure hypothesis has been developed to rationalise the effect of ions chiefly on the hydrophobic effect. Nevertheless, here, in the context of cellobiose solubilisation, the order of solubility enhancement ability, with respect to changing the cation, coincides with an increase in ion charge density ( $\text{Zn}^{2+} > \text{Li}^+ > \text{Na}^+ > \text{K}^+$ ). So, what is the mechanism upon which the charge density increases solubilisation?

According to the water structure hypothesis, solubilisation is caused by the breaking of water structure around the hydrophobic group. Cellobiose hydration behaviour exhibits the opposite trend to this hypothesis (Section 2.6), hence the role of charge density should be reconsidered. Figures 2.3 and 2.5 highlight, instead, the importance of increasing *preferential* cellobiose-salt affinity over simply the cellobiose-salt affinity (Meaning that the comparison between salt and water interactions leads to the driving forces as opposed to one individual interaction). This is consistent with the previous identification of preferential interaction as the driving force of the Hofmeister effect.<sup>197</sup>

## 2.8 Summary and cellobiose as an analogue

### 2.8.1 molecular scale solubility explanation

Elucidation of the mechanism of cellulose dissolution has been hampered by the lack of a theoretical framework that can explain solubility on a molecular scale, as well as lack of standard model systems that enable the direct experimental measurements of cellulose-solvent interactions in a reproducible manner. To overcome these hindrances, we identified and quantified the driving forces of solubilisation using cellobiose as a model system whose solubility in the presence of Hofmeister salts have been reported recently in the literature. The rigorous statistical thermodynamic framework, which has a track record of clarifying the microscopic basis of solvation in wide-ranging fields, has been applied to reveal the solubilisation mechanism at odds with many of the classical hypotheses.

In cellobiose, the driving force for solubilisation is the preferential accumulation of salt ions around the solute molecules, which is stronger than cellobiose hydration. Even though the salt accumulation weakens as the concentration of salts in solution, the increasing cellobiose *dehydration* keeps the cellobiose-salt interaction still preferential. The increasing dehydration is at odds with the classical “water structure” hypothesis for chaotropic solubilisation which predicts the increase in cellobiose *hydration*.

Hence the classical hypothesis regarding the role of ionic charge density on water structure breaking and making should be revised: the larger charge density leads to preferential interaction with cellobiose. That the concentration of ions around cellobiose is the key towards solubilisation is consistent with the



classical hypothesis that emphasised the importance of cellulose-ion binding as the driving force. (Section 2.1) However, in contrast to the classical hypothesis that invoked the favourable entropy of mixing between cellulose polyelectrolyte and small charged ions in solution as the driving force, the theory used here links the ion accumulation and solubilisation directly; the approach based on entropy of mixing (or more accurately “entropy of assimilation”)<sup>184</sup> suffers from entropy-enthalpy compensation that prevents us from directly linking solubility with solution structure. Self-association of salts in bulk solution has been identified also as a minor contribution that reduces the efficiency of solubilisation.

## 2.8.2 Cellobiose as a cellulose analogue

This chapter’s identification of the roles of cellulose-salt and cellulose-water interactions on solubilisation provides a basis for applying these insights to cellulose in a quantitative manner. To do so, the extent to which cellobiose is a good representation of cellulose must be established.

In shorter chain oligo-saccharides that may act as analogues, such as cellobiose, water solubility increases with increasing temperature.<sup>137,165,198</sup> Qualitatively, adding co-solutes that promote cellulose solubility also improve cellobiose’s solubility (Section 2.1). However, their temperature dependence is sometimes different as cellobiose solubility in alkali solutions increases with temperature while cellulose solubility increases at lower temperatures.<sup>137,199</sup>

Despite this, cellobiose is likely a reasonable model examining the interactions between salts and cellulose-type (cellulosic) molecules in solution if the difference in excluded volume (i.e., the size of the molecules in solution) is taken into account.<sup>200,201</sup>

To extend the insights from this chapter to cellulose, an investigation into the group additivity of solvation is required that applies cellulose analogues of longer chain lengths. It may be that study of anomalous temperature dependence requires water insolubility of the solute, as the shorter chain oligosaccharides are able to dissolve in water up to 10 DP.<sup>59</sup> Chapter 1 identified that there are problems with cellulose solubility, the application of KB theory relies on accurate measures of solubility. Hence, investigating the extent to which solubility problems occur in cellulose oligomers (or the overall effect of DP on these problems) is crucial to enable the application of KB theory to cellulose. A sample which suffers to a lesser extent from solubility quantification problems, yet still demonstrates enhanced solubility in low temperature alkaline solutions would be ideal.

# CHAPTER 3: DEVELOPMENT OF CELLULOSE SOLUBILITY METHODS FOR STATISTICAL THERMODYNAMIC DATA ACQUISITION

Quantifying cellulose solubility is crucial for understanding its dissolution mechanism as well as its rational exploitation, yet the reported data are often unsuitable for use in statistical thermodynamic analyses. These analyses are indispensable for the elucidation of molecular interaction information about the solution state of dissolved cellulose (Chapter 1 and 2). Here, the causes for inaccuracies and uncertainties which prevent the use of cellulose solubility measurements are identified, through systematic solubility measurement of a series of amorphous cellulose samples with varied degree of polymerisation (DP) in LiOH (aq) solutions.

## 3.1 Introduction

The last decade has seen a resurgence of study into the mechanism behind cellulose (in)solubility in water, with extensive discussions on its driving forces and, at times, the molecular interactions that lead to them (Section 2.1).<sup>101,109,157</sup> However, to make the discussion more quantitative, a reliably quantitative solubility measurement is essential (Section 1.6),<sup>202-204</sup> because, through these measurements, molecular interactions in solution can be quantified (Section 1.5.2).<sup>3,116,121,176</sup>

Although cellulose solubility has been studied for over a century, yet the solubility data available in the literature may not be applicable to statistical thermodynamics due to the following problems:

- (1) Cellulose samples are polymeric and may have kinetic limitations to their quantification.

(2) The diverse nature and non-uniformity of cellulose samples.

(3) Errors and discrepancies dependent on choice of method.

**Incomplete dissolution (1):** For small and simpler solutes, when solubility saturates exactly the maximum amount of solute has been dissolved in the solution at equilibrium. This is referred to as “thermodynamic solubility” (or, at times, “equilibrium solubility”).<sup>205</sup> For most cases with small molecules, thermodynamic solubility is reached when a solute is dissolved up to saturation. However, most of the less harsh (and more environmentally friendly) cellulose solvents are poor solvents, and thus one needs to perform certain pre-treatments (ball-milling, steam explosion, etc.) to enhance their dissolving ability (Section 1.2).<sup>106,206,207</sup> These pre-treatments reduce the influence of the presence of other components and intermediate steps in the dissolution mechanism which can prevent solubility data from being taken under thermodynamic equilibrium condition.<sup>208</sup> Values of cellulose solubility taken under a non-equilibrium condition could lead to misleading results and interpretations through statistical thermodynamics. However, complete removal of the factors that lead to recalcitrance do not provide an adequate representation of cellulose (Section 2.8).

**Non-uniformity of samples (2):** Solubility is affected by significant variations in physical and chemical properties between cellulose samples, such as crystallinity<sup>41-43</sup>, crystal size, crystal allomorph<sup>41,45</sup>, molecular weight (or degree of polymerisation, DP)<sup>46,47</sup>, macroscopic structure<sup>209-211</sup>, and residual impurities such as lignin or hemicelluloses. (Box 1.1) Separating the contributions to solubility/insolubility from these variables are difficult as they are interconnected<sup>45</sup>. For example, crystallinity’s contribution to the dissolution mechanism becomes more influential at high values of DP<sup>45,46</sup>. Additionally, pre-processing methods (Box 1.2) often reduce DP, crystallinity, and macroscopic structures simultaneously<sup>106,142,208,212</sup>. Consequently, it can be difficult to

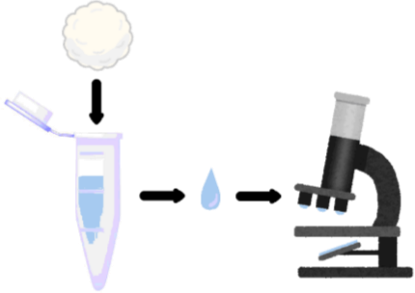
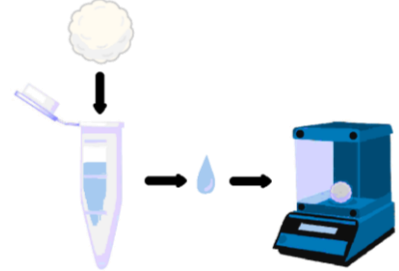
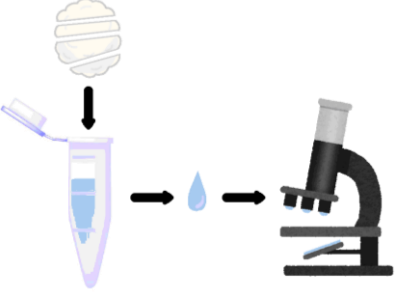
determine causal links between one variable and improved dissolution. This means that interpretation of and comparison between data from the literature can be difficult.

**Non-standardised methodology (3):** The methods used for solubility measurements are not standardised, as summarised in Table 3.1. Each method has different potential inaccuracies which affect its solubility measurement. As a result, one cannot compare the data of solubility measurement between the different methods. Many of these solubility measurements have been performed with commercial purpose; that is a solubility measurement performed in order to know if the solvent can produce a cellulose solution highly-concentrated enough for fiber spinning.<sup>53,213,214</sup> Quantification is not the aim in such measurements. This indicates that choice of data from the literature is important when considering which can be used for statistical thermodynamic analysis.

### 3.1.1 Quantification methods

Utilising cellulose solubility measurements that have been made using these methods can be problematic if the method's aim is not to quantify the concentration of molecules in solution.. The commonly used methods which will be examined in this chapter are listed in Table 3.1 and discussed below along with example of studies which use them.

**Table 3.1:** Schematic depictions of relevant quantification methods in cellulose solubility measurement, separated by method of addition and of measurement.

Solute addition	Solute measure	Description	Illustration
Single Aliquot	Visual/ Optical	A known mass of cellulose is added to a solvent. It is visually confirmed to be dissolved or undissolved.	
Single Aliquot	Solute Recovery	A known mass of cellulose is added to a solvent. The supernatant is dried and weighed to determine the proportion that dissolved.	
Incremental	Visual/ Optical	Cellulose is incrementally added to a solvent. The saturation point is visually confirmed by the appearance of aggregates.	

**Single aliquot addition**

Single aliquot & visual/optical (SA/VO) solubility tests are often performed as an indicator of the processing capability of cellulose, or for analytical tests, on a set cellulose weight percent<sup>43,144,199,215</sup>. As a consequence, they are predominantly qualitative in nature (i.e, they observe if cellulose is dissolved or not and do not quantify its concentration), this will not be examined in this chapter.<sup>38,94,152,216-218</sup> Methods using single aliquots of cellulose & solute recovery (SA/SR) are able to quantify solubility<sup>82,103,219,220</sup>. However, this method sometimes measures solubility as the fraction of the aliquot which can be dissolved, as opposed to the total concentration<sup>45</sup>. Consequently, some inaccuracy can be introduced into measurements of this type. The difficulty of completely dissolving a single added aliquot of cellulose is well known.

### **Incremental addition**

More recently, the difficulty of dissolving a single aliquot of cellulose has been circumvented by the addition of repeated small aliquots of cellulose to reach a point of saturation denoted by appearance of precipitates<sup>93</sup> detected by naked eye, microscope or by turbidity (the latter being most effective<sup>221</sup>). These incremental & visual/optical (Inc/VO) methods (See Table 3.1) allow the measurement of solubility to be quantitative<sup>93,222-224</sup>. However, it is not clear if this sample addition method suffers from the same problems as seen in single aliquot addition. Consequently, it is unclear as to whether this method of solubility measurement introduces inaccuracies. This will be clarified in this chapter.

Point (3) demonstrates that the quantitative accuracy of some methods to measure cellulose solubility could be low. This is especially prominent in unmodified cellulose. Points (1) and (2) demonstrate that the majority of cellulose solubility data cannot be used for statistical thermodynamic analyses. This severely limits the ability of theoretical approaches to extract meaningful

information from data and consequently hampers attempts to clarify the driving forces of cellulose solubility from microscopic and mechanistic standpoints. Correctly quantified solubility measurements will pave the way towards understanding molecular interactions that lead to dissolution of cellulose. If the intent is to produce measurements of cellulose solubility which can be used for theoretical studies, samples must be standardised and an analogue which avoids the problems discussed above must be established.

### 3.1.2 Choice of samples and solvent

As mentioned in chapter 1, the solubility of cellulose is strongly influenced by the parameters inherent to cellulose samples such as crystallinity, crystal allomorph, molecular weight (or degree of polymerisation, DP), and microstructure. This chapter aims to focus solely on the effect of DP as a single variable, while the influence of other parameters are significantly reduced. For this, amorphous regenerated cellulose (cellulose II) is an ideal sample as it has low crystallinity and can be easily produced.

To prepare amorphous regenerated cellulose, two solvent systems are well known: lithium chloride (LiCl)/dimethylacetamide (DMAc)<sup>225,226</sup> and concentrated phosphoric acid (H<sub>3</sub>PO<sub>4</sub>) solutions.<sup>227</sup> The former, LiCl/DMAc system, is known to give amorphous cellulose upon coagulation, while maintaining the DP.<sup>147,225,228-<sup>230</sup></sup> On the other hand, H<sub>3</sub>PO<sub>4</sub> is known to suffer from a drastic decrease in the DP through acid hydrolysis,<sup>231</sup> leading to oligomeric cellulose.<sup>58</sup> By utilising these two contrasting solvent systems, 4 samples were prepared: amorphous Avicel, CC31, and filter paper pulp (FP) regenerated from LiCl/DMAc system and amorphous hydrolysed Avicel regenerated from H<sub>3</sub>PO<sub>4</sub> system. To identify the DP ranges covered by these samples, size exclusion chromatography with multi-angle laser light scattering (SEC-MALLS) was employed (the method used is described in section 3.2.3). As can be seen from the DP distribution shown in



Figure 3.1, these four samples covered a wide range of DP from about 10 to 3000. In addition, through these dissolution-coagulation processes, the effect of microstructure inherent to the starting cellulose samples such as remaining fibrous or plant cell wall structure, was eliminated. Hence, it is unlikely that there are multiple stages in this dissolution process and these experiments can focus on developing a sample and method which can generate data that be used for statistical thermodynamic analysis.

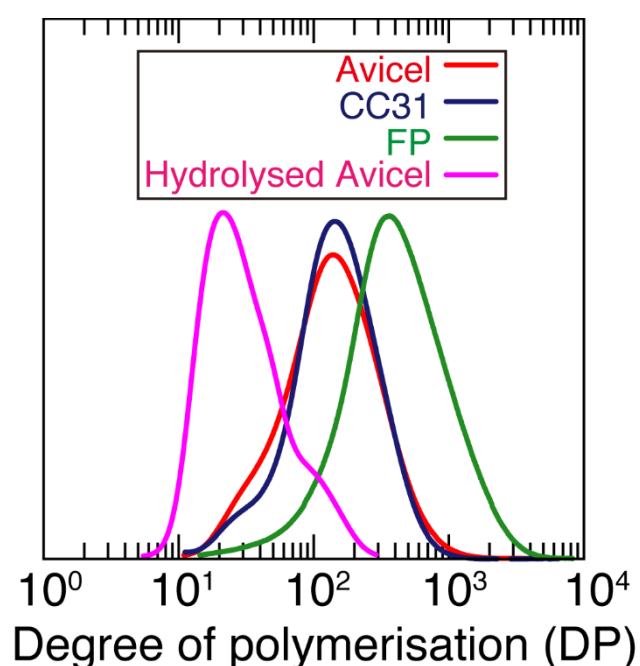


**Figure 3.1:** DP distribution of amorphous Avicel, CC31, and filter paper pulp (FP) regenerated from LiCl/DMAc system and amorphous hydrolysed Avicel regenerated from H<sub>3</sub>PO<sub>4</sub> system.

As a target cellulose solvent system for solubility tests, aqueous lithium hydroxide (LiOH) solution was selected. The reasons behind this choice are as follows: 1) aqueous LiOH shows poorer solubility without additives (such as urea) despite its potential environmental-friendliness, and thus awaits further improvement in solubility, 2) this poor solubilisation ability has a maximum

within easy-to-study ranges of solute concentration. Hence, viscosity does not get too high in these solutions making it easier to separate dissolved sample from undissolved. 3) its anomalous temperature dependence is still not completely understood and therefore it is a system in which more experiments are needed, and finally 4) the decrease in DP during dissolution is significantly reduced in large DP molecules compared to more successful aqueous solvent systems containing transition metal ions, such as "Cuan" and "Cadoxen".<sup>232,233</sup> By contrasting the solubility behaviour of amorphous cellulose with various DPs, this chapter aims to discuss how DP affects the deviation from complete dissolution of the sample. Using this information, it should be possible to design an analogue and a method which can be used to study interactions in cellulose solutions (post-dissolution) *via* solubility measurements that can be used with statistical thermodynamics.

## 3.2 Experimental

### 3.2.1 Materials

Purified water was used throughout this study (Milli-Q Advantage A10, Merck, Germany). The cellulose samples used were: Avicel PH-101 (Sigma-Aldrich), CC31 cotton cellulose (Whatman) and ashless filter paper (FP) pulp (hydrolysed cotton for ashless grade) (Advantec MFS, Japan). Phosphoric acid 85% (Fluorochem), lithium hydroxide monohydrate (Alfa Aesar), sodium borohydride (Aldrich), N-N-dimethyl-acetamide (Wako Chemicals, Tokyo) and lithium chloride (Wako Chemicals, Tokyo) were all of reagent grade and used without further purification.

### 3.2.2 Sample preparation

#### **Preparation of amorphous cellulose through phosphoric acid hydrolysis**

The phosphoric acid hydrolysis of cellulose (to produce the “hydrolysed Avicel” sample) was carried out by adopting a conventional protocol<sup>58</sup>. First, a 2 L vessel was charged with 31.57 g of Avicel, 1 kg of 85% phosphoric acid ( $\text{H}_3\text{PO}_4$ ) and 62.5 g of  $\text{H}_2\text{O}$ . The large-scale aggregates of cellulose were broken up manually and the vessel was then stirred with a magnetic stirrer bar. After 24 h of stirring, the vessel was inverted for a further 24 h. After, the vessel was restored to an upright position. Stirring continued for 5 additional days before the stirrer bar was removed. The vessel was then left in storage at room temperature for 22 additional days. The total hydrolysis time was 29 days. The obtained hydrolysed cellulose was recovered with a water/acetone solution (75/25 volume ratio). The recovered solid was washed with  $\text{H}_2\text{O}$  repeatedly until neutral pH was achieved.

### **End group reduction**

To prevent beta peeling in the alkaline environment, the reducing end group of hydrolysed Avicel was converted to an alcohol using the following method <sup>234</sup>. The hydrolysed Avicel was dissolved in 2.5 molar aqueous LiOH and, using excess NaBH<sub>4</sub>, the end group was reduced. The reaction mixture was stirred for 2 h at room temperature to evolve the majority of the gas before the flask was sealed to be stored at 4.5 °C for 16 h. The resultant sample was analysed by SEC-MALLS to determine its DP.

### **Preparation of amorphous cellulose samples through dissolution and coagulation**

To produce amorphous cellulose, the Avicel, CC31 and FP cellulose samples were dissolved in 8 wt% LiCl / 92 wt% DMAc as reported previously <sup>235</sup>, and coagulated with water under agitation with a homogeniser (ULTRA-TURRAX, IKA, Germany). The cellulose solutions were also subjected to the analysis by SEC-MALLS, providing degree of polymerisation (DP) details.

## **3.2.3 Solubility test protocols**

Solubility tests based on the methods listed in Table 3.1 were carried out with an aim to compare these methods and quantify to what extent each method is able to produce data for use in statistical thermodynamic analyses. The protocols used are summarised below.

### **Solubility determination using single aliquot addition with solute recovery**

Firstly, a known mass of cellulose was weighed into a 2 mL tube into which 1 mL of aqueous LiOH ( $1.993 \pm 0.013$  mol dm<sup>-3</sup>) was added. The solution was agitated by Eppendorf Thermomixer at 10 °C and 1200-1400 RPM for 24 h. After agitation, the dissolved fraction of cellulose was separated from the undissolved fraction by centrifugation at 10 °C and 16000-18000 g for 20 minutes.

Subsequently an aliquot of the supernatant was extracted by micro-pipette and weighed. The dissolved cellulose within the supernatant was then precipitated by the addition of ethanol. The precipitate and undissolved fraction were washed multiple times separately. For washing, ethanol and subsequently water/ethanol solutions (75/25, 50/50, 25/75 and 0/100 volume ratios) were used in consecutive order until a neutral pH was reached. Finally, samples were freeze dried at  $-87\text{ }^{\circ}\text{C}$  to recover dissolved and undissolved fractions as solids. These solids were weighed to quantify solubility.

### **Solubility determination using incremental addition with solute recovery**

Firstly,  $< 0.015\text{ g}$  ( $\sim 1.5\text{ wt\%}$  of final solution) of cellulose was weighed into a 2 mL tube into which 1 mL of aqueous LiOH ( $1.993 \pm 0.013\text{ mol dm}^{-3}$ ) was added. Secondly, the solution was agitated by Eppendorf Thermomixer at  $10\text{ }^{\circ}\text{C}$  and 1200-1400 RPM for 24 h. The first and second steps were repeated 2-5 times to produce solutions of varying cellulose concentration. After final agitation, the dissolved fraction of cellulose was separated from the undissolved fraction by centrifugation at  $10\text{ }^{\circ}\text{C}$  and 16000-18000 g for 20 minutes. Subsequently, these fractions were extracted, washed and recovered in the same manner as the single aliquot addition method.

### **Solubility determination using incremental addition with visual quantification**

A known mass of cellulose was weighed into an 8 mL sample vial into which 5 mL of aqueous LiOH ( $1.993 \pm 0.013\text{ mol dm}^{-3}$ ) was added. The solution was stirred with a magnetic flea at  $10\text{ }^{\circ}\text{C}$  for 1 h. After stirring, if no fragments of cellulose were visible to the naked eye, a further known mass of cellulose was added to the vial. This process was repeated until fragments of cellulose were visible to the naked eye. At which point, the solution was stored at  $10\text{ }^{\circ}\text{C}$  for 24 h to ensure equilibration. Repeated determinations, using smaller increments of

added cellulose, were carried out to improve the precision of the measurement<sup>93</sup>. Solubility was quantified by the total amount of added cellulose before appearance of visible fragments.

### **SEC-MALLS analysis**

SEC-MALLS was performed by collaborators, Noriyuki Isobe, Yuko Ono and Akira Isogai. The system consisted of a guard column (KD-G, Shodex, Japan), a SEC column (KD-806M, Shodex, Japan), a MALLS detector (DAWN HELEOS-II,  $\lambda = 658$  nm, Wyatt Technologies, USA), and an RI detector (Optilab T-rEX,  $\lambda = 658$  nm, Wyatt Technologies, USA). 1.0 w/v% LiCl/DMAc was used as an eluent. Detailed protocol is described elsewhere.<sup>147</sup> It should be noted that the study cited here notes that the effect of eluent choice on DP distributions are negligible for the method used.

### Box 1.4a: Additional details of solute recovery solubility tests

Solute recovery experiments were made in two different labs whose equipment varied. Due to this fact, there are minor differences in protocol between some of the 7 runs completed for hydrolysed Avicel solute recovery (Figure S1). For run 1 (which was discarded due to incomplete sample processing) and run 7, the cooled agitation chamber rotated a platform with horizontal sample tubes at ~200 RPM. The cooled centrifuge was run at 20000 g to separate undissolved fraction from dissolved fraction. In contrast to this, runs 2-6 used vertical Eppendorf tubes, cooled and shaken at 1200-1400 RPM. The cooled centrifuge was run at 16000-18000 g to separate undissolved and dissolved fractions. The timescales for the dissolution stage of solubility tests were 16-24 hours. All incremental solubility tests were carried out under the same conditions as runs 2-6.

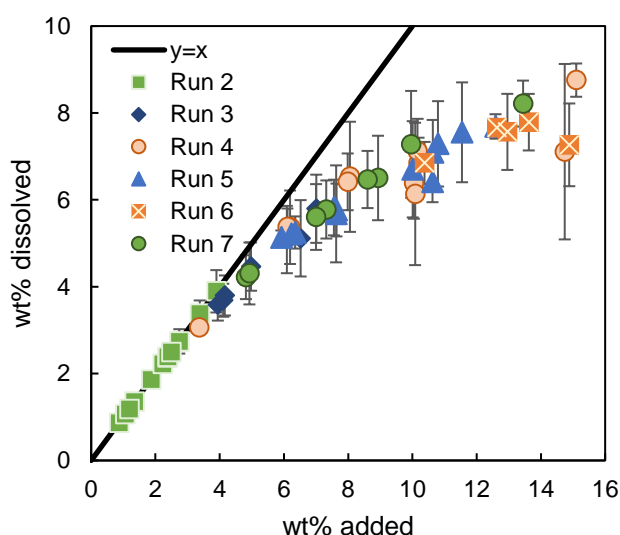


**Figure S1:** Raw data of all single aliquot/solute recovery experiments on hydrolysed Avicel.

Two methods were employed in the washing steps for solute recovery. Each sample, after precipitation, was washed with varying EtOH/H<sub>2</sub>O ratios (Section 3.2.3). During washing, precipitate was re-dispersed in fresh EtOH/H<sub>2</sub>O aliquot. Runs 1-4 achieved this by overnight agitation. However, this method led to long experimental timescales due to numerous washing stages. Therefore, a new methodology was employed for runs 5-7 in which the compressed material was carefully broken apart and dispersed in the liquid using a plastic rod or spatula.

### Box 1.4b: Error calculation and weighted averages

Average (apparent) values of solubility from each fraction, compensating for solute losses were calculated by:

$$App = \frac{D+(T-U)}{2} \quad (S1)$$

Where D is dissolved fraction, T is total added and U is undissolved fraction.

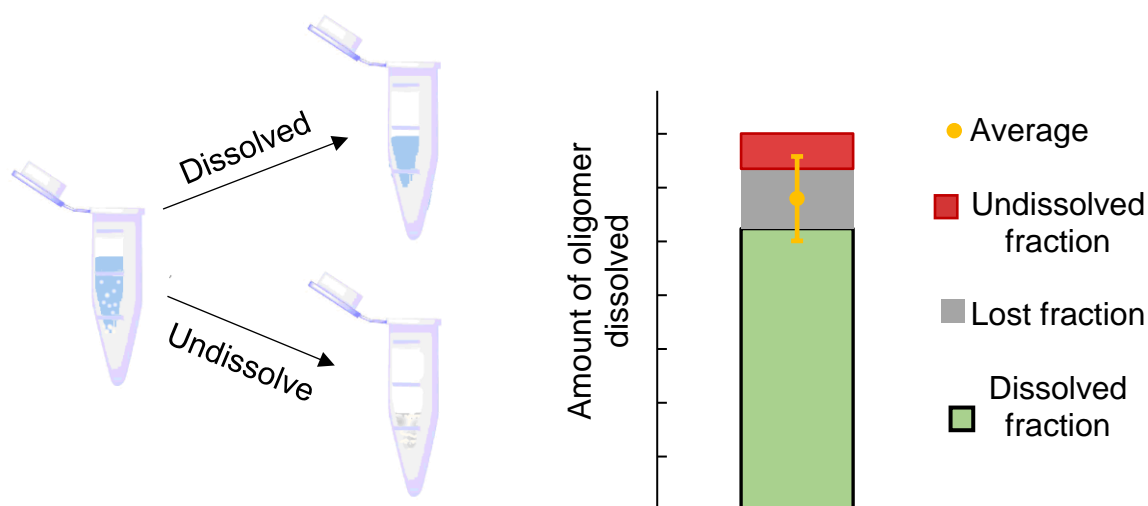


**Figure S2:** Schematic depiction of apparent solubility value calculation.

The standard error of the averaged (or apparent) solubility value was calculated using a combination of the measurement imprecision and the size of the unaccounted fraction. Multiple repeats to calculate apparent solubility values were carried out and error bars included. Averaging of these repeats was carried out using a weighting method, similar to the one employed by Gale *et al.*<sup>93</sup> The weighting attributed to each value is calculated by:

$$w_i = \frac{1}{\sigma_i^2} \quad (S2)$$

where  $\sigma_i$  is the standard error related to App in Equation S1.

This weighting value was used to calculate the contributions of a range of values ( $v_1 \dots v_n$ ) to the weighted average value, according to how well their dissolved and undissolved fractions agree:

$$v_{avg} = \frac{\sum_1^n v_i w_i}{\sum_1^n w_i} \quad (S3)$$

Hence, data used for Figure 3.2 onward had a weighting applied based on the errors associated with the gap between “dissolved” and “undissolved” fraction data points (Eq. S2 and S3) unless noted otherwise. This weighting gives a larger contribution from points whose “dissolved” and “undissolved” fraction were closer together.



### 3.3 Results and discussion

#### 3.3.1 Comparison with cellulose: DP dependence in dissolution behaviour for Single Aliquot experiments

In order to determine the correlation between DP and the dependence of solubility on solute initial concentration, all amorphous cellulose samples were subjected to the solubility measurement using single aliquot addition and solute recovery quantification (Section 3.2.2). The aqueous LiOH was at  $1.993 \pm 0.013$  mol cm<sup>3</sup>) and 10 °C. Results were plotted in Figure 3.2 below.

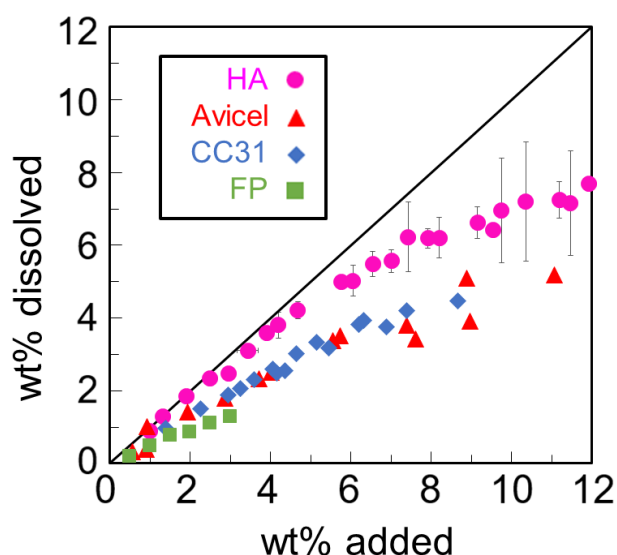


**Figure 3.2:** Solubility of cellulose samples in 2 molar LiOH (aq) solution at 10 °C plotted against the size of the aliquot of solute added, in weight percent. (Error bars calculated by procedure in Box 1.4. and not available for CC31 and FP due to the small quantity of available sample.)

It was found that all samples showed a deviation from total dissolution of cellulose below its saturation point. For hydrolysed Avicel, complete dissolution did occur below 3 wt%. However, after this point, there is incomplete dissolution

of the aliquot added. Within the range of values that lie between the point at which solubility deviates and the saturation point, solubility measurements could be taken erroneously, leading to an incorrect data point for solubility. Comparing this behaviour to the longer chain cellulose samples, the dependence of DP on the solubility behaviour can be examined. Cellulose samples regenerated from the LiCl/DMAc system showed incomplete dissolution below the saturation point along almost the whole of the range tested. The level-off DP celluloses Avicel ( $DP_w \sim 200$ ) and CC31 ( $DP_w \sim 190$ ) showed a very similar solubility profile, thereby confirming that the sample preparation (which employed dissolution and coagulation) was effective in eliminating innate microstructural difference due to their respective sample origins (Avicel from wood and CC31 from cotton). FP having much higher DP ( $DP_w \sim 710$ ), showed significant incomplete dissolution, even at  $< 1$  wt%. Hence, regardless of the quantity of added cellulose, FP cellulose may not display complete dissolution in this solvent.

To summarise, as DP increased, the fraction of the added cellulose that was not dissolved also increased. This implies that the incomplete dissolution can be reduced by decreasing the average DP of the solute. The point at which a solute's solubility deviates from full dissolution of the solute could be taken as a quantifiable metric for DP's influence on incomplete dissolution. The solid line in Figure 3.2 describes full dissolution. The points at which each sample's data-set intersect with this line were  $\sim 2.5$  wt% for hydrolysed Avicel,  $< 1.3$  wt% for CC31,  $\sim 0.9$  wt% for Avicel and  $< 0.5$  wt% for FP. This point, compared to the sample's saturation point determines the range of values that could be measured as their "solubility". The wider this range, the less likely that solubility measurements of samples such as these from the literature can be trusted. Additionally, these values provide a quantifiable point up to which we can estimate a solute is able to be fully dissolved, which could be used to choose sizes of aliquots for

incremental addition methods. In contrast, generally in the literature, these small aliquots are chosen arbitrarily, leading to possible inaccuracy.

This possible cause for inaccuracies in solubility measurements could be explained by the hypothesis that the partition between incomplete and complete dissolution could depend on either the extent of cellulose aggregation or meta-stability of a fraction of the solution in an intermediate swollen/penetrated state<sup>54,211</sup>. The amorphous nature of the samples tested here means that they are completely swellable with solvent<sup>236,237</sup>. This solvent accessible but entangled state<sup>54</sup> could be meta-stable, with cellulose unable to disperse completely in solution due to solvent cohesion forces<sup>49</sup>. This is plausible as some solvents are able to only swell cellulose<sup>238</sup>. The efficacy of using incremental addition to reduce the impact of these problems and whether that in itself allows us to make accurate quantitative measures of the solubility is investigated in the next section. Incremental addition should have a reduced impact from these intermediate states. Hence, it should also be possible to confirm this hypothesis if incremental addition alone reduces the incomplete dissolution significantly.

### 3.3.2 Influence of incremental addition on solute recovery measurements

In addition to the single aliquot (SA) measurements, the incremental addition (Inc) method (Table 3.1) was tested to see if Inc displays reduced incomplete dissolution below the saturation point by using hydrolysed Avicel regenerated from H<sub>3</sub>PO<sub>4</sub>. Here, the samples were recovered in the same manner as the single aliquot /solute recovery method, to isolate the effect of the addition method on solubility.

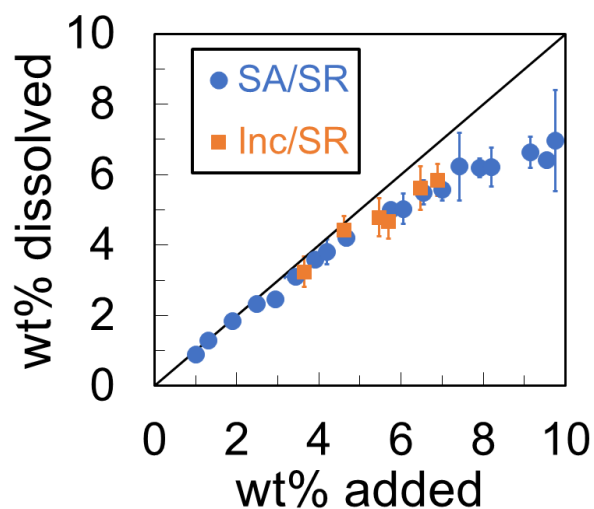


**Figure 3.3:** Solubility of hydrolysed Avicel measured by the addition of incremental aliquots of < 1.5 wt%. Compared with the solubility profile obtained from single aliquot/solute recovery measurements.

Figure 3 demonstrates that the incremental addition (Inc) and single aliquot (SA) were identical, both showing a continued increase of solubility above the expected saturation point and deviation from total dissolution. Hence, incremental addition itself does not provide the accurate (and singular) value for solubility needed for statistical thermodynamic analysis. This agreement between Inc and SA indicates that kinetics of dissolution is not the cause of incomplete dissolution. Therefore, in these amorphous samples, the incomplete dissolution results from the equilibrium state, namely, the equilibrium between *Dissolved cellulose*  $\leftrightarrow$  *Aggregated cellulose*. This equilibrium is dependent on solute concentration<sup>220,239</sup>. Whether this aggregation is due to saturation or the formation of undissolved fractions depends on the solution. Indeed, turbidity, a measure related to solute aggregation, is used to determine the point at which saturation occurs in some solubility measurements<sup>93,222-224</sup>. Increases in aggregation lead finally to either precipitation or gelation, phenomena observed in celluloses of higher DP and crystallinity<sup>240,241</sup>.

### 3.3.4 Incremental Addition: Visual/Optical measurement of saturation point

Incremental solute addition is often adopted to circumvent the difficulties in quantifying solubility. In these studies, the appearance of solids in the solution is used to mark saturation<sup>93,222-224</sup>. The presence of incomplete dissolution in the solubility profiles observed in Figures 3.2 and 3.3 point out a potential problem in the visual/optical quantification methodology. The solid line in Figure 3.4 indicates the point at which the aggregates visible to the naked eye started to appear during incremental addition.

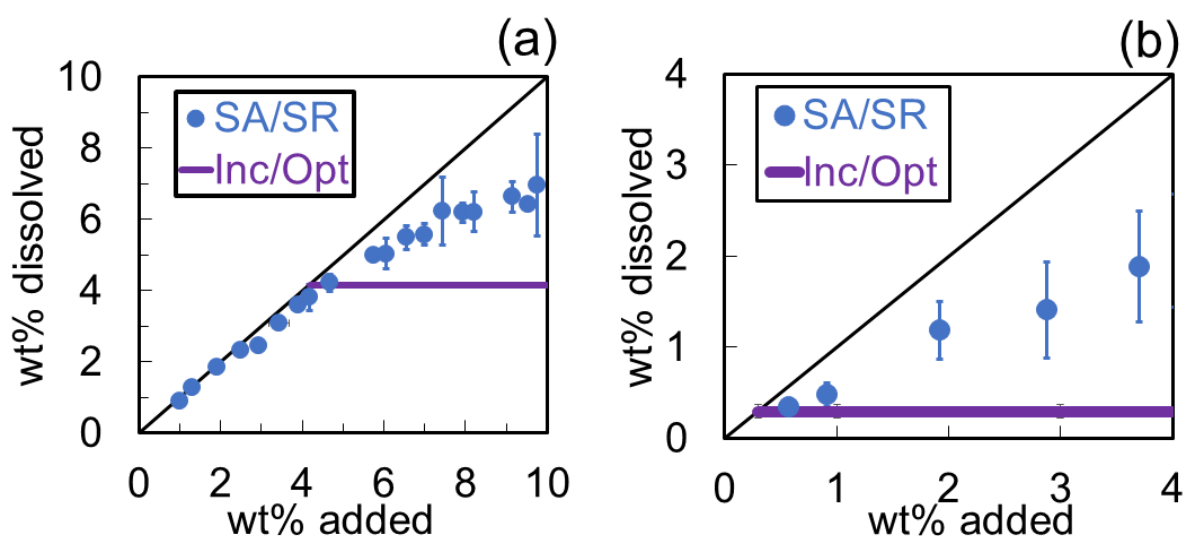


**Figure 3.4** Saturation point determined by incremental addition of hydrolysed Avicel regenerated from  $\text{H}_3\text{PO}_4$  and Avicel regenerated from  $\text{LiCl}/\text{DMAc}$  at  $10^\circ\text{C}$  in 2 molar  $\text{LiOH}$  (aq) (Shown in purple, line thickness represents error bars) compared with the solubility profile obtained from single aliquot/solute recovery measurements.

The saturation point, according to this method is shown in purple on Figure 3.4:  $4.16 \pm 0.05$  wt% for hydrolysed Avicel and  $0.29 \pm 0.7$  wt% for the amorphous Avicel sample which were close to the point where single aliquot/solute recovery data showed deviation from complete dissolution. This shows that the solute

induced self-aggregation leading to incomplete dissolution was large enough for visual observation, which means that Inc/VO solubility tests cannot quantify the maximum solubility of cellulose in these samples but rather the maximum complete dissolution of cellulose. This gives further credence to the idea that the studied methods can produce a range of results for the solubility of the same sample. As such, one cannot use them directly for statistical thermodynamic analysis without further investigation.

### 3.3.5 Origin of incomplete dissolution

The origin of incomplete dissolution must be understood in order to design an analogue/methodology combination which gives the type of low uncertainty in the saturation point needed. Traditionally, one would define the saturation point as the point at which aggregation of solutes is first observed. However, because more solute dissolves above this point, the true value of saturation in this system is unclear. To investigate the origin of incomplete dissolution, the dissolved fraction and undissolved fraction (corresponding to the aggregates), recovered from single aliquot experiment, were subjected to SEC-MALLS analysis.

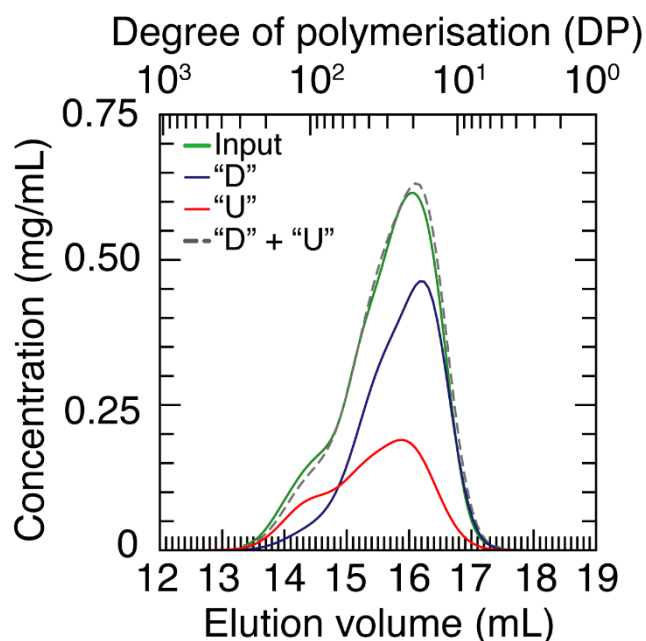


**Figure 3.5:** SEC-MALLS elution profiles for hydrolysed Avicel (HA) before solubility tests ("Input") overlaid with elution profiles for the dissolved ("D") and undissolved ("U") fractions of HA. The "D" and "U" samples were taken from the SA/SR batch at  $11.85 \pm 0.19$  wt% added (Figure 2). The concentration of profiles "D" and "U" were normalised with respect to the peak area of "Input" by taking account of the mass recovered for each fraction (Where D was  $66.2 \pm 1.6$  % and undissolved was  $36.0 \pm 1.6$  % of the mass of "Input").

Figure 3.5 demonstrates that there is a significant difference in the DP within the dissolved and undissolved fractions. Using peak deconvolution on Figure 3.5, it is possible to separate out the proportional distribution of DP present in the Initial, Dissolved and Undissolved samples. Analysis of this data can tell us, in a more quantitative manner, the impact of DP on solubility. The deconvoluted peaks are tabulated in Table 3.2.

**Table 3.2:** Deconvoluted SEC-MALLS peaks describing the DP distribution within Initial, Dissolved and Undissolved samples.

Sample	Peak DP	Proportion within sample (wt%)
Initial	108.8	12.3
	33.2	36.4
	17.2	41.3
Dissolved (D)	102.9	4.5
	30.4	49.3
	15.8	46.2
Undissolved (U)	103.4	23.0
	45.8	27.9
	22.2	49.1

Table 3.2 shows that higher DP molecules have limited solubility; they do exist in the dissolved fraction, but in proportionally smaller amounts than the initial fraction. This suggests that DP is a dominant factor leading to insolubility. Additionally, the undissolved fraction contains lower DP molecules in proportionally smaller amounts than the initial and dissolved fractions. Consequently, there is not a hard DP limit for solubility *per se*. However, DP within the sample does have a significant effect on how soluble each fraction is. Table 3.2 also demonstrates that the continued increase in solubility with the addition of cellulose, beyond the first formation of aggregates, is likely due to solute molecules of a shorter chain length which continue to dissolve up to a higher concentration than the median length molecule. This would be exacerbated in samples of high DP dispersity which suggests that samples with high DP dispersity have a higher incidence of incomplete dissolution.



### 3.3.6 Comparison between methods

This section summarises and compares how each solubility method under or overestimates solubility, and why. Single aliquot addition with solute recovery (SA/SR) provides basic quantification, limited by choice of aliquot size and recovery processing problems. This information could be applied to determine which measurements could be used for statistical thermodynamic analysis and which is the optimal choice to produce data with low uncertainty with respect to the saturation point. The several stages of sample processing required to recover solute for quantification could lead to further errors caused by solute loss during centrifugation.<sup>209</sup> Incorrect choice of aliquot size can either under- or over-estimate the solubility value (Figure 3.2) due to incomplete dissolution or additional dissolution of low DP solutes. Incremental addition with solute recovery gives data which is also affected by incomplete dissolution. For the shorter chain sample, hydrolysed Avicel (HA), the addition method does not make a large difference to the observed solubility trend. In contrast, incremental addition with visual/optical quantification always underestimates cellulose solubility for samples with incomplete dissolution, because the first point of incomplete dissolution is taken as saturation. It is likely that more of the shorter chain molecules in the sample can be dissolved beyond this point. Figure 3.5 illustrates the effect of DP on the aggregation that leads to incomplete dissolution.

Furthermore, the approximate saturation points for both solute recovery methods are comparable. However, the values of these saturation points can be erroneous and the values obtained from incremental/optical measurements are consistently lower. Our results demonstrate that incomplete dissolution is present in every method. The incomplete dissolution observed in the hydrolysed Avicel (average DP 44) sample was mostly dominated by solute aggregation, as

evidenced by the equivalent solubility profiles between the addition methods (Figure 3) and the SEC-MALLS analysis. Fewer molecules of low DP were aggregated and therefore undissolved, as confirmed by the higher proportion of short chain molecules in the dissolved fraction compared to the initial sample (Figure 3.5, Table 3.2). In this sample, higher DP ( $> 100$  DP) molecules were more likely to be aggregated than the average DP, leading to incomplete dissolution. The presence of incomplete dissolution leads to a significant and systematic error in solubility quantification within any measurement that it affects.

## 3.4 Conclusions

### 3.4.1 Insights into quantification problems

Through the study of cellulose samples with a range of DPs the problems inherent in the quantification of cellulose have been investigated with an aim to determine the optimal method to produce data for application to statistical thermodynamic analysis. This has revealed the following insights:

Incomplete dissolution (ID), namely, the fractionation of solute into dissolved and undissolved states below the saturation point, is present in all cellulose samples and all solubility methods studied. Within the samples studied, ID becomes less dominant as degree of polymerisation (DP) decreases, but is still present in hydrolysed Avicel, a sample of low DP and crystallinity. In this sample, ID was caused by solute induced self-aggregation dependent on the concentration of the solute. Higher DP molecules were proportionally more present in undissolved fractions and hence their aggregation is likely the major cause of ID. Due to the influence of ID, samples with reduced DP and crystallinity show fewer quantification inaccuracies.

However, for every solubility quantification method, ID of cellulose samples led to inaccurate quantification of the solubility, or multiple possible values for solubility. In the case of solute recovery methods, the several stages of sample processing required to recover solute for quantification could lead to further errors. Surprisingly, although the Incremental/Optical quantification method was introduced to circumvent solubility inaccuracy caused by intermediate stages, errors still persist due to incomplete dissolution. In fact, it is less accurate than solute recovery methods in which a correctly sized aliquot of solute is chosen. These persistent errors are due to the appearance of aggregates being used as a sign of saturation being reached in solution. However, in poor solvents or in

cases with a wide DP dispersity, incomplete dissolution leads to aggregates appearing before true maximum solubility is achieved.

### 3.4.2 Design of an analogue

Based on the above clarifications, it is recommended to measure sample DP and DP dispersity before quantifying solubility. With an aim to understand the cellulose dissolution mechanism through molecular interactions, accurate solubility measurements can be obtained using a cellulose oligomer analogue of < 40 DP with uniform DP as this analogue would be completely soluble in poor solvents such as LiOH, would still retain insolubility in water and would not show incomplete dissolution due to DP dispersity. However, one would have to consider how an analogue's dissolution differs mechanistically from cellulose (such as presence of aggregation, intermediate states, etc.). If the study requires the use of Avicel or other cellulose samples as opposed to an analogue, quantitative accuracy can be optimised by measuring soluble and insoluble fractions with SEC-MALLS (Figure 3.5) or by measuring solubility across the whole range of added cellulose (Figure 2). Alternatively, solubility could be quantified using a calibration curve based on physical properties of solutions such as density, refractive index or turbidity and their dependence on cellulose concentration. Based on such calibration, accurate, in situ solubility could be measured (where complete dissolution is possible.)

Further work demonstrating the efficacy of a homogenous oligomer analogue below 50 DP combined with this chapter, can provide an analogue which does not suffer from the problems discussed here. To produce such an analogue, hydrolysis should progress for an extended period of time until all cellulose is either water soluble (and can be removed), or of 15 degrees of polymerisation.<sup>58</sup>

# CHAPTER 4: UNDERSTANDING MOLECULAR INTERACTIONS IN MACROSCOPIC TRANSITIONS

Chapter 2 began to study the driving forces on the molecular scale behind the dissolution of cellulose. Exploitation of carbohydrates is not limited to dissolution and therefore ones understanding must move beyond the molecular basis of the dissolution process. Control of macroscopic phases and states of carbohydrate polymer assemblies such as gelation and gelatinisation (as defined in Section 4.1) are crucial in many applications (Chapter 1).

Though these systems work on a larger scale compared to our previous chapters, it is possible to extend the theory for co-solute induced solubilisation to the transitions involving these carbohydrate polymer assemblies. Due to the abundance of clear transition data available in the starch gelatinisation literature, the study on which this chapter is based was focused on starch gelatinisation. Through which this chapter aims to develop particle scale theory that could be applied to cellulose but also aims to make progress in the understanding of starch gelatinisation through statistical thermodynamics.

## 4.1 Introduction

Starch exists in the form of semi-crystalline granules that consist of two types of polysaccharides: non-branched amylose and branched amylopectin. Upon heating in the presence of excess water, the granule goes through gelatinisation, which is the process comprised of swelling of granules and partial leaching of amylose<sup>242,243</sup>. This is comparable to the swelling stage that we see in cellulose dissolution, differing mainly due to the presence of amylopectin and structural differences between starch granules and cellulose fibres (or cellulose crystal moieties). What is particularly important is the control of gelatinisation process by the addition of small molecule components (co-solutes), such as salts and

sugars,<sup>1,243,244</sup> which has been exploited routinely in cooking and food processing.

Despite decades of investigations by the employment of a variety of experimental techniques ranging from microscopy and calorimetry<sup>2,242</sup> to rheological and NMR measurements,<sup>1,245,246</sup> the understanding on a molecular scale of how salts affects gelatinisation remains incomplete. Indeed, the influence of salts on starch gelatinisation can be measured through how gelatinisation temperature  $T_g$  and the enthalpy of gelatinisation  $\Delta H_g$  change with co-solute concentration, which is probed using differential scanning calorimetry (DSC).<sup>247</sup> The advantage of this approach is that, despite the irreversibility of the transition,<sup>248</sup> sufficiently slow heating rates can eliminate kinetic contributions,<sup>249,250</sup> thereby enabling the application of equilibrium statistical thermodynamics, such as the Flory theory.<sup>251</sup> Still, the universal difficulty which has yet been overcome is the lack of a direct link between the experimental observation and gelatinisation temperature shift in a quantifiable manner, namely putting numbers to each of the contributions and comparing the relative importance between them. The need for the application of physical theory is clear in cases such as these, as discussed in Chapter 1.

Within the literature, experimental observation generally points out the importance of the following two contributions to salt induced changes in gelatinisation:<sup>1,2,252–254</sup>

- 1) Starch-cation interaction (leading to the decrease of  $T_g$ )
- 2) “Water structure” (leading to additional changes in  $T_g$ )

Beyond the consensus on the existence of the above two driving forces, there is little agreement on their causes and relative importance<sup>1,2</sup>, which reflects the

lack of a reliable link between the change of  $T_g$  and the microscopic interactions that take place in solution.

The paradigm for explaining how salts affect hydration of solutes and polymers has long been the concept of the “water structure”<sup>185</sup>, which is considered to be the driving force for the hydrophobic effect<sup>190</sup>, and the ion-induced hydration change is rationalised via the change of water structure. As discussed in Chapter 2, the difficulty of this paradigm arises from the fact that not only has the “water structure” been ambiguously defined but also the how it influences the thermodynamics of hydration has never been quantified.<sup>175,255</sup>

Hence, the aims of the theoretical studies within this chapter are threefold:

- 1) to quantify starch-water and starch-salt interactions and to identify the dominant contributions;
- 2) to clarify if there is any relationship between starch-water and starch-salt interactions;
- 3) to identify the molecular scenario behind 1 and 2.

To achieve these aims, it is indispensable to base the analysis on established statistical thermodynamics, which has clarified how additives and co-solutes can influence solubility (Chapter 2), macromolecular stability and gelation based solely on experimental data.<sup>116,124,176</sup> For this application, this theory must be extended beyond the molecular level interpretation used in Chapter 2. Here the statistical thermodynamic approach is extended to starch gelatinisation, by utilising the extensive experimental data on the role of salts and sugars on gelatinisation of sago starch.<sup>1,2,256</sup> The systems studied here are starch/ salt/ water and starch/ sugar/ water, with the main focus being on salts. This focus had been chosen because salts' concentration dependence has similar driving

forces to cellobiose solubility in electrolyte solutions (as noted above) and also has a large impact on gelatinisation temperature and enthalpy. Varying the anion/cation can extract information about these dependencies.



## 4.2 Statistical thermodynamics of starch gelatinisation in the presence of salts

### 4.2.1 Thermodynamics of starch gelatinisation

To elucidate from calorimetric data how the addition of co-solutes, such as salts, affect the gelatinisation on a molecular scale, here we construct a statistical thermodynamic theory. To this end, let us consider a three-component solution consisting of starch ( $i = u$ ), water ( $i = 1$ ), and co-solute ( $i = 2$ ). For co-solute concentration, we use the molar scale,  $c_2$ , or its chemical potential,  $\mu_2$ .

Within starch gelatinisation there are multiple transitions as temperature increases.<sup>257</sup> Here, the major endothermic transition will be used to describe gelatinisation for simplicity.<sup>258</sup> The gelatinisation endotherm refers to the so called M1/M2 endothermic peak in the DSC of gelatinisation. It describes the major transition in gelatinisation and is irreversible. This peak has been referred to as the swelling, decrystallisation and leaching peak.<sup>247</sup> The remaining 2 enthalpic transitions often observed in gelatinisation DSC (M3 and M4) are also endothermic but reversible and they have been attributed to structural rearrangements ("settling") after gelatinisation. Figure 4.1 shows the presence of M1, M2 and M3 endotherms in a DSC thermogram for gelatinisation.

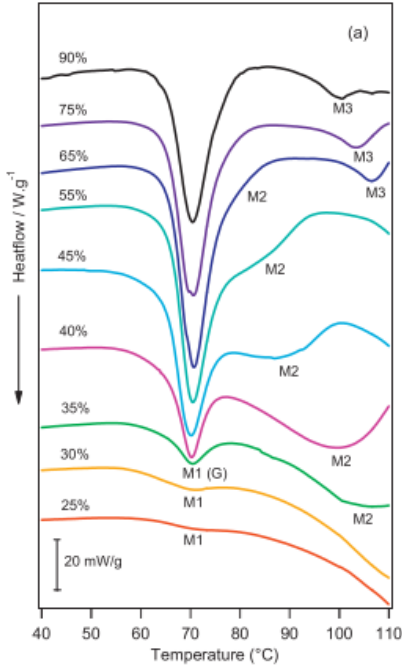


**Figure 4.1 (Left):** DSC thermogram of wheat starch within a range of water contents (25-90%) as seen in Day et al.<sup>243</sup>

This figure shows the presence of M2 and M3 endotherms alongside the primary gelatinisation endotherm (M1). The M2 endotherm combines with the M1 endotherm at higher water content (As noted by Patel<sup>259</sup>). As water content is high in aqueous solutions, the M1 endotherm is usable for full gelatinisation process for this study.

Following Ahmad and Williams,<sup>1</sup> the  $T_g$  data used in our study is the peak temperature. Since initial and final temperatures are affected by increasing co-solute concentration, the peak temperature is more likely to be the most consistent measure of  $T_g$  attainable.<sup>249</sup> Under this setup, how salt concentration changes the free energy (and therefore the chemical potential) difference between the gelatinised and granular states of the starch,  $\Delta\mu_{u,g}$ , can directly be obtained from  $T_g$  and  $\Delta H_g$ . To do so,  $\Delta\mu_{u,g}$ , which is the function of temperature  $T$ , pressure  $P$  and salt chemical potential  $\mu_2$  can be expanded around a point on the gelatinisation equilibrium as:

$$\delta\Delta\mu_{g,u} = \left(\frac{\partial\Delta\mu_u}{\partial T}\right)_{P,\mu_2} \delta T + \left(\frac{\partial\Delta\mu_u}{\partial P}\right)_{T,\mu_2} \delta P + \left(\frac{\partial\Delta\mu_u}{\partial\mu_2}\right)_{T,P} \delta\mu_2 \quad (4.1)$$

where  $\delta$  signifies a small change of the variables in question.  $\Delta\mu_{g,u}$  is denoted as  $\Delta\mu_u$  from now onward in this chapter for simplicity.

Along the equilibrium line,  $\Delta\mu_u = 0$ , Eq. (4.1) can be rewritten as:

$$0 = -\frac{\Delta H_g}{T_g} \delta T + \Delta V_g \delta P + \left(\frac{\partial\Delta\mu_u}{\partial\mu_2}\right)_{T,P} \delta\mu_2 \quad (4.2)$$

where the equilibrium condition was used to yield  $\left(\frac{\partial \Delta\mu_u}{\partial T}\right)_{P,\mu_2} = -\Delta S_g = -\frac{\Delta H_g}{T_g}$  and  $\Delta V_g$  is the volume change that accompanies gelatinisation.

Under a constant pressure,  $\delta P = 0$ , we also obtain <sup>124</sup>:

$$\left(\frac{\partial \Delta\mu_u}{\partial \mu_2}\right)_{T,P} = \frac{\Delta H_g}{T_g} \frac{\delta T_g}{\delta \mu_2} \quad (4.3)$$

Eq. (4.3) will lead to the determination of starch-water and starch-salt affinities, as will be shown in the next section. The present theoretical framework relies only on the existence of the gelatinisation as a phase transition, which is observed in pure water and in the presence of salts alike.

#### 4.2.2. Statistical thermodynamics of starch gelatinisation

Calorimetric data on gelatinisation, analysed via Eq. (4.3) yields the free energy change  $\Delta\mu_u$  that accompanies gelatinisation transition. How  $\Delta\mu_u$  depends on salt concentration  $c_2$  reveals quantitative microscopic information by using statistical thermodynamic relationships, as will be shown below.

To this end, below lies a summary of what gelatinisation process consist of according to the consensus of the field <sup>242,249,260,261</sup>:

- (a) the leaching of amylose into solution,
- (b) loss of crystallinity and swelling of the granules.

In the scope of statistical thermodynamics, these processes correspond to:

- (a) solvation of amylose from the solid state to a molecularly dispersed solution with water and salts
- (b) expansion of a granule and penetration of solution into the granule.

Hence both processes accompany solvation changes and macroscopic structure changes within the granule.

Such solvation changes can be interpreted microscopically, based on the difference in solvent and co-solute densities between the vicinity of starch and the bulk solution. This is enabled by extension of the Kirkwood-Buff integrals (KBIs) to the gelatinised and semi-crystalline states. This vicinity-bulk density difference can be captured quantitatively using the change of KBIs between these two states,<sup>120,262</sup> defined as<sup>119</sup>:

$$G_{ui}^{\alpha} = \int [g_{ui}^{\alpha}(\vec{r}) - 1] d\vec{r} \quad (4.4)$$

where  $g_{ui}^{\alpha}(\vec{r})$  refers to the distribution function between a state (either gelatinised  $\alpha = g$  or semi-crystalline  $\alpha = c$  state) of the starch ( $u$ ) and species  $i$  (either water  $i = 1$  or cosolute  $i = 2$ ). Hence,  $G_{ui}^{\alpha}$  signifies the net increase or depletion of the species  $i$ , within each state, around the starch macromolecular assembly compared to a component of the bulk solution.<sup>124,263</sup>  $G_{ui}^{\alpha}$  has also been interpreted as the net “affinity” between species  $u$  and  $i$ .<sup>3,121</sup> The KBI changes in Eq. (5.4) accompany the semi-crystalline (granular) state  $\rightarrow$  gelatinised state transition, such that  $\Delta G_{ij} = G_{ij}^g - G_{ij}^c$ . Note that this deals with “starch” (which consists of amylose and amylopectin) as an averaged single entity. Consequently, the part of amylose that leaches upon gelatinisation is still being an integral part, statistical thermodynamically, of starch, or the species  $u$ .

KBI changes are linked to the free energy change upon gelatinisation through the following relationship, equivalent to Eq. 2.6:<sup>174</sup>

$$-\left(\frac{\partial \Delta \mu_u}{\partial \mu_2}\right)_{T,P} = c_2(\Delta G_{u2} - \Delta G_{u1}) \quad (4.5)$$

This is based on the same assumption of negligible inter-particle interactions. However, the particle definition for the interpretation of Eq. (4.5) in this chapter is the whole granule itself, as opposed to an individual starch molecule. This equation plays a central role in the analyses within this chapter.

### 4.2.3 Determining starch-water and starch-salt affinity changes

The KBI change for the starch-water and starch-salt affinities and how they vary with co-solute concentration can tell us about the changes in interactions upon gelatinisation and how they are affected by co-solutes. This will allow us to determine whether the co-solute or the solvent have the biggest effect on variations in gelatinisation temperature. These KBIs can be determined by supplementing Eq. (4.3) with the following independent relationship:<sup>174</sup>

$$\Delta V_u = -c_1 V_1 \Delta G_{u1} - c_2 V_2 \Delta G_{u2} \quad (4.6)$$

where  $V_i$  represent the partial molar volume of the species  $i$ .

Eqs. (4.3), (4.5) and (4.6) yield the following useful formulae for the calculation of KBIs at  $c_2 \rightarrow 0$  limit:

$$\Delta G_{u2} = -\frac{\Delta H_g}{T_g} \frac{\delta T_g}{\delta c_2} - \Delta V_u \quad (4.7)$$

$$\Delta G_{u1} = -\frac{1}{c_1 V_1} \Delta V_u \quad (4.8)$$

In bulk water,  $c_1 V_1 = 1$ , whereas in aqueous starch solution,  $c_1 V_1$  may deviate from 1. However, this does not affect the result of the interpretation of  $\Delta G_{u1}$  due to its negligibly small value as discussed in Section 4.5. Eqs. (4.7) and (4.8) can yield starch-water and starch-salt affinity changes whenever calorimetric and volumetric data on gelatinisation are both available.

## 4.2.4 The effect of bulk solution structure

Salts, according to the classical paradigm, change water structure, which modulates the strength of the hydrophobic effect and consequently the gelatinisation free energy<sup>174</sup>. Here we aim to quantify how the bulk solution structure affects gelatinisation. To do so, note that we have considered  $\mu_2$  or  $a_2$  (salt ion activity) as the measure of co-solute concentration.

However, co-solute concentration is considered usually in molarity. The gap between the chemical potential of salts ( $\mu_2 = \mu_2^\theta + RT \ln a_2$ ) and molarity gives rise to,<sup>171</sup> as introduced in Section 2.3:

$$\left(\frac{\partial \ln a_2}{\partial \ln c_2}\right)_{T,P} = \frac{1}{1+c_2(G_{22}-G_{21})} \quad (4.9)$$

This means that the self-association of salts ( $G_{22}$ ) in preference to salt hydration ( $G_{21}$ ) effectively reduces the number of salts, thereby leading to the per-mole inefficiency for starch solvation.<sup>176</sup> However, note that the L.H.S. of Eq. (4.9) tends to 1 as  $c_2 \rightarrow 0$ , meaning that this inefficiency term disappears at low salt concentration.

## 4.2.5 Source and analysis of experimental data – non-linear regressions

At dilute salt concentration, it is possible to obtain both calorimetric and volumetric data for starch gelatinisation based on data available in the literature<sup>242,250,264</sup>. The most systematic set of data uses sago starch.<sup>242,250,264</sup> It should be noted that sago starch retains typical compositional, structural, and physical characteristics similar to the other starches such as potato and corn.<sup>265</sup> However, whether the salt concentration dependence of other starches proceeds in a qualitatively similar way to sago<sup>2,266-268</sup> or differently<sup>243,253,254,269</sup>

still awaits an extensive experimental clarification. Despite this, theoretical method developed in this chapter can readily be applied to any starch if calorimetric and volumetric data on gelatinisation has been measured along the concentration of salts.

$\Delta V_u$ , as used in Eqs. 4.7 and 4.8, can be calculated for dilute solutions from the pressure dependence of  $T_g$  using the following relationship:<sup>174</sup>

$$\left(\frac{\partial \Delta \mu_u}{\partial P}\right)_{T, N_1; c_2 \rightarrow 0} = (\Delta V_u)_{c_2 \rightarrow 0} = \frac{\Delta H_g}{T_g} \frac{\delta T_g}{\delta P} \quad (4.10)$$

This means that both  $\Delta G_{u1}$  and  $\Delta G_{u2}$  can be determined from the experimental data at the dilution limit of salts. However, the volume change on gelatinisation has not been measured at higher salt concentrations, and is qualitatively inconsistent in the literature,<sup>243,269,270</sup> which means that only the KBI difference  $\Delta G_{u2} - \Delta G_{u1}$  is available. And consequently, due to the lack of experimental data,  $\Delta G_{u1}$  and  $\Delta G_{u2}$  cannot be determined separately at higher salt concentrations. Additionally,  $\Delta G_{ui}^0$  values do not exist at high salt concentrations as Eqs. 4.7 and 4.8 are predicated on the dilute salt condition.

For processing the experimental data, the following expression, equivalent to Eq. (4.4) has been used for convenience:<sup>174,271</sup>

$$\frac{\Delta H_g}{T_g} \frac{\delta T_g}{\delta \mu_2} = \frac{\Delta H_g}{RT_g^2} \left(\frac{\delta T_g}{\delta c_2}\right) \left(\frac{\delta c_2}{\delta \ln a_2}\right)_{T,P} \quad (4.11)$$

To study molecular level interactions using KBIs calculated using Eqs. (4.5) and (4.11), several fitting functions were required. Namely, enthalpy ( $\Delta H_g$ ), temperature of gelatinisation ( $T_g$ ) and salt activity ( $\mu_2 = \mu_2^0 + RT \ln a_2$ ) dependence on salt concentration ( $c_2$ ). These will be detailed in the section below.

## 4.3 Data processing methods

### 4.3.1 Enthalpy fitting

For enthalpy, continuous data is needed to use Eqns. (4.5) and (4.11) because  $T_g$  and  $H$  values at the same concentration are not always available. The enthalpy fitting equations, shown in Table 4.1, produced continuous data points for each salt studied. The fitting is shown in Figure 4.2 below.

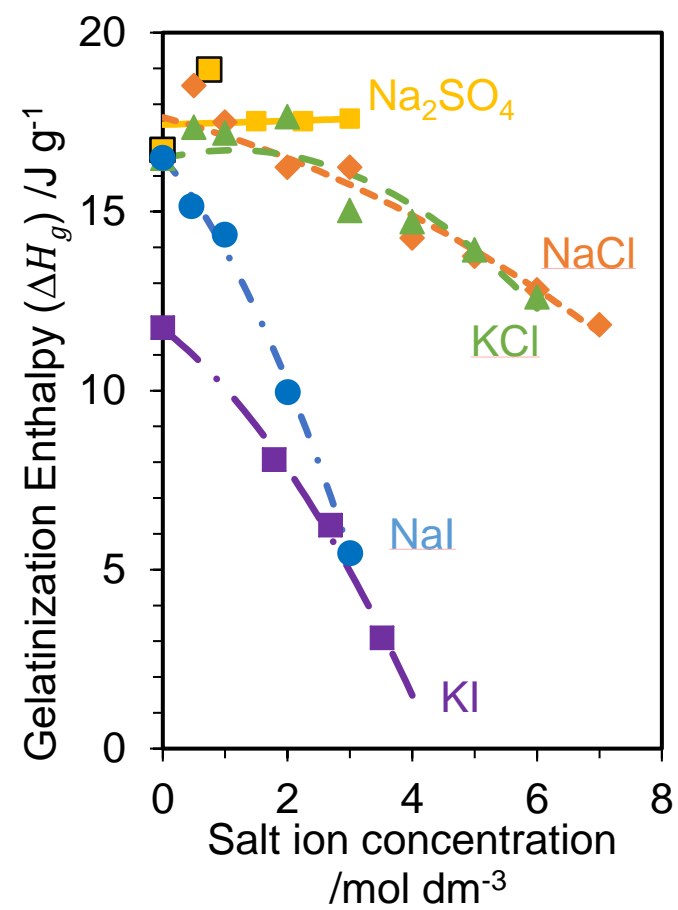


**Figure 4.2:** Fitting of enthalpy data collected from the literature<sup>1,2</sup> using parameters summarised in Table 4.1. Unfitted points highlighted with black outline.



It should be noted that, for the Na<sub>2</sub>SO<sub>4</sub> dataset, significant over-fitting was required to include all points, as such two points were excluded from the fitting. Hence, when those datapoints were used in calculations the individual point was calculated outside of the overall trend.

**Table 4.1:** Coefficients from the equation,  $\Delta H_g = A + Bc_2 + Cc_2^2$ , used for fitting calorimetric  $\Delta H_g$  data. These coefficients have no physical meaning and exist simply to provide a continuous set of data.

Salt	A	B	C
Na <sub>2</sub> SO <sub>4</sub>	17.43	0.053	0
NaI	16.50	-2.03	-0.552
KI	11.72	-2.70	-1.209
NaCl	17.63	-0.453	-0.058
KCl	16.48	0.420	-0.186

The  $T_g$  fitting was required to obtain  $\frac{\delta T_g}{\delta c_2}$ . Its fitting is shown in Figure 4.3 and Table 4.2 shows the equations and coefficients used.  $T_g$  and  $\Delta H_g$  data for NaCl, KCl, NaI and  $\text{Na}_2\text{SO}_4$  were obtained from Ahmad & Williams<sup>1</sup> and for KI was obtained from Jane.<sup>2</sup>

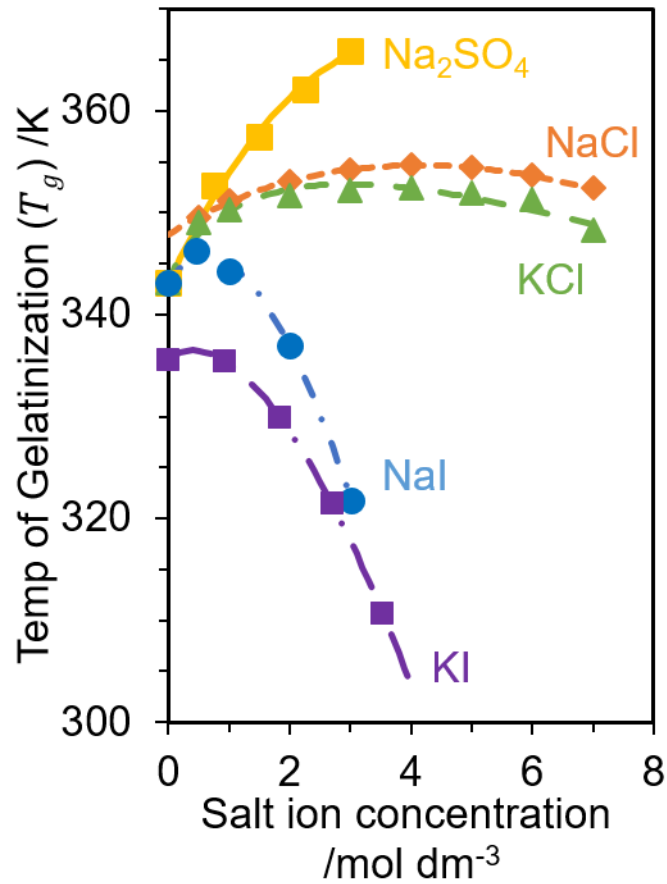


**Figure 4.3:** Fitting of  $T_g$  data from the literature<sup>1</sup> to obtain  $\frac{dT_g}{dc_2}$ , using parameters summarised in Table 4.2.

**Table 4.2:** Coefficients from the equation,  $T_g = A + Bc_2 + Cc_2^2 + Dc_2^Z$ , to fit experimental gelatinisation temperature data.

Salt	A	B	C	D	Z
Na <sub>2</sub> SO <sub>4</sub>	343.2	37.05	-14.72	0	0
NaI	343.1	9.483	-26.10	18.48	2.099
KI	335.6	13.22	0	-20.32	1.521
NaCl	347.9	3.920	-2.809	2.046	2.069
KCl	343.1	19.31	1.182	-185.1	1.044

### 4.3.2 Salt activity fitting

$\frac{\delta c_2}{\delta \ln a_2}$  is required for the calculation of preferential interaction via Eqs. 4.3, 4.5 and 4.11. The method for fitting activity data for  $\frac{\delta c_2}{\delta \ln a_2}$  is based on the same method established in Section 2.4 and expanded upon for use in starch gelatinisation in the Appendix.<sup>3,177</sup> The activity data used was from various sources.<sup>182,272-274</sup> Note that activity data for certain salts (KSCN and NaNO<sub>3</sub>) were not available at the temperature required; their dilute concentration behaviour has nevertheless been calculated. It should be noted here that these same fitting values were used to calculate the salt self-association provided by Eq. (4.9) through the straightforward relationship between  $\frac{\delta c_2}{\delta \ln a_2}$  and  $\frac{\delta \ln a_2}{\delta \ln c_2}$ .

From the values for  $\Delta H_g$ ,  $T_g$ ,  $\frac{\delta T_g}{\delta c_2}$  and  $\frac{\delta c_2}{\delta \ln a_2}$  obtained in this section, preferential interaction KBIs were calculated using Eqs. (4.3), (4.5) and (4.11). These are presented in Figure 4.4.

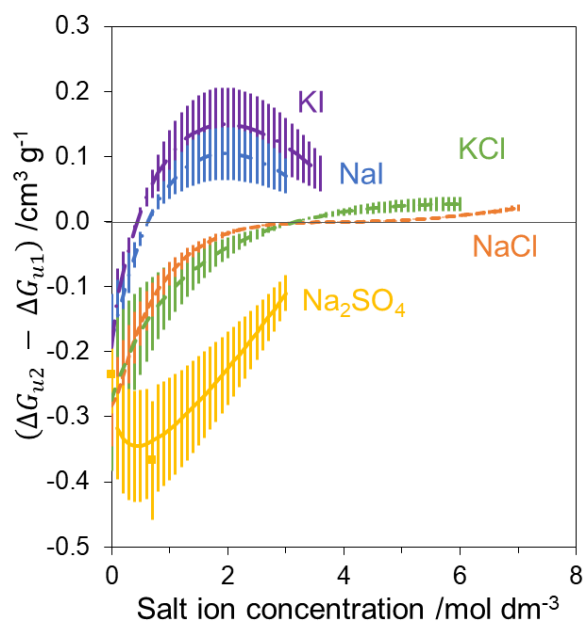


**Figure 4.4:** Preferential affinity of salt with starch or water with starch, described by  $\Delta G_{u2} - \Delta G_{u1}$  values from Eq. (4.11) for all of the salts studied, and its dependence on salt ion concentration. The individual data points in the  $\text{Na}_2\text{SO}_4$  dataset that lay outside of smoothed data fit (Figure 4.2) are denoted by yellow square markers.

Error bars, denoted in the style established in chapter 2 show that, despite fitting errors, the groupings according to cation remain consistent. It should be noted that, in the case of  $\text{Na}_2\text{SO}_4$ , the equations used to fit the data were simplified and some points lay far from the curve due to the small number of data points (Figure 4.2). In these cases, to avoid overfitting, the outlying data points were used in place of the smoothed data when calculating KBIs (Figure 4.4). This has led to a small number of individual points that lie slightly away from the curve (yellow squares). These points do not appear to break observed trends in the data.

## 4.4 Starch gelatinisation under dilute salt concentration

Based on the theory presented in Section 4.2, this section clarifies how salts affect gelatinisation through the starch-water and starch-salt average affinity changes that have been quantified via the KBI changes summarised in Figure 4.4. Preferential starch-salt interaction over starch-water interaction ( $\Delta G_{u2} - \Delta G_{u1}$ ) alone cannot explain the driving forces behind starch gelatinisation.

Consequently, individual contributions from salt and water to starch gelatinisation were calculated by Eqs. 4.7 and 4.8.

At low salt concentration, all the salts studied here (KCl, NaCl, Na<sub>2</sub>SO<sub>4</sub>, NaI and KI) raise the gelatinisation temperature. This salt-induced destabilisation of gelatinisation can be attributed to the dominant and large negative  $\Delta G_{u2}^0$  compared to the negligible contribution from  $\Delta G_{u1}^0$  (100-300 times smaller) seen in Table 4.3, where  $\Delta G_{u1}^0$  and  $\Delta G_{u2}^0$  denote KBIs under infinite salt dilution, calculated from Eqs. (4.7) and (4.8).

**Table 4.3:**  $\Delta G_{u1}^0$  and  $\Delta G_{u2}^0$  of a range of salts upon gelatinisation of sago and wheat (for KI only) starch.<sup>1,2</sup>

Salt	Na <sub>2</sub> SO <sub>4</sub>	NaNO <sub>3</sub>	KCl	NaCl	KI	NaI	KSCN
$\Delta G_{u2}^0$ (cm <sup>3</sup> g <sup>-1</sup> )	-0.63 ± 0.16	-0.5 ± 0.4	-0.39 ± 0.16	-0.34 ± 0.08	-0.040 ± 0.015	-0.19 ± 0.08	0.09 ± 0.06
$\Delta G_{u1}^0$ (cm <sup>3</sup> g <sup>-1</sup> )	0.0021± 0.0005	0.0021± 0.0005	0.0021± 0.0005	0.0021± 0.0005	0.0021± 0.0005	0.0021± 0.0005	0.0021± 0.0005

Errors for  $\Delta G_{u2}^0$  from fitting errors in  $\Delta V_u$  and  $\frac{\delta T_g}{\delta c_2}$ ,  $\Delta G_{u1}^0$  errors simply from fitting errors in  $\Delta V_u$  calculation. It should be noted that none of the error bounds lead to possible changes in sign.

The negligible contribution from  $\Delta G_{u1}^0$  is contradictory to the prevalent hypothesis that salt-induced gelatinisation change is driven by the starch hydration changes caused by the ion's effect on the "water structure".<sup>2,244,254</sup>

What, then, does the dominant contribution, i.e., the negative  $\Delta G_{u2}$  signify? The spectroscopic evidence demonstrates binding of cations to the OH groups of starch,<sup>1,2,245</sup> and the ability of anions to form complexes with amylose.<sup>275,276</sup> Considering that the direction of the transition for KBI changes is defined as granular  $\rightarrow$  gelatinised, this means that cations and/or anions at low concentration are bound more strongly to the pre-gelatinisation granular state than to the gelatinised state. This interpretation may seem at odds with the changes that take place upon gelatinisation, in particular the leaching of amylose into aqueous solution, since binding to aqueous amylose is possible in both anions and cations, one would expect an increase in binding.<sup>276,277</sup> Additionally, channels of amorphous starch, which are more easily penetrable upon gelatinisation, extend into the hilum (centre) of the starch granule.<sup>275,278,279</sup> This suggests that more area is available for binding. However, these apparent paradoxes between negative dilute  $\Delta G_{u2}$  values and the contributions which suggests binding should increase upon gelatinisation can be resolved by taking into account the following effects, on each ion, of the structural properties of starch granules:<sup>280,281</sup>

- 1) Extruded amylose "needles" have been observed for granules in solution, which has been referred to as the "hedgehog effect".<sup>282</sup> This expands the volume of the granule and hence the area which excludes salts.
- 2) Starch granules exhibit semi-permeable membrane-like behaviour on cations and whole salts, preventing them from entering the granule until a certain threshold of concentration is achieved (discussed later in this chapter), which explains how exclusion occurs mechanistically.

This semi-permeable membrane-like behaviour is likely present until the granule is fully diaphanous (i.e., translucent, swollen).<sup>283,284</sup> (Note that this effect is present in the endotherm for the initial stage of gelatinisation, which we focus on in this chapter).<sup>247</sup>

These features of the granule's structure lead to exclusion behaviour in both anions and cations at low salt concentration. Exclusion is used here to refer to the case where  $\Delta G_{u2}$  has a negative value.<sup>124,271</sup> This can be interpreted in terms of the definition of KBIs given in Eq. (4.4), which signify the distributions of salt ions or water molecules around starch. Indeed, any reduction in the distribution of co-solute molecules around the solute or surface is due to changes in their binding strength or access to the solute.<sup>113,123</sup>

The effect of the semi-permeable membrane-type behaviour of starch granules requires further discussion. It prevents cations from interacting with the majority of the constituent molecules of starch inside the granule.<sup>282,283</sup> Large negative  $\Delta G_{u2}$  at this concentration is consistent with this experimental observation. It should be noted that this "semi-permeable membrane"<sup>282,283</sup> is not strictly a semi-permeable membrane as defined in thermodynamics textbooks.<sup>285</sup> It excludes cations but not anions, which suggests that this phenomenon is an ion-interaction induced ion concentration difference mediated by the presence of the granule envelope.<sup>283</sup> Anions are able to penetrate into the granule from aqueous solution.<sup>282</sup> Therefore, some mechanistic barrier to their entry at low concentration must exist, leading to this reduction in access to the solute. These anion exclusion effects could be due to cation – anion pairing, with cations unable to enter the starch structure.<sup>282</sup> This suggestion is supported for low salt concentration because Figure 4.5 shows that there is minor salt self-accumulation at low concentration for all salts, as calculated by Eq. (4.9).

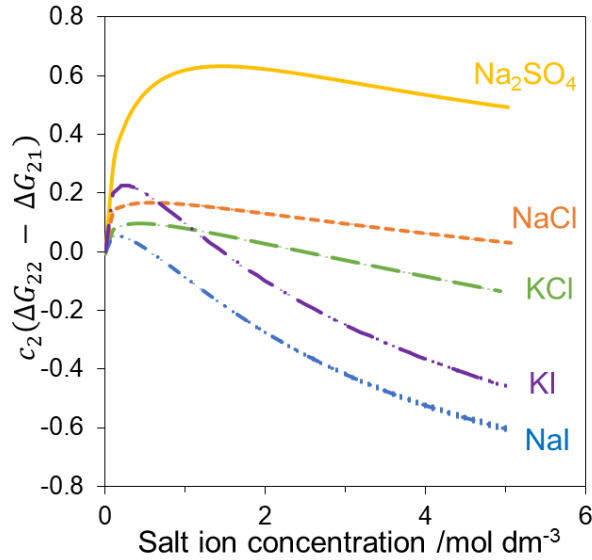


**Figure 4.5:**  $c_2(G_{22} - G_{21})$ , the salt ion self-association in bulk solution and its dependence on salt concentration. Calculated using Eq. (4.9).

It should be noted that error bars are included in Figure 4.5, however, they are negligible.

As an additional consideration, kinetic effects are likely not the cause of  $\Delta G_{u2}^0$ 's negative value,<sup>249</sup> even though heating rates are generally higher than responses in starch systems.<sup>286</sup> However, the relatively slow heating rate in the main source of our data (0.1 K min<sup>-1</sup> for all salts except KI)<sup>1</sup> shows little difference at infinite dilution from the comparatively faster heating rate for KI (10 K min<sup>-1</sup>).<sup>2</sup> This factor of 100 change in heating rate does not lead to a change in sign of  $\Delta G_{u2}^0$ , providing an evidence against the kinetic interpretation. (However, Shiotsubo and Takahashi concluded that heating rates of above 0.5 Kmin<sup>-1</sup> have contributions from kinetic limitations and hence any interpretations of the KI data have an additional assumption that it is not largely influenced by kinetic contributions which may not be accurate.<sup>250</sup>)

The dilute-salt KBIs have shown that, when transitioning from granule → gelatinised starch, there is no marked increase in binding of ions at low



concentration, instead salt exclusion is in effect. These contributions from both anions and cations lead to a negative  $\Delta G_{u2}^0$ . In contrast to the previous hypothesis that the ion binding on the granule state stabilises this state and hence hinders gelatinisation,<sup>2</sup> it is the difference in ionic affinity between the gelatinised and granular states as well as its dependence on ionic strength that is crucial in this case.

It is interesting to note that the weaker co-solute interaction with the gelatinised state can also be observed for sugars (Table 4.4), which also exhibit dominant, albeit lower in magnitude, negative  $\Delta G_{u2}^0$  values as the driving force for the suppression of gelatinisation. (Sugars, as co-solutes, in fact show no  $T_g$  decrease).<sup>256</sup>

**Table 4.4:** Dilution limit KBIs of a range of monosaccharides upon gelatinisation of sago starch.<sup>256</sup>

Sugar	Maltose	Fructose	Glucose	Ribose
$\Delta G_{u2}^0$ ( $\text{cm}^3 \text{g}^{-1}$ )	-0.047	-0.018	-0.013	-0.0021

Sugars are widely known to be preferentially excluded from the biomolecular surfaces, through which more compact conformational states (native protein structures, aggregates or gels) are stabilised.<sup>174</sup> The fact that sugars and salts both show negative  $\Delta G_{u2}^0$  values on gelatinisation suggest that exclusion contributes to the mechanism of gelatinisation as sugars do not demonstrate stoichiometric binding and their mechanism is more significantly influenced by exclusion.<sup>174</sup> Hence, the structural properties of the granule in its gelatinised state may play a key role in how co-solutes modulate gelatinisation.

## 4.5. Starch gelatinisation under increased salt concentration

### 4.5.1. The origin of the $T_g$ maxima

The above sections have shown that the salt effect on starch gelatinisation at  $c_2 \rightarrow 0$  is dominated by a large negative change of  $\Delta G_{u2}$ , which originates from a significant reduction of salt-starch interaction when the starch gelatinises. Here, this view will be extended to observe how  $\Delta G_{u2}$  changes with the concentration of salts, aiming at drawing a molecular picture from the calculated KBIs. Because of the lack of literature data on  $\Delta V_g$  along salt concentrations of different salts, we cannot use Eqs. (4.3) and (4.4) to separate  $\Delta G_{u1}$  and  $\Delta G_{u2}$ . However, it is possible to calculate the difference  $\Delta G_{u2} - \Delta G_{u1}$  via Eqs. (4.4) and (4.11) from  $\frac{\Delta H_g}{T_g} \frac{\delta T_g}{\delta \mu_2}$  for all salts. Figures 4.2 and 4.3 show that  $T_g$  goes through a maximum in all salts studied except  $\text{Na}_2\text{SO}_4$ . Consequently, at the corresponding salt concentration,  $\Delta G_{u2} - \Delta G_{u1}$  changes its sign from negative to positive (Figure 4.4). This KBI sign change will be rationalised in this section on a molecular basis.

Figure 4.4 demonstrates that preferential salt-starch binding in the gelatinised state, signified by a positive  $\Delta G_{u2} - \Delta G_{u1}$  value, promotes gelatinisation. Preferential salt-starch binding occurs when changes in salt ion binding overcomes the contributions from changes in exclusion and starch-water interaction. Changing the anions significantly effects the dependence of  $\Delta G_{u2} - \Delta G_{u1}$  on concentration, whereas changing the cation does not, as demonstrated by the grouping of anions in Figure 4.5. This corroborates the evidence in the literature suggesting that anion binding changes are most important in determining overall binding changes,<sup>1,2,282</sup> and can also inform our understanding of the mechanism:

- Salts with  $\text{I}^-$  anions'  $\Delta G_{u2} - \Delta G_{u1}$  values start negative and quickly become positive with addition of salt. These anions are capable of forming

inclusion complexes with starch and overcome the exclusion forces to pass more easily into the granule<sup>276</sup>. Therefore, penetrated anions promote gelatinisation to occur from the hilum outward, as it does in pure water<sup>275,278,282</sup>.

- Salts with Cl<sup>-</sup> anions require a higher concentration to overcome the exclusion forces as demonstrated by Figure 4.4. This suggests that they would be more likely to bind externally or just inside the channels. Salt ions therefore have less access to starch molecules within the granule and promote gelatinisation from the periphery. This peripheral gelatinisation has been seen in LiCl and CaCl<sub>2</sub> most notably.<sup>2,283</sup>
- Finally SO<sub>4</sub><sup>2-</sup> anions, within the data range studied,<sup>1</sup> do not overcome the exclusion forces and, from Figure 4.3, do not reduce the  $T_g$  at any salt concentration. This suggests that their inability to penetrate the granule, or to access enough starch for significant binding (due to exclusion), prevents them from assisting in gelatinization.

#### 4.5.2. Salt accessibility to, and association with, starch

The changes that occur in  $\Delta G_{u2} - \Delta G_{u1}$  can therefore be attributed to the salt's accessibility to the starch rather than water's, which is always present in the hilum. Indeed, the increasing  $\Delta G_{u2} - \Delta G_{u1}$  indicates that salt-gelatinized affinity becomes stronger than salt-granular at higher salt concentrations. Supporting this with the following spectroscopic, microscopic and swelling data in the literature can give us a stronger interpretation of what is occurring.

Firstly, increased salt accessibility to the gelatinised state at higher salt concentrations is possible when there is a significant salt-dependent structural change that opens up the gelatinised surface or strong salt ion binding. Experimental evidence for this comes from the salt-dependent swelling change

observed by DSC <sup>270</sup> and optical microscopy <sup>287,288</sup>. Secondly, the strength of conjugation of anions with their cations reduces the anion binding in gelatinized starch <sup>282</sup>. This discovery, which is based on short range NMR measurements, still holds true for longer ranges as quantified by  $c_2(G_{22} - G_{21})$ , in Figure 4.5.

This term signifies preferential salt self-association for the bulk solution in this system, thereby supporting this relationship between bulk phase ion self-association and the binding strength of the anion. As  $c_2$  increases, in Figure 4.5, we can observe this relationship:

- $\text{Na}_2\text{SO}_4$  shows strong self-association, and consequently does not demonstrate dominant binding in the gelatinized state.
- $\text{NaCl}$  and  $\text{NaI}$  show minor self-association with very minor dissociation at higher  $c_2$ . Their gelatinized state binding increase requires more salt ions than potassium salts.
- $\text{KCl}$  and  $\text{KI}$  initially show a change from minor self-association to minor self-dissociation. They demonstrate faster increases in gelatinized state binding.

This further supports the dominance of salt-starch binding effects and helps to explain the mechanism behind  $\Delta G_{u2}$  sign changes. It should be noted that salt accumulation itself is a secondary effect and does not directly change the sign of  $\Delta G_{u2}$ .

## 4.6. Advantages over the current polymer theory

### 4.6.1. Quantifying co-solute exclusion

We have shown that the change from co-solute exclusion from the gelatinized state at lower concentration to co-solute binding is responsible for the existence of the peak in  $T_g$ . Indeed, all salts in dilution studied in this chapter counteract gelatinization because they are more excluded from the gelatinized state than from the granular state. Such exclusion can be quantified as the negative contribution to KBIs. In contrast, the approaches based on polymer theory relies on the Flory  $\chi$  parameter<sup>251,289</sup>, which is the difference in the contact energies. Because  $\chi$  parameters are based solely on contact energies in the lattice model, it cannot easily deal with the free energy contribution arising from the exclusion of co-solutes, as has been recognised in biophysics, for a long time, in terms of the crowding effect.<sup>290</sup> The theory of co-solutes based on KBIs can naturally handle crowding and binding alike.

### 4.6.2. Other processes involving starch

The advantages of the approach proposed here for gelatinisation can naturally be extended to other processes involving starch, such as retrogradation and the salt effect thereupon. The prevalent approach in the literature is to start from the starch-water system as the reference state, and to consider how salt affects starch hydration<sup>291</sup>. According to this view, salt affects retrogradation by predominantly disturbing hydrogen bonding and water structure, which is a view similar to gelatinisation<sup>292</sup>. Still, as we have shown in this chapter, a presumed link between salt-induced hydration changes and the state change in starch have never been linked in a quantitative manner. However, a potential difficulty in extending our current approach to retrogradation would be the two-step

characteristics of the retrogradation process due to the different crystallization behaviours of amylose and amylopectin <sup>293</sup>.

### 4.6.3 Extension and application to cellulose

The advantages of this method over other approaches to understanding polymer systems highlighted above (4.5.1) could also be beneficial when applied to cellulose. Swelling and gelation are macroscopic shifts in the structure of cellulose in solvents. Theoretical understanding of these processes is, for the most part, based on a step by step description of what happens during the process as opposed to the molecular interactions.<sup>294</sup> Hydrogel systems, at least in Methyl - Cellulose are reversible, maintain equilibrium at isothermal conditions and are thermo-dependent. There appears to be a "gelation" transition occurring in the DSC that can be measured.<sup>295</sup>

Gelation is defined as the "process of random linking of subunits to larger and larger molecules by formation of an infinite network...", which defines a critical "gel point" where the system behaves neither as "liquid nor as a solid on any length scale."<sup>296</sup> In general, chemical gelation with covalent bonds are irreversible and physical gels due to entanglements or ion crosslinking are reversible.<sup>296</sup> Reversible gelation occurs via sol-gel transition.<sup>296,297</sup>

Using a well-defined transition, such as the sol-gel transition, statistical thermodynamic theory similar to the one defined in this chapter could be applied to cellulose. These transitions are generally limited to functionalised cellulose. This theory could be applied to understand the interactions which drive these transitions, allowing for more intelligently designed hydrogels or for a greater understanding of the precipitation point.

## 4.7. Conclusion

Understanding the gelatinisation of starch requires a theoretical framework that can extract microscopic information from the literature's abundant experimental data in a quantitative manner. This chapter has used recent developments in statistical thermodynamics and adapted them to extract the starch-water and starch-salt affinity changes that occur during gelatinisation, in a manner beyond the capabilities of traditional polymer theory. How the temperature of gelatinisation depends on salt concentration can be rationalised by the exclusion of salts at low salt concentrations from the gelatinised state and salt anion accessibility to the inside of the starch granule at increased concentration. Briefly, at low salt concentrations, salts are excluded from the surface of gelatinised starch. However, when reaching a higher salt concentration, this exclusion is overcome, allowing salt anions to penetrate the gelatinised granule and bind within. This means that once preferential binding of salt ions over water molecules is reached, gelatinisation temperature begins to decrease. Furthermore, the mechanism that leads to the increases of salt binding upon gelatinisation at high concentrations has been discussed. Showing the importance of salt-starch interactions when compared to water-starch interactions (Section 4.4), contrary to historical assumptions, and to include discussion about the influence of starch structural components on binding to the gelatinised state. Finally, it was noted that the salt anion accessibility informs whether gelatinisation progresses from the hilum or the periphery of the starch granule.

The theory in this chapter has attributed the suppression of gelatinisation at low salt concentrations to the exclusion of salts from the gelatinised state. Such an exclusion effect, recognised in biophysics as one of the dominant roles of

some co-solutes, has been beyond the reach of the polymer theory,<sup>251</sup> for whom the interaction is defined in terms of the contact energy differences.

The gelatinisation temperature goes through maximum at higher salt concentrations, whose cause has been identified as the increase of salt binding on the gelatinised state, as has been inferred by experiments.<sup>2</sup> The increase of salt binding is tied to salt accessibility to the inside of the starch granule. This accessibility has been shown to inform whether gelatinisation progresses from the hilum or the periphery of the starch granule, in support of evidence presented by Jane. The negligible contribution of changes in water effects demonstrated here does not agree with the traditional approaches that have attempted to attribute the salt effect to the change of starch hydration.

The methodology from the present study could also be applied to important processes involving cellulose, such as swelling and gelation, where reversible transitions are present. This is possible due to the general nature of this theory and its application to transition processes. However, elucidating molecular interactions becomes more difficult for processes such as gelation and gelatinisation when compared to solvation. As demonstrated in this chapter, macrostructures lead to a need for a much larger number of additional structural measurements to clarify the meaning of the KB parameters.



## CHAPTER 5: CONCLUSION AND FUTURE WORK

The goals of this thesis were threefold. Firstly, to apply a statistical thermodynamic theory to understand the microscopic interactions that drive cellulose solubility. Secondly, to extend this statistical thermodynamic theory to particles as opposed to molecules which enabled studies into gelatinisation and gelation of polysaccharides. And thirdly, to circumvent quantification issues that are present when acquiring solubility data which is critical for such studies.

Significant progress has been made on all of these goals. This progress and the future work remaining to complete these goals will be summarised in this chapter.

### 5.1 Insights into the mechanism of cellulose solubility in aqueous solvents

Knowledge of the driving forces or properties of cellulose that lead to insolubility have been well established in previous research (Chapter 1). A simple summary of this knowledge is that (1) hydrogen bonding causes interactions which must be disrupted and (2) hydrophobicity causes instability in solution that requires stabilisation (alleviation).

The studies in this thesis have focused on dissolved cellulose in solution. This allowed clarification of the interactions present in solvents which are able to dissolve cellulose and therefore overcome the above driving forces. These interactions appear to be dependent on the solvent used to dissolve cellulose. In electrolyte solutions, two prominent molecular interactions were identified within the dissolution mechanism of cellobiose (Chapter 2). Through KB theory the dominance of each contribution was quantified to show that ion accumulation (which matches with the “charging up” hypothesis in cellulose) was the dominant factor in solubilisation. Through examining changes in the water

structure this chapter contradicted the hypothesis that hydrophobicity is important in electrolyte solutions of cellulose. This result suggested that the competition between water-cellobiose and salt-cellobiose interactions is the most important molecular level driving force for solubilisation.

## 5.2. Improvements to the experimental quantification of cellulose solubility

Cellulose solubility in poor solvents cannot be quantified, to an accuracy which is acceptable for theoretical applications, due to a number of problems which have been clarified in chapter 3. The most impactful of these problems being incomplete dissolution (ID), the fractionation of solute into dissolved and undissolved states below the saturation point, which is present in cellulose samples of  $> 40$  DP. The presence of incomplete dissolution leads to a significant and systematic error in solubility quantification of cellulose. The mechanism for ID of amorphous cellulose was determined to be solute induced self-aggregation at equilibrium dependent on the presence of longer chain ( $> 100$  DP) cellulose molecules in the sample.

The importance of the choice of sample in solubility experiments has been highlighted (Chapter 3). Reducing DP of cellulose reduces the extent of incomplete dissolution which makes accurate solubility quantification easier. However, an analogue can only be used to investigate a property of cellulose it retains; how it differs from cellulose in terms of dissolution mechanism must be considered. Water soluble oligomers such as cellobiose therefore struggle to reproduce the hydrophobic nature of cellulose. An oligomer analogue of between 10 and 40 DP would therefore likely provide an adequate representation of cellulose interactions as water soluble cellulose oligomers typically have  $DP < 10$ .<sup>59</sup> Above 40 ID becomes a significant problem (Chapter 3). If this analogue has a well resolved DP, this would allow for accurate solubility

quantification. Isogai et al provide a method to produce a DP 15 oligomer consistently,<sup>58</sup> with an increased duration of hydrolysis when compared to the hydrolysed sample in chapter 3.

On the other hand, higher DP cellulose should be used in cases where an investigation into cellulose dissolution mechanisms aims to understand the influence of macroscopic structures of cellulose (Section 1.2). Consequently, improvements or replacements for existing quantification methods should be established because solubility measurements which use cellulose suffer from incomplete dissolution (Chapter 3). Chapter 3 suggested improvements using analytical quantification (SEC-MALLS). Alternatively, solubility could be quantified by measurement and analysis of the full solubility profile of a sample with respect to added solute (Figure 3.2).

This section has highlighted important problems to be considered for poor solvents and inhomogeneous samples. These insights should help to inform future experiments to produce accurate measurements which can be used in theoretical analysis.

### 5.3. Future work based on this thesis

For a complete resolution of the questions posed in this thesis, research is required into (1) further experimental improvements towards quantitative solubility measurements and (2) addition data and analysis to reveal aspects of the cellulose dissolution mechanism that have not been completely resolved.

#### 5.3.1 Experimental improvements

**Understanding the impact of filtration or centrifugation on quality of supernatant sampling**

Setting aside incomplete dissolution, separation of the undissolved solute aggregates from saturated supernatant appears to have an impact on the accuracy of all non-optical solubility methods, although the extent of its impact is unknown (Section 3.3.6). Continued use of these methods requires an understanding of whether to use filtration or centrifugation.

Gale et al have suggested that cellulose solutions which are too viscous cannot be filtrated.<sup>93</sup> There are examples of use of filtration in cellulose solutions,<sup>298</sup> although many are filtering derivatised cellulose.<sup>38,299</sup> Hence, an investigation into the limit at which filtration could be used would enable filtration as an option for separation of supernatant samples (Chapter 3).

Centrifugation has been shown to lead to losses in material.<sup>300</sup> However, there is an additional consideration that incomplete sedimentation of aggregates, when sampling supernatant without filtration, could lead to overestimation of the quantity of cellulose dissolved. A rigorous study of the samples produced from varying centrifugation methods in each solvent could resolve this by revealing an optimal method for each solvent.

### 5.3.2 Additional research into dissolution mechanism

The insights gained from this thesis into the dissolution of cellulose raise further questions. Chapter 2 highlighted the importance of ion accumulation around cellobiose in electrolyte solution. Whether this persists to higher DP cellulose requires confirmation by experiment. In addition to this, the gaps in understanding of the cellulose dissolution mechanism provide significant opportunity for research.

#### **Applying thermodynamics to understand cellulose solubility driving forces**

Cellulose dissolution is governed by the principles of thermodynamics.<sup>118</sup> Hence, the contribution from possible driving forces of solubilisation can be

quantified in terms of their respective contribution to thermodynamic quantities, such as the Gibbs free energy when dissolution takes place under constant temperature and pressure. In addition, how solubility changes with temperature is not only an important practical question when optimising dissolution condition but also a thermodynamic question, whose driving forces can be understood by the use of entropy and enthalpy.

Chapter 2 implemented KB theory to understand molecular interactions related to water structuring and hydrophobicity in a case where temperature dependence is “traditional” (ie increases with increasing T). This showed that, at a molecular level, water structuring is not alleviated by addition of salts. Suggesting that hydrophobicity is not the driving force in electrolyte solutions. However, cellobiose does not have the same water solubility as cellulose. This leads to motivation for a study into anomalous temperature dependence using cellulose samples of higher DP, which are not water soluble.

Hydroxide solutions show anomalous solubility behaviour, where cellulose dissolution becomes more prominent at low temperature.<sup>103,137</sup> Bergenstråhle-Wölert et al have implied, through simulation, the presence of hydrophobicity in this mechanism.<sup>137</sup> A rigorous study based on these initial results could confirm the presence of hydrophobicity as a driving force in this dissolution mechanism and eventually, combined with KB theory, lead to a complete determination of the dissolution mechanism in this solvent.

### **Simulation to complete the molecular level picture of cellulose’s dissolution mechanism**

Some driving forces and molecular interactions present in some cellulose solutions have been established, through KBIs, in this thesis. To clarify the exact interaction within the molecular-based mechanism of the role of individual ions

on KBIs and solubility, an extensive molecular dynamics simulation is required, following recent progress in protein simulation's resolution of the same problem.<sup>301</sup>

Having singled out preferential interaction as the dominant driving force of the Hofmeister effect for cellobiose (Chapter 2), the next step is to elucidate the mechanism of preferential interaction on a molecular basis. If a recent computational approach,<sup>302</sup> based on the KB theory of solutions could be translated to use in polysaccharides, individual molecular level interactions that make up preferential ion-cellulose affinity could be specified. This computational approach applies statistical thermodynamics to quantify the effect of different types of electrostatic and non-electrostatic interactions (including configurational and excluded volume effects) on how ions affect protein stability. If this type of simulation were applicable to cellulose, the ability to elucidate these effects would be ideal for resolving remaining questions about cellulose's solvation mechanism.

Alternatively, an approach which has seen some use in the cellulose field, molecular dynamics (MD), could be applied. Some simulations using this method have provided valuable insights into cellulose solution driving forces.<sup>137,162</sup> Hence, MD could be applied to simulate exact positions and arrangements of the cellulose molecules which could also reveal a complete molecular picture of the dissolution mechanism when coupled with KBIs.

Those who specialise in these fields would have greater insight into the optimal method for determining the molecular based mechanism. MD has been more frequently applied to cellulose and therefore groundwork has already been laid. However, statistical thermodynamics simulations rely on the same experimental solution parameters as KBIs and the same assumptions as KB theory.<sup>303</sup>

## **Extending KB theory to cellulose particles**

Chapter 4 successfully extended KB theory, with some additional assumptions, to focus on the interactions of larger scale particles with solvent components. This allowed for some insights into the starch gelatinisation mechanism which more clearly explain the effect of salts on the macroscopic starch granules. Using this chapter as a guide it should be possible to study gelation, a well-defined transition which cellulose and its derivatives can undergo, and the interactions which influence it. Where a gelation or precipitation is reversible, this extended macro-scale KB theory is useful (Section 4.6.3), in fact, similar methods have already been applied to gelation in other polysaccharides.<sup>124,174</sup>

Hydrogels are an important upcoming cellulose material with applications in medicine and bio-materials (Section 1.1).<sup>77</sup> A study based on the theory developed in Chapter 4 could aid in future intelligent design of hydrogels, whose tuneable properties are already being developed.<sup>23,294,304</sup>

## Final thoughts...

This thesis has demonstrated well the efficacy of using solution theory developed from the basis Kirkwood and Buff laid out in the 50s.<sup>119</sup> The many developments since have provided a platform of statistical thermodynamic theory which can be applied to a huge range of solutions.<sup>113,305-308</sup> Using some of these developments, this thesis and work that leads on from it can produce a full molecular level mechanism of cellulose dissolution and other polysaccharides. Although these lofty goals are the end point that I hope to achieve, much ground work still remains, as demonstrated by the need for Chapter 3. It is my hope that any who read this text see the benefit to the cellulose community that this work should provide.



## Appendix – Fitting and methodology for salt activities in starch systems

This appendix describes the full method of salt activity fitting in the context of starch gelatinisation (chapter 4), this method is almost identical to the one used in chapter 2, however differs in requirements for preferential interaction as shown in Eq. A1.

### Concentration dependence of salt activity

A value of  $\frac{1}{c_2} \frac{\delta c_2}{\delta \ln a_2}$  is required for the calculation of Eqs. (4.5) and (4.9), using Eq. (4.11).

From Eqs. (4.3), (4.5) and (4.11) in the main text:

$$\Delta G_{u2} - \Delta G_{u1} = -\frac{1}{c_2} \left( \frac{\partial \Delta \mu_u}{\partial \mu_2} \right)_{T,P} = -\frac{1}{c_2} \frac{\Delta H_g}{T_g} \frac{\delta T_g}{\delta \mu_2} = -\frac{1}{c_2} \frac{\Delta H_g}{RT_g^2} \left( \frac{\delta T_g}{\delta c_2} \right) \left( \frac{\delta c_2}{\delta \ln a_2} \right)_{T,P} \quad (\text{A1})$$

and similarly, from Eq. (4.9):

$$\frac{1}{1+c_2(G_{22}-G_{21})} = \left( \frac{\partial \ln a_2}{\partial \ln c_2} \right)_{T,P} = c_2 \left( \frac{\partial \ln a_2}{\partial c_2} \right)_{T,P} \quad (\text{A2})$$

This can be obtained from osmotic coefficient ( $\varphi$ ) data for salts at close to  $T_g$ , which is available in the literature for some of the salts studied. The fitting of

$\frac{\delta c_2}{\delta \ln a_2}$  requires electrolyte activity models which have been adapted from

Robinson and Stokes by addition of the final two terms of the following equation:<sup>3,177</sup>

$$\frac{\partial \ln \gamma_2}{dm_2} = -\frac{\alpha}{2\sqrt{m_2}} \left( \frac{1}{(1+\beta\sqrt{m_2})^2} \right) + 2c + 3dm_2 \quad (\text{A3})$$

The parameters  $\alpha$ ,  $\beta$ ,  $c$  and  $d$  are obtained using fittings based on  $\varphi$  as described in Section 2.4. The fittings are displayed below in the section “Activity Fitting” below.

Eq. (A3) can be rewritten in terms of the molarity concentration scale ( $c_2$ ).

$$m_2 \frac{\partial \ln a_2}{\partial c_2} = m_2 \left( \frac{\partial \ln \gamma_2}{\partial m_2} + \frac{\partial \ln m_2}{\partial m_2} \right) \frac{dm_2}{dc_2} \quad (\text{A4})$$

$$= \frac{dm_2}{dc_2} \left[ \left( -\frac{\alpha}{2} \left( \frac{\sqrt{m_2}}{(1+\beta\sqrt{m_2})^2} \right) + 2cm_2 + 3dm_2^2 \right) + 1 \right]$$

Note that the presence of the multiplier  $m_2$  is to avoid dividing by zero as  $m_2 \rightarrow 0$ .

Converting  $m_2$  to  $c_2$  yields  $c_2 \left( \frac{\partial \ln a_2}{\partial c_2} \right)_{T,P}$  which can be inverted for its use in Eq. (A1).

### Activity fitting (Osmotic coefficients)

Here we obtain the fitting parameters  $\alpha, \beta, c$  and  $d$  from experimental osmotic coefficients ( $\phi$ ). This fitting uses the following expression for  $\phi$ , equivalent to Eq. (2.12), from which Eq. (A3) can be directly calculated:

$$\phi = 1 - \frac{\alpha\sqrt{m}}{3} \left( \frac{3}{(\beta\sqrt{m})^3} \left[ 1 + \beta\sqrt{m} - 2 \ln(1 + \beta\sqrt{m}) - \frac{1}{1+\beta\sqrt{m}} \right] \right) + cm + dm^2 \quad (\text{A5})$$

to produce a functional form which is able to fit to a range of osmotic coefficient data. It should be noted here that this is based on an empirical model which is supposed to approximate the value of osmotic coefficients (by Robinson and Stokes)<sup>177</sup>, its only goal is to provide a high quality fit to a range of data inputs in a form that allows differentiation to produce  $\frac{\partial \ln \gamma_2}{\partial m_2}$  using the relationship between  $\phi$  and  $\ln \gamma_2^m$  which is quickly obtainable from Eq. (2.10) and the definition of the molal activity coefficient ( $\gamma_2^m$ )  $\rightarrow (a_2 = m_2 \gamma_2^m)$ :

$$\ln \phi \ln x_2 = \ln a_2 = \ln(m_2 \gamma_2^m) = \ln m_2 + \ln \gamma_2^m \quad (\text{A6})$$

based on a method developed by Robinson and Stokes. A comparison of fitting data vs experimental data is included here for the fitting used to determine water activity in solutions for chapter 4.

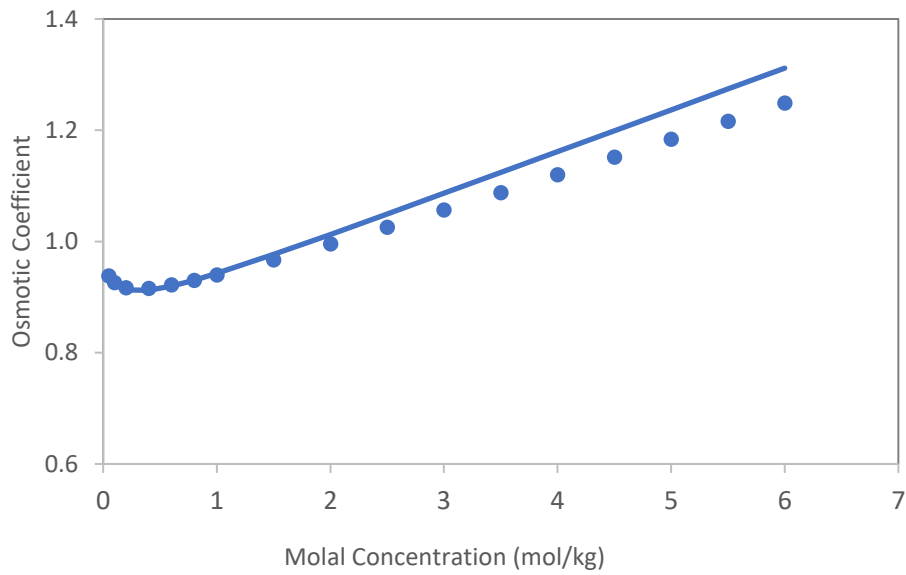


**Figure A.1:** Osmotic coefficient of NaCl at 348K (75 °C).<sup>309</sup>

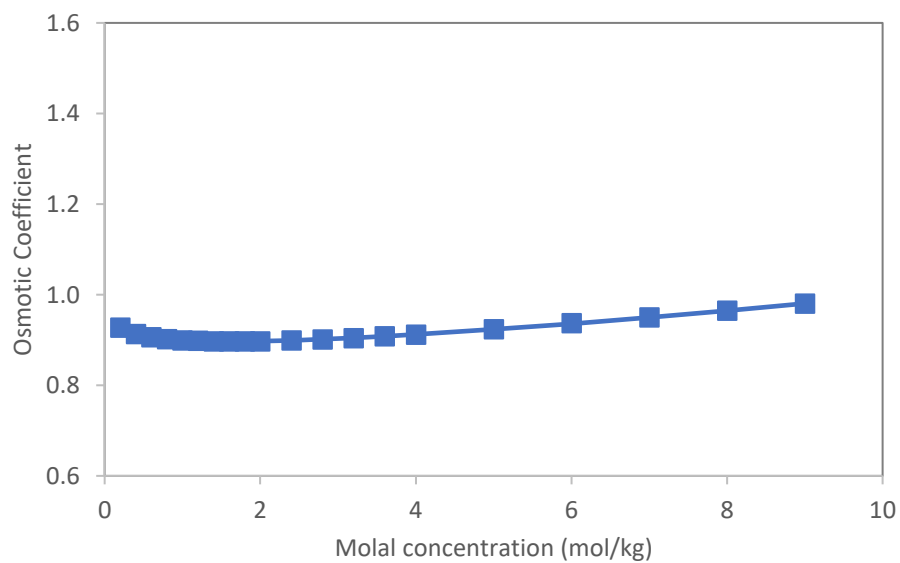


**Figure A.2:** Osmotic coefficient of KCl at 353K (80 °C).<sup>273</sup>

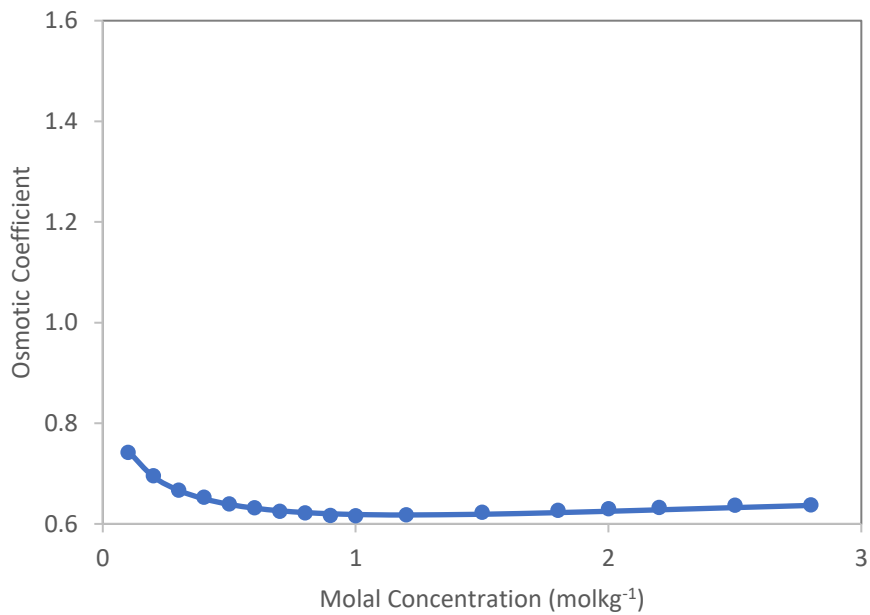


**Figure A.3:** Osmotic coefficient of Na<sub>2</sub>SO<sub>4</sub> at 353K (80 °C).<sup>274</sup>

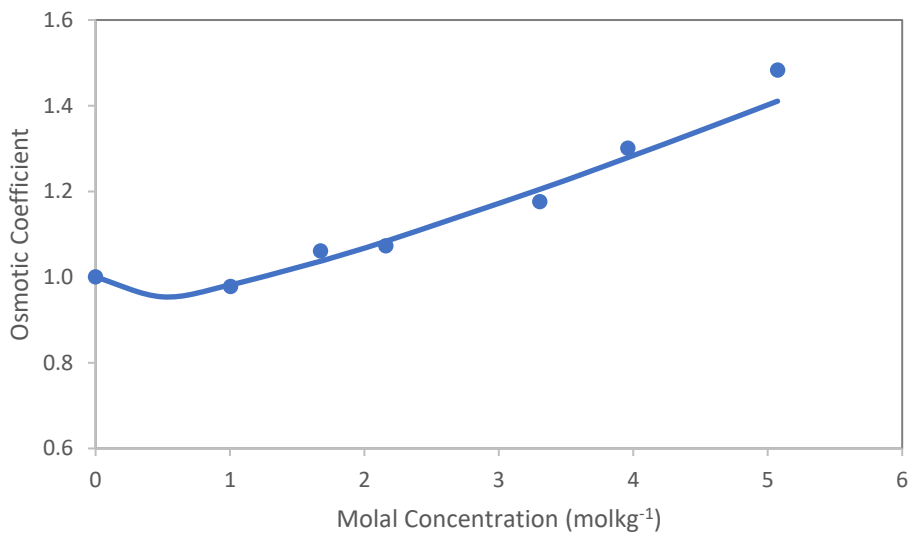


**Figure A.4:** Osmotic coefficient of NaI at 353K (80 °C) (extrapolated from trend seen in reference).<sup>272</sup>

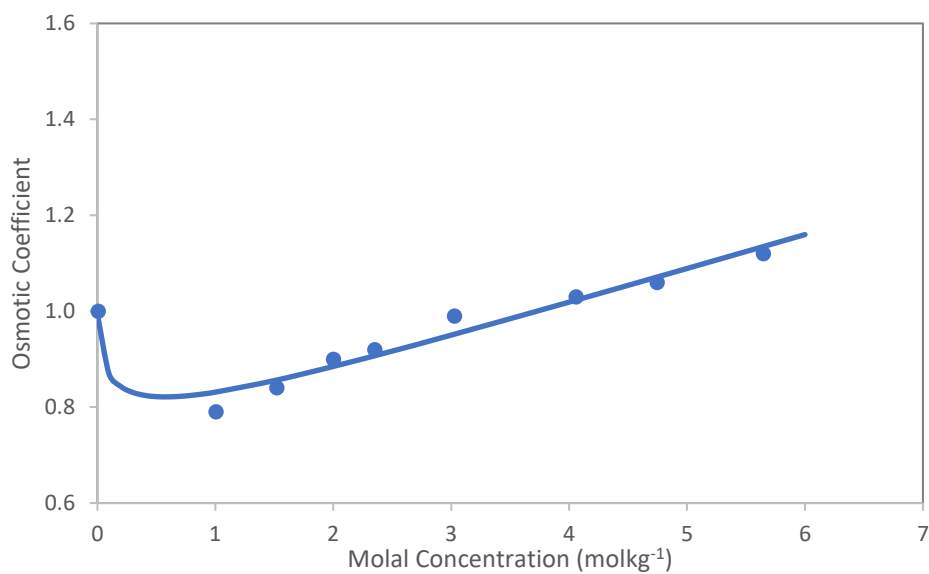


**Figure A.5:** Osmotic coefficient of KI at 333K (60C).<sup>272</sup>

The fitting coefficients for Eq. (A5) obtained are shown in the table below.

**Table A.1:** Fitting coefficients for osmotic coefficient in equation A5.

Salt	a	b	c	d
NaCl	0.707	0.7158	0.02213	0.0008313
KCl	0.7669	0.7461	0.006698	0.0004836
Na <sub>2</sub> SO <sub>4</sub>	1.088	3.835	0.02949	-0.003654
NaI	0.536	0.002508	0.1596	0
KI	1.921	0.9032	0.06769	0

## References

- 1 F. B. Ahmad and P. A. Williams, *Biopolymers*, 1999, **50**, 401–412.
- 2 J. L. Jane, *Starch - Stärke*, 1993, **45**, 161–166.
- 3 T. W. J. Nicol, N. Isobe, J. H. Clark and S. Shimizu, *Phys. Chem. Chem. Phys.*, 2017, **19**, 23106–23112.
- 4 T. W. J. Nicol, N. Isobe, J. H. Clark, N. Matubayasi and S. Shimizu, *Food Hydrocoll.*, 2019, **87**, 593–601.
- 5 M. Pauly and K. Keegstra, *Plant J.*, 2008, **54**, 559–568.
- 6 J. D. DeMartini, S. Pattathil, J. S. Miller, H. Li, M. G. Hahn and C. E. Wyman, *Energy Environ. Sci.*, 2013, **6**, 898.
- 7 B. P. Mooney, *Biochem J*, 2009, **418**, 219–232.
- 8 V. Menon and M. Rao, *Prog. Energy Combust. Sci.*, 2012, **38**, 522–550.
- 9 N. Reddy and Y. Yang, *Trends Biotechnol.*, 2005, **23**, 22–27.
- 10 A. D. French, *Cellulose*, 2017, **24**, 4605–4609.
- 11 D. J. Cosgrove, *Plant Physiol. Biochem.*, 2000, **38**, 109–124.
- 12 B. G. Davis, *Carbohydrate Chemistry*, Oxford University Press, Oxford, 2002.
- 13 C. Olsson and G. Westm, in *Cellulose - Fundamental Aspects*, InTech, 2013, pp. 143–178.
- 14 D. Klemm, B. Heublein, H. P. Fink and A. Bohn, *Angew. Chemie - Int. Ed.*, 2005, **44**, 3358–3393.
- 15 M. Sinnott, in *Carbohydrate Chemistry and Biochemistry: Structure and Mechanism*, The Royal Society of Chemistry, Cambridge, 2007, pp. 276–281.
- 16 R. Karnani, M. Krishnan and R. Narayan, *Polym. Eng. Sci.*, 1997, **37**, 476–483.

- 17 A. K. Mohanty, M. Misra and G. Hinrichsen, *Macromol. Mater. Eng.*, 2000, **276–277**, 1–24.
- 18 J. Tiller, P. Berlin and D. Klemm, *Biotechnol. Appl. Biochem.*, 1999, **30 ( Pt 2)**, 155–62.
- 19 C. Liu and H. Baumann, *Carbohydr. Res.*, 2002, **337**, 1297–1307.
- 20 H. Dong, J. F. Snyder, D. T. Tran and J. L. Leadore, *Carbohydr. Polym.*, 2013, **95**, 760–767.
- 21 H. Zhang, F. Zhang and J. Wu, *React. Funct. Polym.*, 2013, **73**, 923–928.
- 22 A. C. Jen, M. C. Wake and A. G. Mikos, *Biotechnol. Bioeng.*, 1996, **50**, 357–364.
- 23 N. Isobe, T. Komamiya, S. Kimura, U.-J. Kim and M. Wada, *Int. J. Biol. Macromol.*, 2018, **117**, 625–631.
- 24 C. Chang and L. Zhang, *Carbohydr. Polym.*, 2011, **84**, 40–53.
- 25 A. K. Bajpai, S. K. Shukla, S. Bhanu and S. Kankane, 2008, **33**, 1088–1118.
- 26 C. Chang, B. Duan, J. Cai and L. Zhang, *Eur. Polym. J.*, 2010, **46**, 92–100.
- 27 C.-H. Zhou, X. Xia, C.-X. Lin, D.-S. Tong and J. Beltramini, *Chem. Soc. Rev.*, 2011, **40**, 5588.
- 28 J. Q. Bond, A. a. Upadhye, H. Olcay, G. a. Tompsett, J. Jae, R. Xing, D. M. Alonso, D. Wang, T. Zhang, R. Kumar, A. Foster, S. M. Sen, C. T. Maravelias, R. Malina, S. R. H. Barrett, R. Lobo, C. E. Wyman, J. a. Dumesic and G. W. Huber, *Energy Environ. Sci.*, 2014, **7**, 1500–1523.
- 29 R. E. H. Sims, W. Mabee, J. N. Saddler and M. Taylor, *Bioresour. Technol.*, 2010, **101**, 1570–1580.
- 30 B. C. Knott, M. Haddad Momeni, M. F. Crowley, L. F. MacKenzie, A. W. Götz, M. Sandgren, S. G. Withers, J. Staišlberg and G. T. Beckham, *J. Am. Chem.*

- Soc., 2014, **136**, 321–329.
- 31 P. Mäki-Arvela, I. Anugwom, P. Virtanen, R. Sjöholm and J. P. Mikkola, *Ind. Crops Prod.*, 2010, **32**, 175–201.
- 32 V. B. Agbor, N. Cicek, R. Sparling, A. Berlin and D. B. Levin, *Biotechnol. Adv.*, 2011, **29**, 675–685.
- 33 E. Melro, L. Alves, F. E. Antunes and B. Medronho, *J. Mol. Liq.*, 2018, **265**, 578–584.
- 34 J. X. Sun, X. F. Sun, R. C. Sun and Y. Q. Su, *Carbohydr. Polym.*, 2004, **56**, 195–204.
- 35 Y. P. Zhang, S. Ding, J. R. Mielenz, J. Cui, R. T. Elander, M. Laser, M. E. Himmel, J. R. Mcmillan, L. R. Lynd, B. Systems and V. Tech, *Biotechnol. Bioeng.*, 2007, **97**, 214–223.
- 36 A. Brandt-Talbot, F. J. V. Gschwend, P. S. Fennell, T. M. Lammens, B. Tan, J. Weale and J. P. Hallett, *Green Chem.*, 2017, **19**, 3078–3102.
- 37 I. Miyamoto, M. Inamoto, T. Matsui, M. Saito and K. Okajima, *Polym. J.*, 1995, **27**, 1113–1122.
- 38 T. Heinze, R. Dicke, A. Koschella, A. H. Kull, E.-A. Klohr and W. Koch, *Macromol. Chem. Phys.*, 2000, **201**, 627–631.
- 39 B. Medronho, A. Romano, M. G. Miguel, L. Stigsson and B. Lindman, *Cellulose*, 2012, **19**, 581–587.
- 40 A. Pinkert, K. N. Marsh and S. Pang, *Ind. Eng. Chem. Res.*, 2010, **49**, 11121–11130.
- 41 J. C. Roberts, in *The Chemistry of Paper*, ed. J. C. Roberts, 1996, pp. 52–68.
- 42 L. Segal, J. J. Creely, A. E. Martin and C. M. Conrad, *Text. Res. J.*, 1959, **29**,



- 786–794.
- 43 K. Kamide, K. Okajima, T. Matsui and K. Kowsaka, *Polym. J.*, 1984, **16**, 857–866.
- 44 M. Ghasemi, P. Alexandridis and M. Tsianou, *Biomacromolecules*, 2018, **19**, 640–651.
- 45 A. Isogai and R. H. Atalla, *Cellulose*, 1998, **5**, 309–319.
- 46 L. A. Ramos, J. M. Assaf, O. A. El Seoud and E. Frollini, *Biomacromolecules*, 2005, **6**, 2638–2647.
- 47 H. Qi, H. Chang and L. Zhang, *Cellulose*, 2008, **15**, 779–787.
- 48 A. Ben-Naim, *Molecular Theory of Solutions*, Oxford University Press, New York, 2006.
- 49 L. Schulz, B. Seger and W. Burchard, *Macromol. Chem. Phys.*, 2000, **201**, 2008–2022.
- 50 Y. H. P. Zhang, S. Y. Ding, J. R. Mielenz, J. B. Cui, R. T. Elander, M. Laser, M. E. Himmel, J. R. McMillan and L. R. Lynd, *Biotechnol. Bioeng.*, 2007, **97**, 214–223.
- 51 G. Mancini, S. Papirio, P. N. L. Lens and G. Esposito, *Energy and Fuels*, 2016, **30**, 1892–1903.
- 52 R. H. Atalla and S. C. Nagel, *Science*, 1974, **185**, 522–524.
- 53 X. Chen, C. Burger, F. Wan, J. Zhang, L. Rong, B. S. Hsiao, B. Chu, J. Cai and L. Zhang, *Biomacromolecules*, 2007, **8**, 1918–1926.
- 54 M. Ghasemi, P. Alexandridis and M. Tsianou, *Cellulose*, 2017, **24**, 571–590.
- 55 M. Ghasemi, M. Tsianou and P. Alexandridis, *Agric. Res. Technol.*, 2018, **16**, 555985.

- 56 O. A. Battista, *Ind. Eng. Chem. Res.*, 1950, **42**, 502–507.
- 57 E. M. de Melo, J. H. Clark and A. S. Matharu, *Green Chem.*, 2017, **19**, 3408–3417.
- 58 A. Isogai and M. Usuda, *Mokuzai Gakkaishi*, 1991, 37, 339–344.
- 59 E. Billès, V. Coma, F. Peruch and S. Grelier, *Polym. Int.*, 2017, **66**, 1227–1236.
- 60 J. T. Oberlerchner, P. Vejdovszky, T. Zweckmair, A. Kindler, S. Koch, T. Rosenau and A. Potthast, *J. Chromatogr. A*, 2016, **1471**, 87–93.
- 61 S. Morales-delaRosa, J. M. Campos-Martin and J. L. G. Fierro, *ChemSusChem*, 2014, **7**, 3467–3475.
- 62 S. Morales-delaRosa, J. M. Campos-Martin and J. L. G. Fierro, *Cellulose*, 2014, **21**, 2397–2407.
- 63 R. B. Chavan and A. K. Patra, *Indian J. Fibre Text. Res.*, 2004, **29**, 483–492.
- 64 US Patent Office, 1952604, 1934, 1–3.
- 65 N. Bywater, *Lenzinger Berichte*, 2011, **89**, 22–29.
- 66 J. T. Marsh, *An Introduction To Textile Finishing*, Chapman and Hall Ltd., London, 2nd edn., 1948.
- 67 A. K. Sengupta, in *Manufactured Fibre Technology*, Springer Netherlands, Dordrecht, 1997, pp. 480–513.
- 68 T. Shaikh, S. Chaudhari and A. Varma, *Int. J. Eng. Res. Appl.*, 2012, **2**, 675–680.
- 69 F. Scientific, *Sodium Hydroxide Material Safety Data Sheet*, 2008.
- 70 F. Scientific, *Carbon Disulfide Material Safety Data Sheet*, 2009.
- 71 WALHI, *ecologistas en accion, ethical consumer and Changing Markets*,

- Chang. Mark.*, 2007.
- 72 W. L. Lim, A. A. N. Gunny, F. H. Kasim, I. M. AlNashef and D. Arbain, *Cellulose*, 2019, **26**, 4085–4098.
- 73 S. Sen, J. D. Martin and D. S. Argyropoulos, *ACS Sustain. Chem. Eng.*, 2013, **1**, 858–870.
- 74 M. Kostag, M. Gericke, T. Heinze and O. A. El, *Twenty-five years of cellulose chemistry: innovations in the dissolution of the biopolymer and its transformation into esters and ethers*, Springer Netherlands, 2019, vol. 26.
- 75 T. Heinze and A. Koschella, *Polímeros*, 2005, **15**, 84–90.
- 76 W. Runckel, MSc Thesis, Oregon State College, 1942.
- 77 S. Wang, A. Lu and L. Zhang, *Prog. Polym. Sci.*, 2016, **53**, 169–206.
- 78 H. P. Fink, P. Weigel, H. J. Purz and J. Ganster, *Prog. Polym. Sci.*, 2001, **26**, 1473–1524.
- 79 G. Brodeur, E. Yau, J. Collier and J. Telotte, , DOI:10.1002/jctb.4972.
- 80 M. Krysztof, K. Olejnik, P. Kulpinski, A. Stanislawska and S. Khadzhynova, *Cellulose*, 2018, **25**, 3595–3607.
- 81 J. B. Binder, J. B. Binder, R. T. Raines and R. T. Raines, *J. Am. Chem. Soc.*, 2009, **131**, 1979–85.
- 82 C. L. McCormick and B. H. Hutchinson, *Macromolecules*, 1985, **18**, 2394–2401.
- 83 A. Potthast, T. Rosenau, R. Buchner, T. Röder, G. Ebner, H. Bruglachner, H. Sixta and P. Kosma, *Cellulose*, 2002, **9**, 41–53.
- 84 European Chemicals Agency, *Agreement of the Member State Committee of the identification of N,N-Dimethylacetamide (DMAC) as a substance of very high*

- concern, 2011.
- 85 K. Saalwächter, W. Burchard, P. Klüfers, G. Kettenbach, P. Mayer, D. Klemm and S. Dugarmaa, *Macromolecules*, 2000, **33**, 4094–4107.
- 86 Vickers Laboratories Ltd, *Cuprammonium hydroxide solution - Safety Data Sheet*, Pudsey, 2013.
- 87 Sigma-Aldrich, *Nickel (II) hydroxide - Safety data sheet*, 2019.
- 88 Sigma-Aldrich, *Tris(2-aminoethyl)amine - Safety data sheet*, 2019.
- 89 E. R. Rene, E. Sahinkaya, A. Lewis and P. N. L. Lens, *Sustainable Heavy Metal Remediation: Volume 2: Case studies*, Springer, 2017.
- 90 Changing Markets Foundation, 2018.
- 91 J. Koch and W. Nowak, *Water Resour. Res.*, 2015, **51**, 806–831.
- 92 T. Liebert, in *Cellulose Solvents: For Analysis, Shaping and Chemical Modification*, American Chemical Society, Washington, 2010, pp. 3–54.
- 93 E. Gale, R. H. Wirawan, R. L. Silveira, C. S. Pereira, M. A. Johns, M. S. Skaf and J. L. Scott, *ACS Sustain. Chem. Eng.*, 2016, **4**, 6200–6207.
- 94 W. Wei, F. Meng, Y. Cui, M. Jiang and Z. Zhou, *Cellulose*, 2017, **24**, 49–59.
- 95 R. C. Remsing, R. P. Swatloski, R. D. Rogers and G. Moyna, *Chem. Commun. (Camb)*, 2006, 1271–1273.
- 96 J. Cai, L. Zhang, S. Liu, Y. Liu, X. Xu, X. Chen, B. Chu, X. Guo, J. Xu, H. Cheng, C. C. Han and S. Kuga, *Macromolecules*, 2008, **41**, 9345–9351.
- 97 C. Zhang, R. Liu, J. Xiang, H. Kang, Z. Liu and Y. Huang, *J. Phys. Chem. B*, 2014, **118**, 9507–9514.
- 98 R. S. Payal and S. Balasubramanian, *Phys. Chem. Chem. Phys.*, 2014, **16**, 17458.

- 99 A. M. Bochek, *Russ. J. Appl. Chem.*, 2003, **76**, 1711–1719.
- 100 K. Kamide, K. Okajima and K. Kowsaka, *Polym. J.*, 1985, **17**, 701–706.
- 101 B. Lindman, G. Karlström and L. Stigsson, *J. Mol. Liq.*, 2010, **156**, 76–81.
- 102 Y. Nishiyama, J. Sugiyama, H. Chanzy and P. Langan, *J. Am. Chem. Soc.*, 2003, **125**, 14300–14306.
- 103 N. Isobe, K. Noguchi, Y. Nishiyama, S. Kimura, M. Wada and S. Kuga, *Cellulose*, 2013, **20**, 97–103.
- 104 L. Alves, B. Medronho, F. E. Antunes, D. Topgaard and B. Lindman, *Cellulose*, 2016, **23**, 247–258.
- 105 L. Alves, B. Medronho, F. E. Antunes, D. Topgaard and B. Lindman, *Carbohydr. Polym.*, 2016, **151**, 707–715.
- 106 M. Kihlman, B. F. Medronho, A. L. Romano, U. Germgård and B. Lindman, *J. Braz. Chem. Soc.*, 2013, **24**, 295–303.
- 107 B. Medronho and B. Lindman, *Curr. Opin. Colloid Interface Sci.*, 2014, **19**, 32–40.
- 108 E. Bialik, B. Stenqvist, Y. Fang, A. Ostlund, I. Furo, B. Lindman, M. Lund and D. Bernin, *J. Phys. Chem. Lett.*, 2016, **7**, 5044–5048.
- 109 W. G. Glasser, R. H. Atalla, J. Blackwell, M. M. Brown, W. Burchard, A. D. French, D. O. Klemm and Y. Nishiyama, *Cellulose*, 2012, **19**, 589–598.
- 110 G. H. Vineyard, *J. Chem. Educ.*, 1949, **26**, 383–385.
- 111 A. K. Bledzki, S. Reihmane and J. Gassan, *J. Appl. Polym. Sci.*, 1996, **59**, 1329–1336.
- 112 J. A. Schellman, *Biophys. Chem.*, 1993, **45**, 273–279.
- 113 S. Shimizu and D. J. Smith, *J. Chem. Phys.*, 2004, **121**, 1148–1154.

- 114 T. W. J. Nicol, N. Matubayasi and S. Shimizu, *Phys. Chem. Chem. Phys.*, 2016, **18**, 15205–15217.
- 115 P. R. Davis-searles, A. J. Saunders, D. A. Erie, D. J. Winzor and G. J. Pielak, *Annu. Rev. Biophys. Biomol. Struct.*, 2001, **30**, 271–306.
- 116 S. Shimizu and C. L. Boon, *J. Chem. Phys.*, 2004, **121**, 9147–9155.
- 117 A. Isogai, *Cellulose*, 1997, **4**, 99–107.
- 118 Z. Liu, C. Zhang, R. Liu and W. Zhang, *Cellulose*, 2015, **22**, 1641–1652.
- 119 J. G. Kirkwood and F. P. Buff, *J. Chem. Phys.*, 1951, **19**, 774–777.
- 120 D. G. Hall, *Trans. Faraday Soc.*, 1971, **61**, 2516–2524.
- 121 A. Ben-Naim, *J. Chem. Phys.*, 1977, **67**, 4884–4890.
- 122 P. E. Smith, *J. Chem. Phys.*, 2008, **129**, 124509/1-124509/5.
- 123 S. Shimizu and N. Matubayasi, *J. Phys. Chem. B*, 2014, **118**, 3922–3930.
- 124 S. Shimizu and N. Matubayasi, *J. Phys. Chem. B*, 2014, **118**, 13210–13216.
- 125 T. W. J. Nicol, MChem thesis, University of York, 2015.
- 126 M. J. Rosen, *J. Am. Oil Chem. Soc.*, 1974, **51**, 461–465.
- 127 P. L. Privalov and S. J. Gill, *Adv. Protein Chem.*, 1988, **39**, 191–234.
- 128 B. Lee, *Biopolymers*, 1991, **31**, 993–1008.
- 129 A. Ben-Naim, *J. Phys. Chem.*, 1978, **82**, 792–803.
- 130 T. Roder, B. Morgenstern and O. Glatter, *Lenzinger Ber*, 2000, 97–101.
- 131 C. Cuissinat and P. Navard, *Macromol. Symp.*, 2006, **244**, 19–30.
- 132 A. Pinkert, K. N. Marsh, S. Pang and M. P. Staiger, *Chem. Rev.*, 2009, **109**, 6712–6728.

- 133 F. Lu, C. Zhang, B. Lu, K. Yu, J. Liu, H. Kang, R. Liu and G. Lan, *Cellulose*, 2017, **24**, 1621–1629.
- 134 B. Cao, J. Du, D. Du, H. Sun, X. Zhu and H. Fu, *Carbohydr. Polym.*, 2016, **149**, 348–356.
- 135 Y. Shang, H. Zhang, X. Zhao, Z. Wang, X. Jiang, L. Zhang, X. Zhou, Q. Gong and Y. Chen, *J. Therm. Anal. Calorim.*, 2012, **111**, 891–896.
- 136 J. B. Taylor, *Trans. Faraday Soc.*, 1957, **7**, 1198–1203.
- 137 M. Bergenstrahle-Wohlert, T. Angles d'Ortoli, N. A. Sjoberg, G. Widmalm and J. Wohlert, *Cellulose*, 2016, **23**, 2375–2387.
- 138 K. Gessler, N. Krauss, T. Steiner, W. Saenger, C. Betzel and A. Sarko, *J. Am. Chem. Soc.*, 1995, **117**, 11397–11406.
- 139 M. Spinu, N. Dos Santos, N. Le Moigne and P. Navard, *Cellulose*, 2010, **18**, 247–256.
- 140 U. Henniges, M. Kostic, A. Borgards, T. Rosenau and A. Potthast, *Biomacromolecules*, 2011, **12**, 871–879.
- 141 Z. Wang, S. Liu, Y. Matsumoto and S. Kuga, *Cellulose*, 2012, **19**, 393–399.
- 142 T. Yamashiki, T. Matsui, M. Saitoh, K. Okajima, K. Kamide and T. Sawada, *Br. Polym. J.*, 1990, **22**, 121–128.
- 143 B. Laszkiewicz and J. A. Cuculo, *J. Appl. Polym. Sci.*, 1993, **50**, 27–34.
- 144 I. Sakurada, *Berichte der Dtsch. Chem. Gesellschaft (A B)*, 1930, **63**, 2027–2042.
- 145 Y. Wang and Y. Deng, *Biotechnol. Bioeng.*, 2009, **102**, 1398–405.
- 146 X. Gong, C. Wang, L. Zhang and H. Qu, *J. Chem. Eng. Data*, 2012, **57**, 3264–3269.

- 147 Y. Ono, T. Ishida, H. Soeta, T. Saito and A. Isogai, *Biomacromolecules*, 2016, **17**, 192–199.
- 148 M. Pincu, E. J. Cocinero, N. Mayorkas, B. Brauer, B. G. Davis, R. B. Gerber and J. P. Simons, *J. Phys. Chem. A*, 2011, **115**, 9498–9509.
- 149 J. B. Taylor, *Trans. Faraday Soc.*, 1957, **53**, 1198–1203.
- 150 H. Sobue, H. Kiessig and K. Hess, *Zeitschrift für Phys. Chemie*, 1939, **43B**, 309–328.
- 151 T. Budtova and P. Navard, *Cellulose*, 2016, **23**, 5–55.
- 152 Y.-J. J. Yang, J.-M. M. Shin, T. H. Kang, S. Kimura, M. Wada and U.-J. J. Kim, *Cellulose*, 2014, **21**, 1175–1181.
- 153 A. L. Dupont, *Polymer (Guildf.)*, 2003, **44**, 4117–4126.
- 154 W. Burchard, N. Habermann, P. Klüfers, B. Seger and U. Wilhelm, *Angew. Chemie Int. Ed. English*, 1994, **33**, 884–887.
- 155 M. Egal, T. Budtova and P. Navard, *Biomacromolecules*, 2007, **8**, 2282–2287.
- 156 Å. Östlund, D. Lundberg, L. Nordstierna, K. Holmberg and M. Nydén, *Biomacromolecules*, 2009, **10**, 2401–2407.
- 157 B. Medronho and B. Lindman, *Adv. Colloid Interface Sci.*, 2015, **222**, 502–508.
- 158 E. Bialik, B. Stenqvist, Y. Fang, A. Ostlund, I. Furo, B. Lindman, M. Lund and D. Bernin, *J. Phys. Chem. Lett.*, 2016, **7**, 5044–5048.
- 159 B. Lindman, B. Medronho, L. Alves, C. Costa, H. Edlund and M. Norgren, *Phys. Chem. Chem. Phys.*, 2017, **19**, 23704–23718.
- 160 L. Alves, B. F. Medronho, F. E. Antunes, A. Romano, M. G. Miguel and B. Lindman, *Colloids Surfaces A*, 2015, **483**, 257–263.
- 161 C. Yamane, T. Aoyagi, M. Ago, K. Sato, K. Okajima and T. Takahashi, *Polym.*



- J.*, 2006, **38**, 819–826.
- 162 M. Bergensträhle, J. Wohler, M. E. Himmel and J. W. Brady, *Carbohydr. Res.*, 2010, **345**, 2060–2066.
- 163 P. E. Smith, *J. Chem. Phys.*, 2008, **129**, 10–15.
- 164 D. Ishii, D. Tatsumi and T. Matsumoto, 2008, **343**, 919–928.
- 165 Z. Liu, C. Zhang, R. Liu, W. Zhang, H. Kang, P. Li and Y. Huang, *Cellulose*, 2016, **23**, 295–305.
- 166 P. K. Banipal, T. S. Banipal, J. C. Ahluwalia and B. S. Lark, *J. Chem. Thermodyn.*, 2000, **32**, 1409–1432.
- 167 P. K. Banipal, T. S. Banipal, B. S. Lark and J. C. Ahluwalia, *J. Chem. Soc. Faraday Trans.*, 1997, **93**, 81–87.
- 168 J. E. Enderby and G. W. Neilson, *Reports Prog. Phys.*, 1981, **44**, 593–653.
- 169 J. E. S. J. Reid, A. J. Walker and S. Shimizu, *Phys. Chem. Chem. Phys.*, 2015, **17**, 14710–14718.
- 170 J. J. Booth, S. Abbott and S. Shimizu, *J. Phys. Chem. B*, 2012, **116**, 14915–14921.
- 171 J. J. Booth, M. Omar, S. Abbott and S. Shimizu, *Phys Chem Chem Phys*, 2015, **17**, 8028–8037.
- 172 I. L. Shulgin and E. Ruckenstein, *J. Chem. Phys.*, 2005, **123**, 054909.
- 173 S. S. Terdale, D. H. Dagade and K. J. Patil, *J. Phys. Chem. B*, 2006, **110**, 18583–18593.
- 174 S. Shimizu, R. Stenner and N. Matubayasi, *Food Hydrocoll.*, 2017, **62**, 128–139.
- 175 S. Shimizu, J. Booth and S. Abbott, *Phys. Chem. Chem. Phys.*, 2013, **15**,

- 20625–20632.
- 176 J. J. Booth, M. Omar, S. Abbott and S. Shimizu, *Phys. Chem. Chem. Phys.*, 2015, **17**, 8028–8037.
- 177 R. A. Robinson and R. H. Stokes, *Electrolyte Solutions*, Butterworth, London, 1959.
- 178 M. Gray, A. O. Converse and C. E. Wyman, *Appl. Biochem. Biotechnol.*, 2003, **105**, 179–193.
- 179 E. Griffiths, *International Critical Tables of Numerical Data, Physics, Chemistry and Technology*, 1927, vol. 119.
- 180 J. I. Partanen, *J. Chem. Eng. Data*, 2016, **61**, 286–306.
- 181 Pitzer and Guillermo, *J. Chem. Inf. Model.*, 1973, **77**, 2300–2308.
- 182 G. Jakli and W. A. Van Hook, *J. Chem. Eng. Data*, 1972, **17**, 348–355.
- 183 I. L. Shulgin and E. Ruckenstein, *J. Phys. Chem. B*, 2006, **110**, 12707–12713.
- 184 A. Ben-Naim, *Am. J. Phys.*, 1987, **55**, 725–733.
- 185 H. S. Frank and F. Franks, *J. Chem. Phys.*, 1968, **48**, 2365–150.
- 186 H. Miyamoto, U. Schnupf and J. W. Brady, *J. Agric. Food Chem.*, 2014, **62**, 11017–11023.
- 187 H. S. Frank and M. W. Evans, *J. Chem. Phys.*, 1945, **13**, 507–532.
- 188 F. Franks, *Biophys. Chem.*, 2002, **96**, 117–127.
- 189 H. S. Chan, S. Shimizu and H. Kaya, *Methods Enzymol.*, 2004, **380**, 350–379.
- 190 K. A. Dill, *Biochemistry*, 1990, **29**, 7133–7155.
- 191 A. W. Omta, M. F. Kropman and S. Woutersen, *Science*, 2003, **301**, 347–350.
- 192 Y. L. A. Rezus and H. J. Bakker, *Phys. Rev. Lett.*, 2007, **99**, 148301.

- 193 S. Shimizu and N. Matubayasi, *Phys. Chem. Chem. Phys.*, 2018, **20**, 5909–5917.
- 194 National Academies Press, in *International Critical Tables of Numerical Data, Physics, Chemistry and Technology*, National Academies Press, Washington, D.C., 1930, pp. 96–306.
- 195 K. D. Collins and M. W. Washabaugh, *Q. Rev. Biophys.*, 1985, **18**, 323–422.
- 196 P. Jungwirth and P. S. Cremer, *Nat. Chem.*, 2014, **6**, 261–263.
- 197 S. Shimizu, W. M. McLaren and N. Matubayasi, *J. Chem. Phys.*, 2006, **124**, 234905.
- 198 X. Zhao, Y. Chen and X. Jiang, *J. Therm. Anal. Calorim.*, 2013, **111**, 891–896.
- 199 J. Zhou and L. Zhang, *Polym J*, 2000, 32, 866–870.
- 200 L. R. Pratt, M. I. Chaudhari and S. B. Rempe, *J. Phys. Chem. B*, 2016, **120**, 6455–6460.
- 201 S. Shimizu and N. Matubayasi, *Biophys. Chem.*, 2017, **231**, 111–115.
- 202 C. Tanford, *J. Mol. Biol.*, 1969, **39**, 539–544.
- 203 H. S. Chan and K. A. Dill, *Annu. Rev. Biophys. Biomol. Struct.*, 2002, **26**, 425–459.
- 204 A. Ben-Naim, *J. Chem. Phys.*, 1971, **54**, 3696–3711.
- 205 H. G. Brittain, Thermodynamic vs. Kinetic Solubility: Knowing Which is Which, <https://www.americanpharmaceuticalreview.com/Featured-Articles/160452-Thermodynamic-vs-Kinetic-Solubility-Knowing-Which-is-Which/>, (accessed 8 August 2019).
- 206 T. M. Wood and J. N. Saddler, *Methods Enzymol.*, 1988, **160**, 3–11.
- 207 T. Yamashiki, T. Matsui, M. Saitoh, K. Okajima, K. Kamide and T. Sawada, *Br.*

- Polym. J.*, 1990, **22**, 73–83.
- 208 Z. Ling, T. Wang, M. Makarem, M. Santiago Cintrón, H. N. Cheng, X. Kang, M. Bacher, A. Potthast, T. Rosenau, H. King, C. D. Delhom, S. Nam, J. Vincent Edwards, S. H. Kim, F. Xu and A. D. French, *Cellulose*, 2019, **26**, 305–328.
- 209 N. Le Moigne, PhD Thesis, École Nationale Supérieure des Mines de Paris, 2008.
- 210 C. Cuissinat and P. Navard, *Macromol. Symp.*, 2006, **244**, 19–30.
- 211 M. Spinu, N. Dos Santos, N. Le Moigne and P. Navard, *Cellulose*, 2011, **18**, 247–256.
- 212 Z. Shi, Y. Liu, H. Xu, Q. Yang, C. Xiong, S. Kuga and Y. Matsumoto, *Ind. Crops Prod.*, 2018, **118**, 48–52.
- 213 L. Zhang, Y. Mao, J. Zhou and J. Cai, *Ind. Eng. Chem. Res.*, 2005, **44**, 522–529.
- 214 J. Cai, L. Zhang, J. Zhou, H. Qi, H. Chen, T. Kondo, X. Chen and B. Chu, *Adv. Mater.*, 2007, **19**, 821–825.
- 215 M. Hattori, Y. Shimaya and M. Saito, *Polym. J.*, 1998, 30, 49–55.
- 216 J. Cai and L. Zhang, *Macromol. Biosci.*, 2005, **5**, 539–548.
- 217 A. Casas, J. Palomar, M. V. Alonso, M. Oliet, S. Omar and F. Rodriguez, *Ind. Crops Prod.*, 2012, **37**, 155–163.
- 218 R. Rinaldi, *Chem. Commun.*, 2011, **47**, 511–513.
- 219 A. Idström, L. Gentile, M. Gubitosi, C. Olsson, B. Stenqvist, M. Lund, K. E. Bergquist, U. Olsson, T. Köhnke and E. Bialik, *Cellulose*, 2017, **24**, 3645–3657.
- 220 M. Gubitosi, H. Duarte, L. Gentile, U. Olsson and B. Medronho, *Biomacromolecules*, 2016, **17**, 2873–2881.

- 221 E. R. D. Seiler, Y. Takeoka, M. Rikukawa and M. Yoshizawa-Fujita, *RSC Adv.*, 2020, **10**, 11475–11480.
- 222 Y.-R. Liu, K. Thomsen, Y. Nie, S.-J. Zhang and A. S. Meyer, *Green Chem.*, 2016, **18**, 6246–6254.
- 223 A. Xu, Y. Zhang, Y. Zhao and J. Wang, *Carbohydr. Polym.*, 2013, **92**, 540–544.
- 224 H. Ren, C. Chen, Q. Wang, D. Zhao and S. Guo, *BioResources*, 2016, **11**, 5435–5451.
- 225 T. Kondo, E. Togawa and R. M. Brown, *Biomacromolecules*, 2001, **2**, 1324–1330.
- 226 C. L. McCormick, P. A. Callais and B. H. Hutchinson, *Macromolecules*, 1985, **18**, 2394–2401.
- 227 N. Andersen, K. S. Johansen, M. Michelsen, E. H. Stenby, K. B. R. M. Krogh and L. Olsson, 2008, **42**, 362–370.
- 228 A. J. Sayyed, N. A. Deshmukh and D. V. Pinjari, *Cellulose*, 2019, **26**, 2913–2940.
- 229 R. Yudianti, A. Syampurwadi, H. Onggo, M. Karina, H. Uyama and J. Azuma, *Polym. Adv. Technol.*, 2016, **27**, 1102–1107.
- 230 B. Zhang, J. Azuma and H. Uyama, *RSC Adv.*, 2015, **5**, 2900–2907.
- 231 S. Wei, V. Kumar and G. S. Banker, *Int. J. Pharm.*, 1996, **142**, 175–181.
- 232 M. R. Kasaai, *J. Appl. Polym. Sci.*, 2002, **86**, 2189–2193.
- 233 J. Oberlerchner, T. Rosenau and A. Potthast, *Molecules*, 2015, **20**, 10313–10341.
- 234 S. Matsuoka, H. Kawamoto and S. Shiro, *Polym. Degrad. Stab.*, 2011, **96**, 1242–1247.

- 235 N. Isobe, S. Kimura, M. Wada and S. Deguchi, *J. Taiwan Inst. Chem. Eng.*, 2018, **92**, 118–122.
- 236 M. Ghasemi, M. Tsianou and P. Alexandridis, *Bioresour. Technol.*, 2017, **228**, 330–338.
- 237 T. Budtova and P. Navard, *Cellulose*, 2016, **23**, 5–55.
- 238 Y. H. P. Zhang, J. Cui, L. R. Lynd and L. R. Kuang, *Biomacromolecules*, 2006, **7**, 644–648.
- 239 S. Shimizu and H. S. Chan, *J. Chem. Phys.*, 2001, **115**, 3424–3431.
- 240 C. Roy, T. Budtova and P. Navard, *Biomacromolecules*, 2003, **4**, 259–264.
- 241 A. Pereira, H. Duarte, P. Nosrati, M. Gubitosi, L. Gentile, A. Romano, B. Medronho and U. Olsson, *Cellulose*, 2018, **25**, 3205–3210.
- 242 I. D. Evans and D. R. Haisman, *Stärke*, 1982, **7**, 224–231.
- 243 L. Day, C. Fayet and S. Homer, *Carbohydr. Polym.*, 2013, **94**, 31–37.
- 244 Q. Li, H. Li and Q. Gao, *Food Hydrocoll.*, 2015, **43**, 803–811.
- 245 P. Chinachoti, V. White, L. Lo and T. Stengle, *Cereal Chem.*, 1991, **68**, 238–244.
- 246 F. Zhu, *Food Hydrocoll.*, 2017, **63**, 611–624.
- 247 C. G. Biliaderis, in *Starch - Chemistry and Technology*, 2009, pp. 293–359.
- 248 J. Lelievre, *Polymer (Guildf.)*, 1976, **17**, 854–858.
- 249 K. Kohyama and K. Nishinari, *J. Agric. Food Chem.*, 1991, **39**, 1406–1410.
- 250 T. Shiotsubo and K. Takahashi, *Agric. Biol. Chem.*, 1984, **48**, 9–17.
- 251 E. Habeych, X. Guo, J. van Soest, A. J. van der Goot and R. Boom, *Carbohydr. Polym.*, 2009, **77**, 703–712.

- 252 E. Chiotelli, G. Pilosio and M. Le Meste, *Biopolymers*, 2002, **63**, 41–58.
- 253 W. Wang, H. Zhou, H. Yang, S. Zhao, Y. Liu and R. Liu, *Food Chem.*, 2017, **214**, 319–327.
- 254 Q. Li, L. Zhang, Y. Ye and Q. Gao, *Food Hydrocoll.*, 2015, **51**, 468–475.
- 255 K. D. Collins and M. W. Washabaugh, *Q. Rev. Biophys.*, 1985, **18**, 323–422.
- 256 F. B. Ahmad and P. A. Williams, in *Gums and Stabilisers for the Food Industry 10*, London, 2000, pp. 255–261.
- 257 C. G. Biliaderis, in *Starch: Chemistry and Technology*, Elsevier Inc., 3rd edn., 2009, pp. 293–372.
- 258 D. Cooke and M. J. Gidley, *Carbohydr. Res.*, 1992, **227**, 103–112.
- 259 B. K. Patel and K. Seetharaman, *Starch/Staerke*, 2010, **62**, 538–546.
- 260 F. B. Ahmad and P. A. Williams, in *Gums and Stabilisers for the Food Industry 11*, eds. P. A. Williams and G. O. Phillips, The Royal Society of Chemistry, 2002, pp. 145–157.
- 261 Y. Ai and J. Jane, *Starch - Stärke*, 2015, **67**, 213–224.
- 262 S. Shimizu, *Proc. Natl. Acad. Sci. U. S. A.*, 2004, **101**, 1195–1199.
- 263 S. Shimizu and N. Matubayasi, *Physica A*, 2018, **492**, 1988–1996.
- 264 J. M. Thevelein, J. A. Van Assche, K. Heremans and S. Y. Gerlsma, *Carbohydr. Res.*, 1981, **93**, 304–307.
- 265 F. B. Ahmad, P. A. Williams, J. L. Doublier, S. Durand and A. Buleon, *Carbohydr. Polym.*, 1999, **38**, 361–370.
- 266 J. O. Brumovsky, L. A. Brumovsky and D. B. Thompson, *Int. J. Food Prop.*, 2006, **9**, 889–896.

- 267 M. Wootton and A. Bamunuarachchi, *Starch - Stärke*, 1979, **31**, 262–264.
- 268 S. Rahman, *Food Properties Handbook*, CRC Press, Boca Raton, FL, 1995.
- 269 M. Hirashima, R. Takahashi and K. Nishinari, *J. Cook. Sci. Japan*, 2004, **37**, 48–56.
- 270 W. X. Zhu, J. Gayin, F. Chatel, K. Dewettinck and P. Van der Meeren, *Food Hydrocoll.*, 2009, **23**, 2204–2211.
- 271 R. Stenner, N. Matubayasi and S. Shimizu, *Food Hydrocoll.*, 2016, **54**, 284–292.
- 272 K. R. Patil, A. D. Tripathi, G. Pathak and S. S. Katti, *J. Chem. Eng. Data*, 1991, **36**, 225–230.
- 273 J. T. Moore, W. T. Humphries and C. S. Patterson, *J. Chem. Eng. Data*, 1972, **17**, 180–182.
- 274 M. EL Guendouzi and M. Aboufaris, *J. Chem. Eng. Data*, 2015, **60**, 2308–2319.
- 275 M. Manca, A. J. J. Woortman, K. Loos and M. A. Loi, *Starch - Stärke*, 2015, **67**, 132–138.
- 276 W. Saenger, *Naturwissenschaften*, 1984, **71**, 31–36.
- 277 Y. Li, S. Lin, J. Hu, G. Liu, G. Zhang, Y. Tu, H. Luo and W. Li, *Carbohydr. Polym.*, 2014, **102**, 489–496.
- 278 P. Chen, L. Yu, G. Simon, E. Petinakis, K. Dean and L. Chen, *J. Cereal Sci.*, 2009, **50**, 241–247.
- 279 A. Buléon, B. Pontoire, C. Riekkel, H. Chanzy, W. Helbert and R. Vuong, *Macromolecules*, 1997, **30**, 3952–3954.
- 280 W. S. Ratnayake and D. S. Jackson, *J. Agric. Food Chem.*, 2006, **54**, 3712–3716.



- 281 S. Brouillet-Fourmann, C. Carrot and N. Mignard, *Rheol. Acta*, 2003, **42**, 110–117.
- 282 C. Y. Lii, P. Tomasik, W. L. Hung and V. M. F. Lai, *Food Hydrocoll.*, 2002, **16**, 35–45.
- 283 Y. J. Wang, M. I. Kuo, L. Wang and J. Patindol, *Starch/Staerke*, 2007, **59**, 445–452.
- 284 L. B. Rockland, F. T. Jones and D. M. Hahn, *J. Food Sci.*, 1977, **42**, 1204–1207.
- 285 I. Prigogine and R. Defay, *Chemical Thermodynamics*, Jarrold and Sons Ltd, Norwich, 1954.
- 286 J. M. V. Blanshard, in *Starch: Properties and Potential*, John Wiley and Sons, New York, 1987, pp. 16–53.
- 287 K. Takahashi, K. Shirai and K. Wada, *J. Japanese Soc. Starch Sci.*, 1981, **28**, 1–8.
- 288 H. Liu, J. Lelievre and W. Ayoung-Chee, *Carbohydr. Res.*, 1991, **210**, 79–87.
- 289 A. H. Clark, *Carbohydr. Polym.*, 2000, **42**, 337–351.
- 290 H.-X. Zhou, G. Rivas and A. P. Minton, *Annu. Rev. Biophys.*, 2008, **37**, 375–397.
- 291 Z. Fu, J. Chen, S. J. Luo, C. M. Liu and W. Liu, *Starch/Staerke*, 2015, **67**, 69–78.
- 292 K. Katsuta, M. Miura and A. Nishimura, *Top. Catal.*, 1992, **6**, 187–198.
- 293 S. C. Alcázar-Alay and M. A. A. Meireles, *Food Sci. Technol.*, 2015, **35**, 215–236.
- 294 N. Isobe, S. Kimura, M. Wada and S. Kuga, *Carbohydr. Polym.*, 2012, **89**, 1298–1300.
- 295 Y. C. Lam, S. C. Joshi and B. K. Tan, *J. Therm. Anal. Calorim.*, 2007, **87**, 475–

- 482.
- 296 Ö. Pekcan and S. Kara, *Mod. Phys. Lett. B*, 2012, **26**, 1230019.
- 297 M. Rubinstein and A. V. Dobrynin, *Curr. Opin. Colloid Interface Sci.*, 1999, **4**, 83–87.
- 298 X. Qin, A. Lu and L. Zhang, *J. Appl. Polym. Sci.*, 2012, **126**, E469–E476.
- 299 S. I. Anisimov, S. Y. Anisimova, A. A. Baldin, E. G. Baldina, V. A. Luzanov and O. O. Denisenko, *Biomed. Eng. (NY)*, 2010, **44**, 130–133.
- 300 L. C. H. Alves, PhD thesis, Universidade de Coimbra, 2015.
- 301 J. Smiatek, *J. Phys. Condens. Matter*, 2017, **29**, 233001.
- 302 S. Murakami, T. Hayashi and M. Kinoshita, *J. Chem. Phys.*, 2017, **146**, 055102.
- 303 M. B. Gee, N. R. Cox, Y. Jiao, N. Benteitis, S. Weerasinghe and P. E. Smith, *J. Chem. Theory Comput.*, 2011, **7**, 1369–1380.
- 304 A. Yethiraj, *Soft Matter*, 2007, **3**, 1099.
- 305 S. Shimizu and N. Matubayasi, *Phys. Chem. Chem. Phys.*, 2016, **18**, 25621–25628.
- 306 S. Shimizu and N. Matubayasi, *J. Mol. Liq.*, 2019, **273**, 626–633.
- 307 J. E. S. J. Reid, C. E. S. Bernardes, F. Agapito, F. Martins, S. Shimizu, M. E. Minas Da Piedade and A. J. Walker, *Phys. Chem. Chem. Phys.*, 2017, **19**, 28133–28138.
- 308 S. Shimizu, *Food Funct.*, 2015, **6**, 3185–3402.
- 309 C. Liu and W. T. Lindsay, *J. Solution Chem.*, 1972, **1**, 45–69.